NASA Contractor Report 4217

Integrated Autopilot/Autothrottle for the NASA TSRV B-737 Aircraft: Design and Verification by Nonlinear Simulation

Kevin R. Bruce
Boeing Commercial Airplane Company
Seattle, Washington

Prepared for
Langley Research Center
under Contract NAS1-14880

National Aeronautics
and Space Administration

**Scientific and Technical
Information Division**

1989

TABLE OF CONTENTS

TABLE OF CONTENTS (Concluded)

LIST OF FIGURES

LIST OF FIGURES (Continued)

LIST OF FIGURES (Concluded)

LIST OF TABLES

1.0 SUMMARY

An integrate autopilot/autothrottle has been developed for implementation on the NASA TSRV B737 airplane. The system was designed using a 'total energy concept'. Certain maneuvers require a net energy change (e.g., an increase in velocity or height) which can be obtained using the throttle. In gusty conditions, the system may only require a redistribution of energy obtained from using the elevator.

The system is intended to achieve:

(1) Fuel efficiency by minimizing throttle activity.

(2) Low development and implementation costs by designing the control modes around a fixed inner loop design.

(3) Maximum safety by preventing stall and engine overboost.

The control law was designed initially using linear analysis techniques and developed using a simplified nonlinear simulation. The system satisfied the design requirements for stability and cross coupling errors during maneuvers. The wind shear criterion (<5 kt vel error) was satisfied during approach while throttle activity was minimized in cruise.

The control law was developed to include additional control modes (e.g., glide slope capture) and modelled on a nonlinear aircraft simulator (i.e., Harris simulator) to confirm the original design results and validate the system for additional flight conditions.

2.0 INTRODUCTION

A new airplane control system must demonstrate more than just good dynamic response to be seriously considered as a replacement for existing systems. In the last decade the dramatic increase in the price of oil, cost of manpower, and amount of air traffic have meant additional constraints on developing a new system. The result of these constraints is that a new system must be designed for:

(1) Fuel Efficiency
(2) Minimum Development, Implementation and Certification Costs
(3) Maximum Safety

The integrated autopilot/autothrottle has been designed with these constraints in mind. To maximize fuel efficiency the integrated autopilot/autothrottle has been designed using the concept of a 'total energy control'.

Consider an airplane flying at some datum condition with an energy level consisting of the sum of the kinetic energy (KE) and potential energy (PE), where the KE is associated with speed and the PE with altitude. In such a condition certain maneuvers may require a net energy change (e.g., an increase in velocity or height) which can be achieved by control of thrust using the throttle. In gusty conditions or during the execution of a double maneuver (i.e., decrease in height coupled with increase in velocity) the net energy change may be small, but the system will require a redistribution of energy which the elevator provides via redistributing energy by trading KE for PE or vice versa.

This concept produces a 'coordinated' response (i.e., the throttle and elevator working in unison to the command inputs or disturbance), whereas in conventional autopilots and autothrottles (i.e., in which the elevator controls height and the throttle speed) the system can produce an 'uncoordinated' response requiring excessive throttle motion.

This system has been designed with a constraint of minimum complexity to lower costs, and thereby reduce software development and verification compared with a conventional system. In achieving this aim, the system has been developed around a generalized inner loop fixed for all control modes, and an outer loop reconfigured for each required control mode. Furthermore, to maximize safety, the engine controller has been designed to include EPR limit protection, while the system incorporates angle of attack limit protection.

This report documents the development of the integrated autopilot/autothrottle and includes:

(1) Linear Design of the System

(2) Development of Additional Features to Improve Performance in Nonlinear and Limiting Conditions

(3) Design of the Engine Controller

(4) Performance Evaluation of the System Using the Harris Nonlinear Flight Simulator.

Detailed system diagrams are included herein to facilitate system software specifications and future flight test of the system.

3.0 NOMENCLATURE

AZCG	Longitudinal acceleration (through center of gravity)
DEC	Elevator command
ELEV	Elevator deflection
EPR_{cmd}	Commanded Engine Pressure Ratio (EPR)
EPR_{min}	Minimum EPR
E_T	Total Energy Controller Error
E_{T_ε}	Total Energy Controller
h	Height
$\dot{h}$	Height rate
$\ddot{h}$	Height acceleration
h_{baro}	Barometric height
H_{cmd}	Height command
I	Inertial height rate
KEPRP	Engine controller forward path gain
KEFB	Engine controller feedback gain
K_v	Velocity error gain
K_h	Height error gain
$K\alpha$	Error gain
P, P_O	Current pressure, pressure at sea level
U_g	Longitudinal gust velocity
$\dot{V}$	Flight path acceleration
V_{AIR}	Air referenced velocity rate
V_{CAS}	Calibrated Air Speed (CAS)
V_e	Equivalent Air Speed (EAS)
$\dot{V}_{e_{max}}$	Maximum EAS
$\dot{V}_\varepsilon$	Velocity rate/acceleration error
V_{eng}, V_T	Thrust derived velocity rate
V_I	Inertially referenced velocity rate
V_p, V_T	True Airspeed (TAS)
THCM	Throttle command
TAUTO	Throttle level angle
W, W_o	Weight, weight at sea level
W_g	Vertical Gust Velocity
α	Angle of attack
γ	Flight path angle
γ_ε	Flight path angle error
δ_ε	Elevator deflection
δ_{THR}	Change in Thrust
$\theta, \dot{\theta}$	Airplane body angle, body rate
τ_K	Complementary filter ($V_{I/AIR}$) time constant
ω_K	Complementary filter bandwidth
ω	Natural frequency
ζ	Damping ratio
ΔT	Thrust change
ΔY	Flight path angle change

4.0 DESIGN AND PERFORMANCE REQUIREMENTS

The following design and performance requirements were imposed on the design to assure satisfactory performance of the final control law:

(1) All vertical control modes should be integrated into a single control law concept. The system should be designed around a fixed inner loop configuration with outer loop control modes generating control signals that are compatible with the inner loop command inputs.

(2) Cross coupling control errors should be minimized and the system should give a balanced performance over all flight conditions. The maximum velocity error should be less than 1 kn for path control, while the maximum height error should be less than 20 ft for speed control.

(3) There should be no overshoot of response for step command inputs. The damping ratio of dominant poles should be greater than 0.7.

(4) Tight speed control is required in conditions of wind shear (max speed error <5 kn). This criterion is considered vital at low speed and altitude conditions.

(5) Throttle activity should be minimized particularly in cruise conditions. However, during approach when wind shear becomes a dominant consideration, the requirement to minimize throttle activity becomes a secondary consideration.

(6) The design should incorporate safeguards to prevent stall and overboost of the engine.

5.0 LINEAR DESIGN

5.1 INTRODUCTION

The concept of 'total energy control' evolved during the evaluation of two preliminary control law schemes. The basic configurations and reasons for rejection of these configurations are presented here.

5.1.1 Configuration 1

Configuration 1 was concerned with integral control of speed through the throttle with proportional and rate control of speed plus integral control of altitude through the elevator. This system was found to require substantial modification to achieve system stability. In addition, performance characteristics were found not to be good.

5.1.2 Configuration 2

Configuration 2 was concerned with integral control of speed through the throttle and integral control of altitude through the elevator with proportional and rate control of speed and altitude through the throttle and elevator. After some modification from the original concept, this design yielded good performance in turbulence, despite that the cross coupling and windshear performance were poor.

Nevertheless, Configurations 1 and 2 did not lend themselves to the single basic control law concept and required considerable software to provide all the additional control modes needed in a practical autopilot design. Therefore, a third control configuration was developed.

5.1.3 Configuration 3

Configuration 3 was concerned with integral control of altitude through the throttle and integral control of speed through the elevator with proportional and rate control of speed and altitude through the throttle and elevator.

This third concept was similar to the technique used by pilots, whereby thrust is trimmed to attain the desired flight path while elevator control is used to stabilize the aircraft and maintain speed. In addition, during operation on the back side of the power curve, this technique is essential because flight path response to elevator is unstable for constant thrust while the relationships:

$$\left(\frac{\Delta\gamma}{\Delta T}\right)_{\delta_e} = \text{constant} \qquad \text{and} \qquad \left(\frac{\Delta V}{\Delta\delta_e}\right)_{T} = \text{constant}$$

remain consistent.

5.2 DEVELOPMENT OF INTEGRATED CONTROL LAW CONFIGURATION

The system shown in Figure 1 represents the original conceptual design which incorporated design features and characteristics identified during the previous autothrottle/autopilot improvement studies. These characteristics are described in the following paragraphs.

5.2.1 Flight Path Inner Control Loop

The flight path inner control loop uses flight path error ($\gamma\varepsilon$) to derive the throttle command signal as flight path angle is directly related to thrust:

$$\Delta T = g\Delta\gamma$$

Altitude and altitude rate control modes are simply outer control loops which generate a γ_{CMD} signal to drive the inner loop.

5.2.2 Inner Speed Control Loop

The inner speed control loop uses flight path acceleration, which is again related to specific thrust:

$$\Delta T \propto \dot{V}$$

True airspeed control forms the outer loop to the flight path acceleration loop. The flight path acceleration command is formed by multiplying airspeed error by the outer loop gain. As with the flight path loop, additional airspeed related control modes can simply be added to the front end of the airspeed control mode. For example, Mach control can be provided by simply converting the change in Mach command to a change in true airspeed.

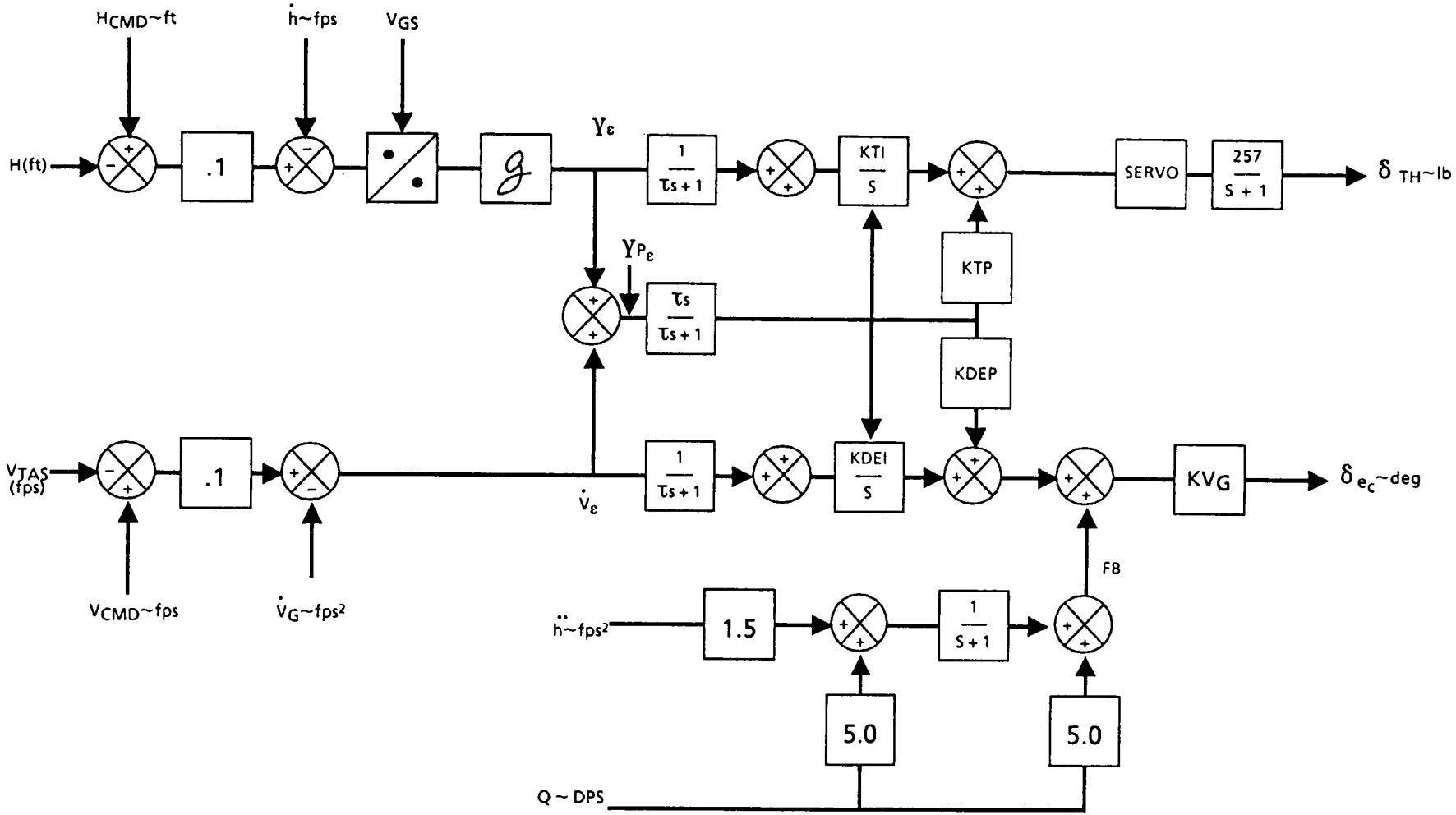

Figure 1. Conceptual Design of Integrated Autopilot/Autothrottle

5.2.3 Flight Path Angle Error Signal

The key design feature is the calculation of the potential flight path angle error signal γ_ε. This signal may be considered as the energy that must be added to the system in order to restore the nominal height and airspeed (e.g., in response to a wind gust). The signal is shaped through a high pass filter and used for short term control of both the elevator and thrust. In constant energy airplane dynamics (e.g., phugoid type motion) the potential flight path angle error signal (γ_ε) would be zero.

5.2.4 High and Low Pass Filters

For large term control, the high and low pass filter yield a unity transfer function for γ_ε, which is then integrated to develop the trimmed throttle position. Similarly, in the elevator path, the filters give a unity transfer function to $\dot{V}_e$, which is then integrated to develop the trimmed elevator position.

5.2.5 Pitch Stability

Short term pitch stability is provided by a conventional θ/θ inner loop.

5.2.6 Outer Loop Gains

The outer loop gains of altitude and speed are selected to provide a good stability and transient response. Further, for speed control, the ratio of airspeed error gain and inertial acceleration gain is selected to achieve maximum cancellation of turbulence induced signal components.

5.2.7 Cross Coupling Signal Paths

The cross coupling signal paths are the same for all control modes in order to achieve consistent control decoupling for each mode.

A stability analysis of this system showed that the system was unstable due to the sign of $\delta_{e/\Delta\gamma}$. The sign must be negative for short term control, but positive for steady state condition. Therefore, the short term elevator and throttle command processing require separate γ_ε and $\dot{V}_\varepsilon$ signal inputs. Crossfeed signals summed downstream of integrators would serve for short term control.

This concept was developed so that the throttle could be used as an energy controller where:

$$E_{T_\varepsilon} = g\gamma_\varepsilon + \dot{V}_\varepsilon$$

In addition, it was considered practical to use $\dot{V}_\varepsilon$ and γ_ε to develop the short and long term elevator command. When the total energy error is zero (i.e., the acceleration error $\dot{V}_\varepsilon$ is equal to $-g\gamma_\varepsilon$), the signal inputs ($\dot{V}_\varepsilon$ and $-g\gamma_\varepsilon$) are equivalent and contribute equally to the elevator command.

This reconfigured system was optimized for high speed (i.e., cruise configuration) as shown in Figure 2. The proportional total energy signal to the throttle has been discarded because a stability analysis indicated that this signal was not required for adequate stability.

The stability characteristics were:

ω	ζ
6.7	.998
6.16	.719
.097	.888

5.3 LOW SPEED CONFIGURATION

The gains derived for the cruise configuration resulted in a slow transient response to command signals at low speed. Root locus analysis techniques were used to obtain an improved response. Figure 3 shows the resulting configuration and gain values. The primary modifications were:

(1) Increased system bandwidth by increasing gains K_h and K_v.

(2) Increased inner loop gains for improved stability.

(3) Change in KDEI, KUD, and KHD gain values to improve cross coupling errors.

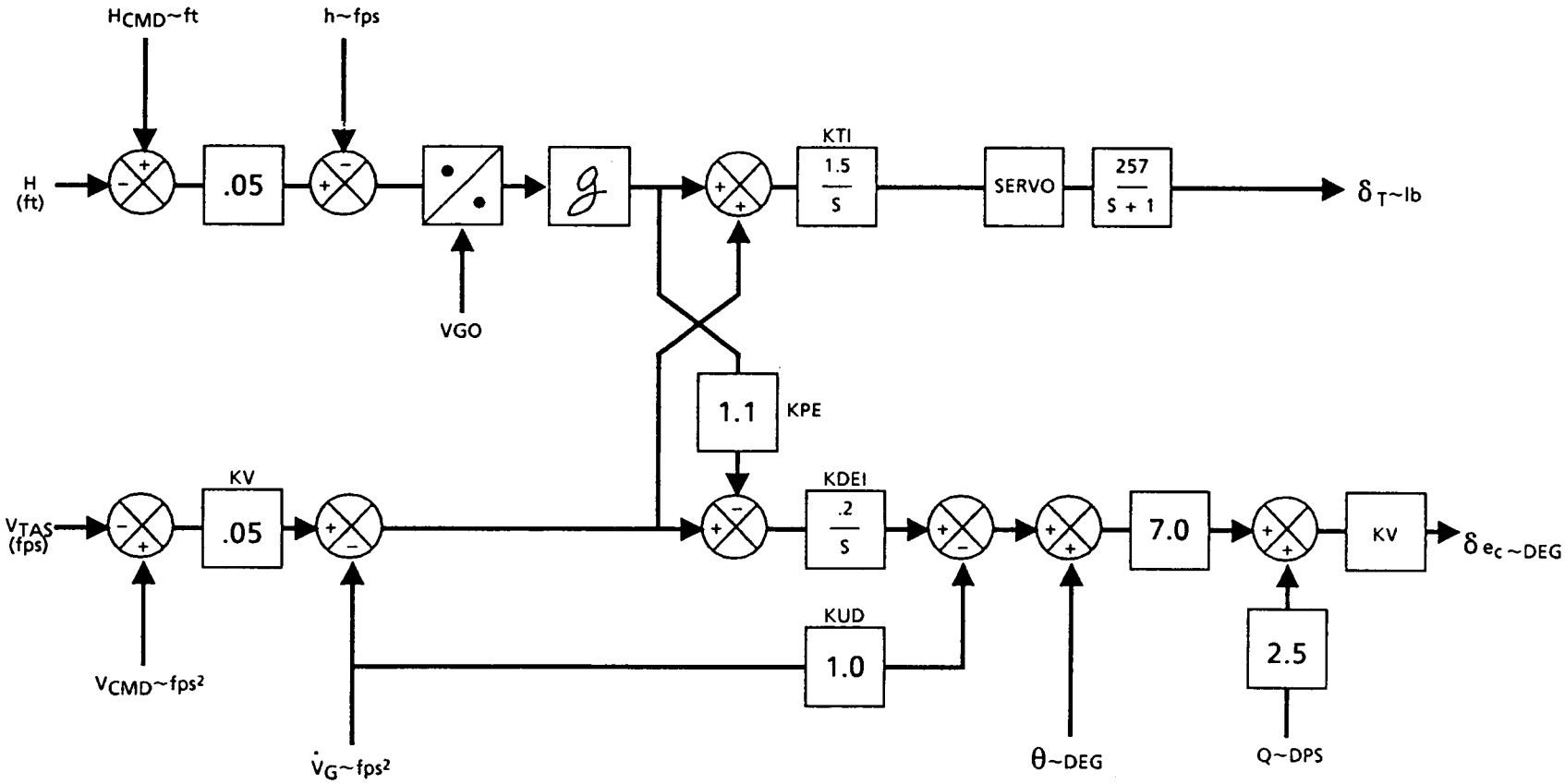

Figure 2. Cruise Configuration

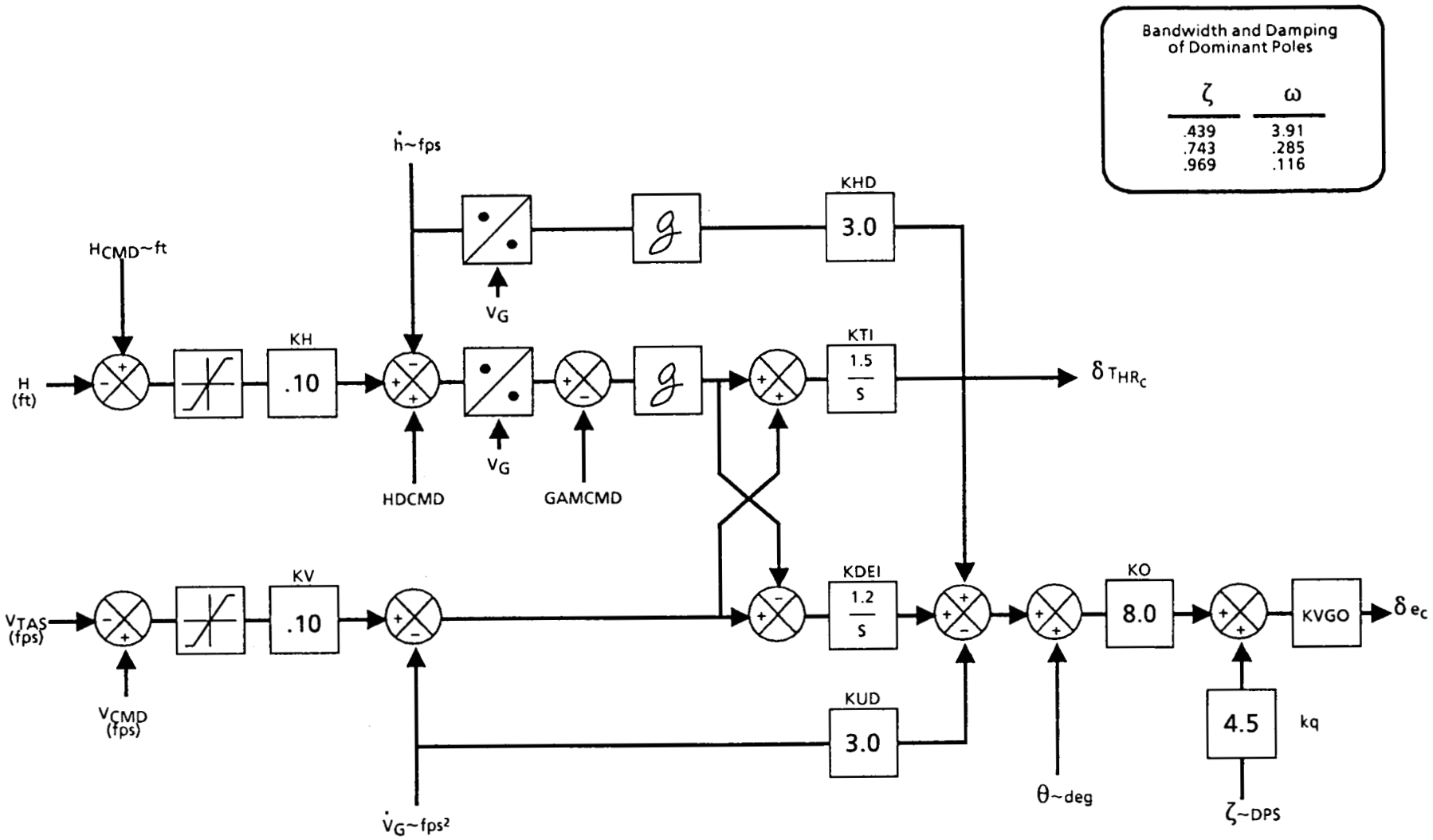

Figure 3. Initial Low Speed Control Law Configuration

The stability characteristics of the system were:

ζ	ω
.439	3.91
.743	.285
.969	.116

Typical transient responses are shown in Figure 4 for a 100-ft step, Figure 5 for a 10-kn step, and Figure 6 for a 3° step in flight path angle.

The double maneuver is of particular interest in examining the performance of the integrated elevator and throttle control law. Figure 7 shows the time response of a conventional autopilot (in altitude hold mode) and autothrottle for a simultaneous commanded 10 kn increase in airspeed and 105 ft decrease in altitude. In this maneuver the throttle moved forward 6° to null the speed error, causing a slow response with overshoot. The same maneuver for the integrated system (fig. 3), shown in Figure 8, gave a smoother response with no altitude or airspeed overshoot. With this maneuver the throttle settled quickly after an excursion of only 2°.

5.4 WIND SPEED AND TURBULENCE PERFORMANCE FOR LOW SPEED CONFIGURATION

The performance of the baseline integrated autopilot/autothrottle in turbulent conditions is shown in Table 1 for 1 fps rms longitudinal and vertical gusts. For comparison purposes, the results obtained for the TCV glide slope track law and autothrottle are also presented. It can be seen that the baseline system has worse path tracking and elevator activity, although airspeed tracking is better particularly in vertical turbulence. The performance of this system in wind shear (1 kn/s horizontal shear) is shown in Figure 9. The 10:1 ratio of inertial acceleration to airspeed causes a 10 kn steady state airspeed error.

Three design modifications were evaluated to improve this performance:

(1) Complementary Inertial/Airmass referenced acceleration
(2) Complementary Airmass/Thrust derived acceleration
(3) Adding a two-dimensional wind stress detector

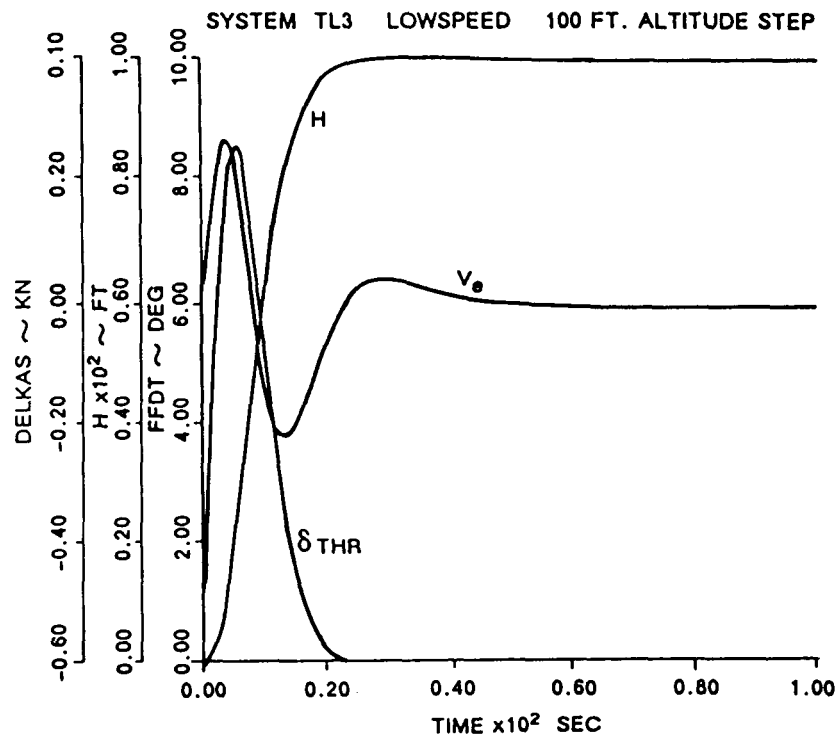

Figure 4. 100-ft Step

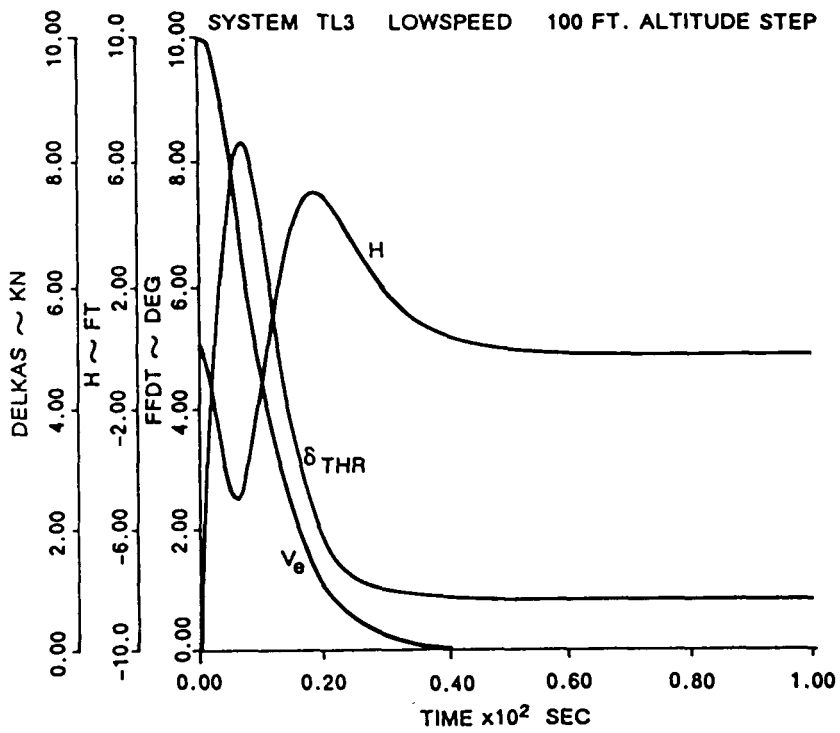

Figure 5. 10-kn Step

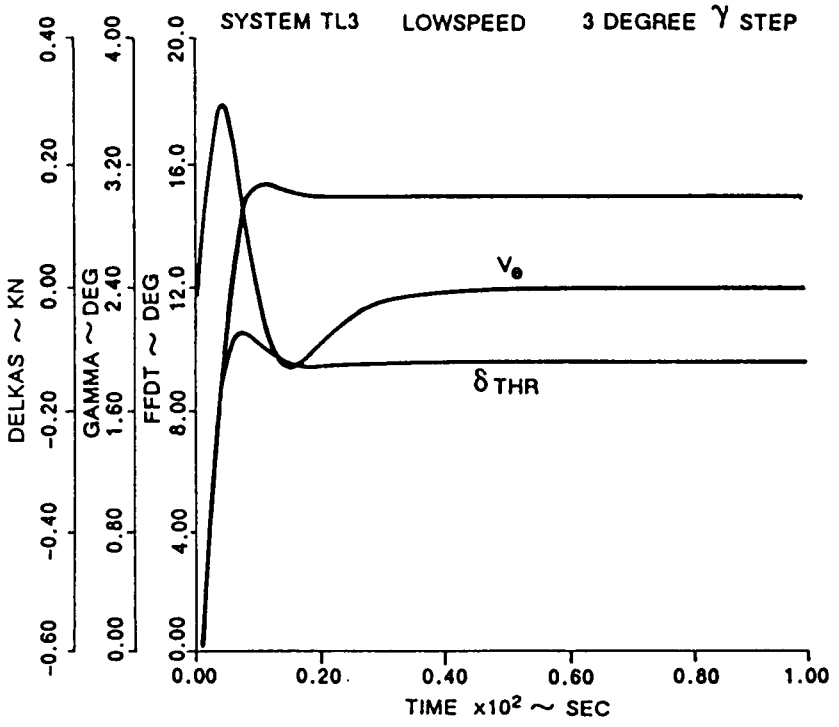

Figure 6. 3° Step in Flightpath Angle

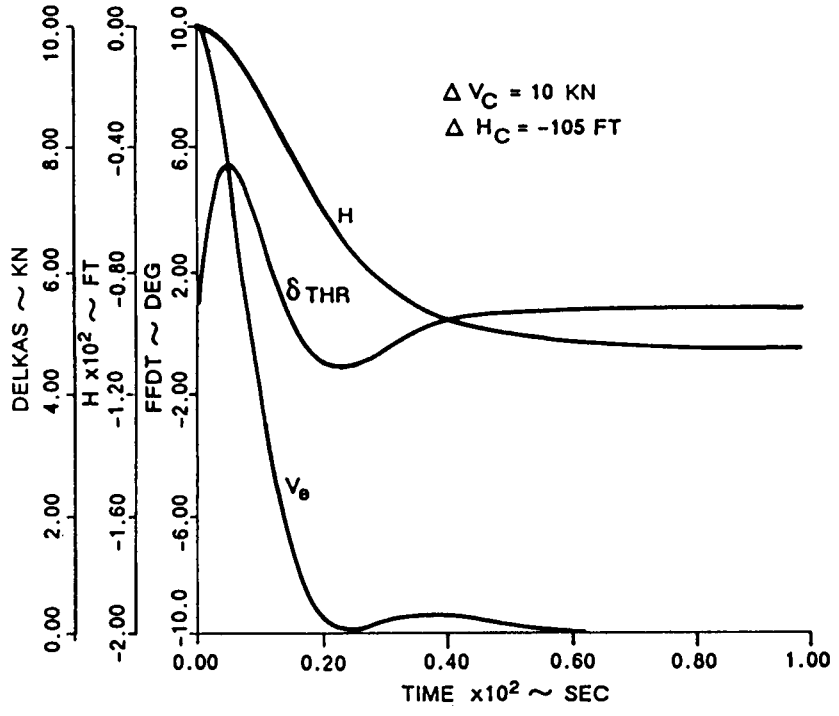

Figure 7. Double Maneuver (Conventional Autopilot)

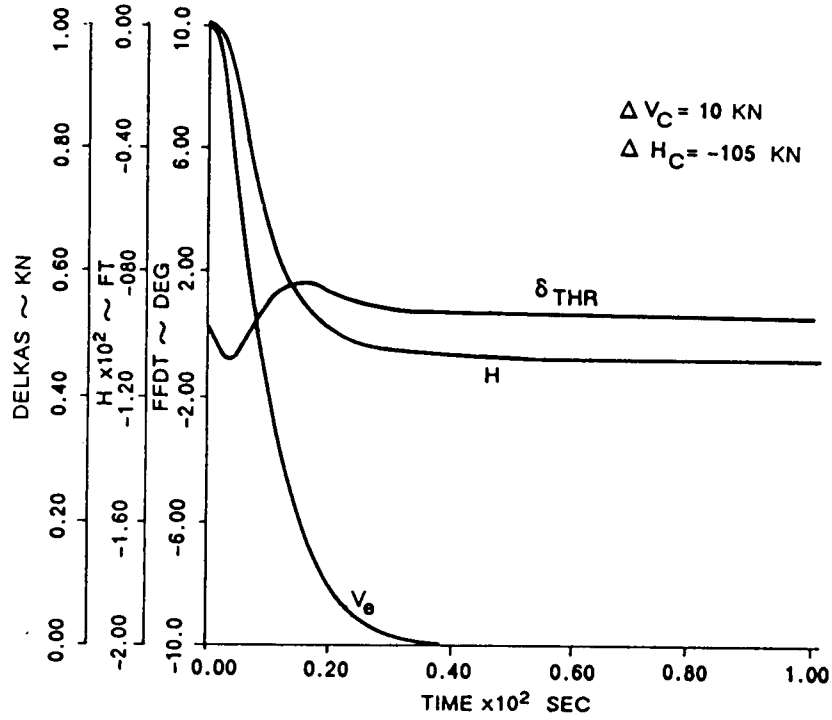

Figure 8. Double Maneuver (Integrated System)

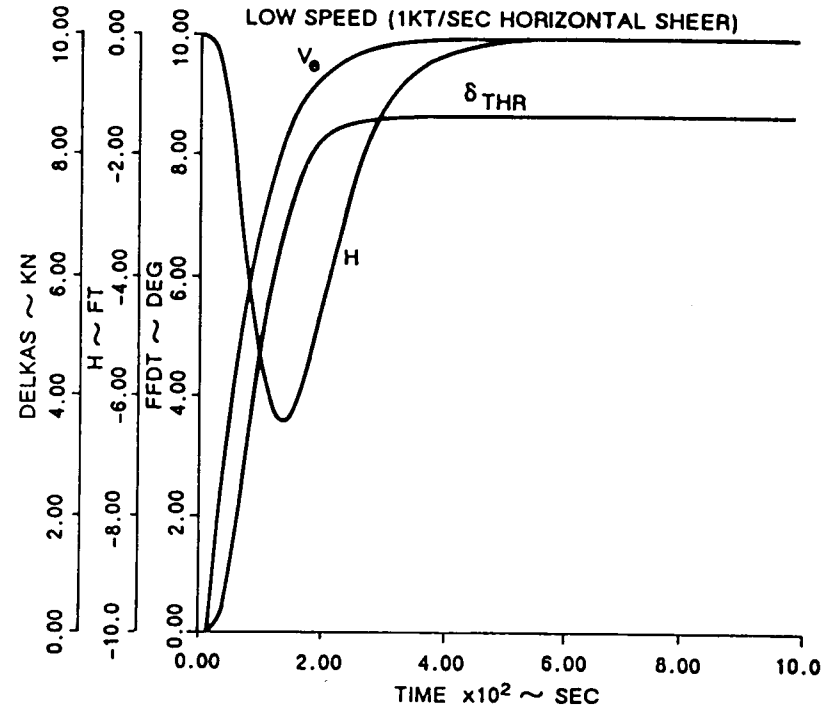

Figure 9. Baseline Systems for 1 kn/s Horizontal Shear

Table 1. RMS Values for Dryden Spectrum Input

NOISE INPUT	OUTPUT	BASELINE SYSTEM	$\dot{V}_I/\dot{V}_{AIR}$ $\tau=20s$	$\dot{V}_{T,\gamma}$ $\tau=20s$	$V_{T,\gamma}$+WSD $\tau=15s$	TCV GLIDE SCOPE* TRACK + A/T
U_g	V_e	.9831	1.013	.9931	.9876	1.025
	H	.6490	1.065	1.0726	1.1826	.4181
	δ_{THR}	.4184	.6383	.6367	.9380	.4047
	δ_e	.3662	.1357	.3319	.7410	.1672
W_g	V_e	.1647	.1574	.5485	.4973	.4486
	H	1.9151	1.973	.9535	1.043	.7916
	δ_{THR}	.8089	.8082	.5224	.6703	.7795
	δ_e	.7056	.6966	.2406	.2282	.3116

* No wind shear detector

The steady state error due to wind shear can be eliminated by the addition of a complementary filter using true airspeed (figs. 10 and 11). Inertial acceleration is filtered through a high pass filter and complemented with a lagged airspeed rate. However, this improvement in wind shear performance is achieved at the expense of throttle activity (Table 1).

An alternative method of obtaining acceleration was considered to determine whether throttle activity could be reduced. This method consisted of deriving an equivalent acceleration signal from engine thrust (EPR) and flight path angle feedback.

The equivalent acceleration signal was approximated by:

$$\dot{V}_{T,\gamma} = \frac{g}{\omega}\Delta T - g\Delta\gamma$$

Drag effects have been neglected. The thrust can be derived from EPR or engine speed (N_1) and flight path angle can be derived by:

$$\gamma = \frac{\dot{h}}{Vg}$$

The acceleration signal $V_{T,\gamma}$ was then used in an identical manner to V_G (i.e., complemented with V_{Air}) as shown in Figure 12.

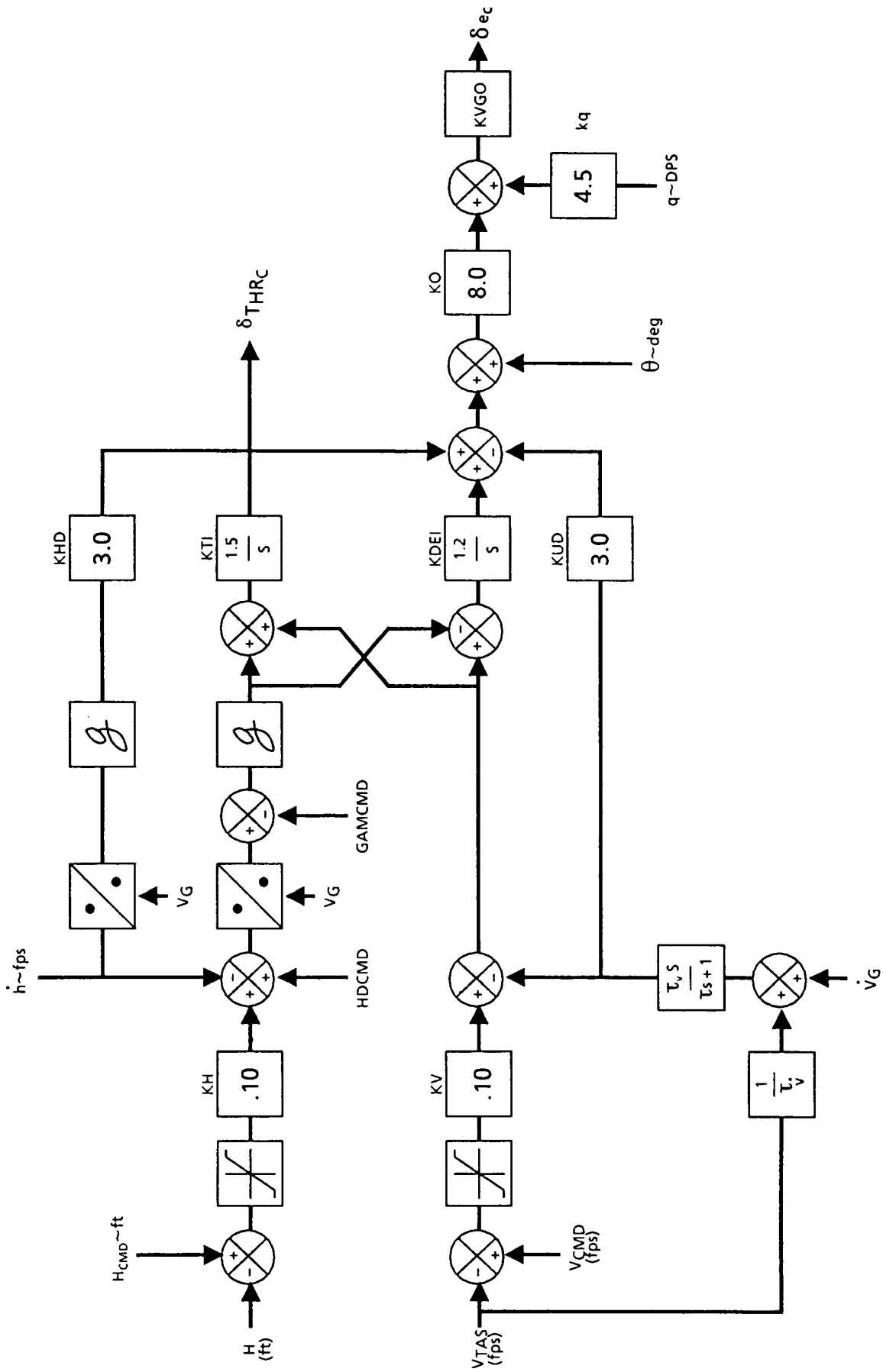

Figure 10. Integrated System with Complementary $\dot{V}$

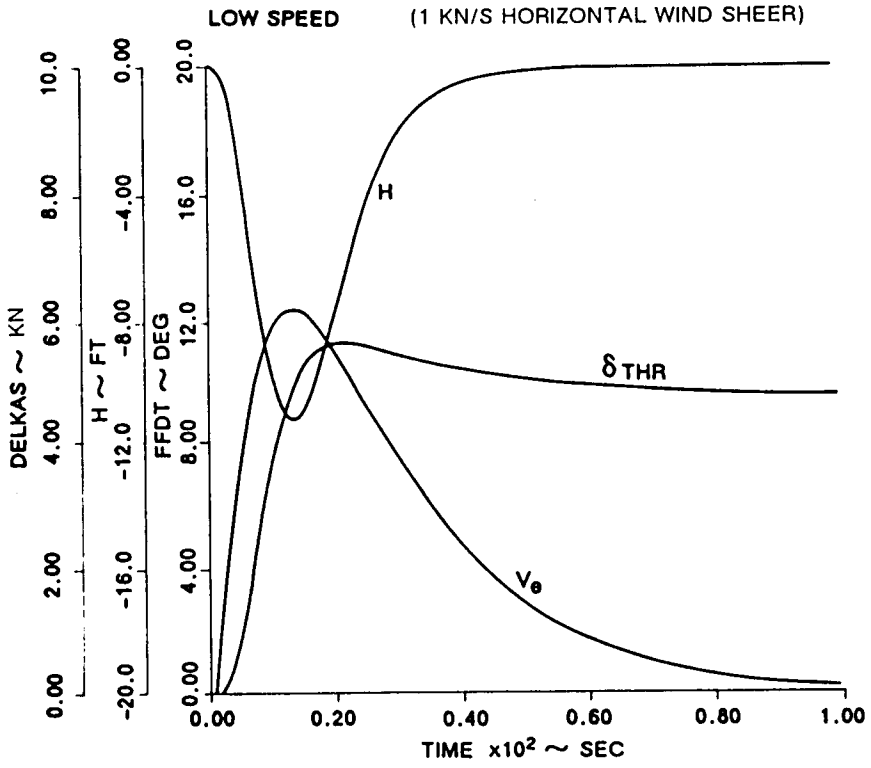

Figure 11. Wind Shear Response with Complementary V

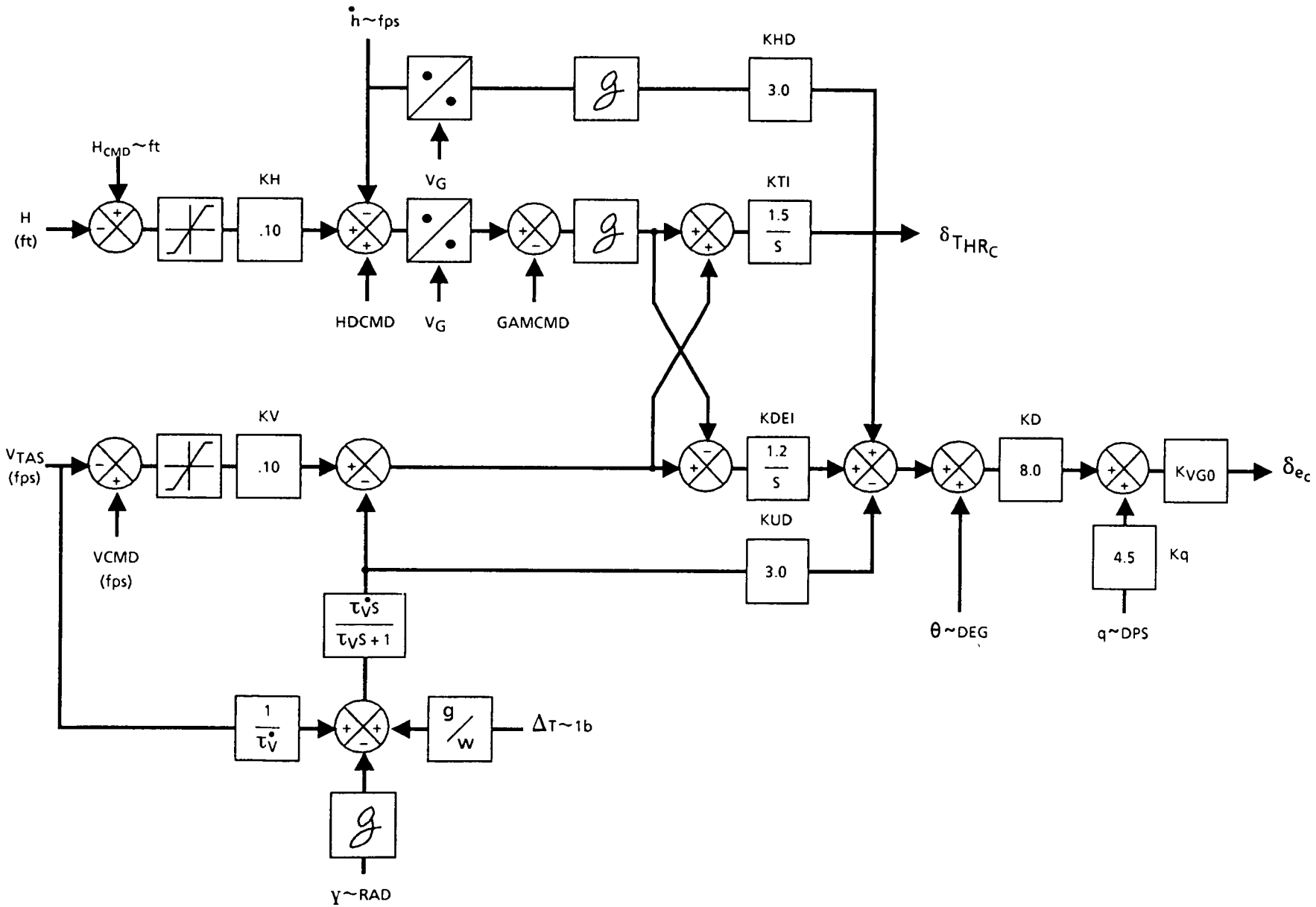

Figure 12. Integrated System with Complementary $\dot{V}_{eng}$

The overall system stability was decreased by using $V_{T,\gamma}$, compared with V_G. The effect of this reduced stability can be seen in Figure 13, which shows nearly twice the error of the baseline system (fig. 4) for a 100-ft step in altitude. Table 2 shows the effect on damping characteristics of varying the $V_{T,\gamma}$, system complementary filter time constant.

Table 2. Effect of Varying the Complementary Filter Time Constant (τ) for $V_{T,\gamma}$ System

τ = 10		τ = 20		τ = 30	
ζ	ω	ζ	ω	ζ	ω
.353	1.82	.359	1.84	.361	1.84
.689	.212	.724	.208	.737	.207

The wind shear performance of this system is compared with the performance obtained with the $\dot{V}_I/\dot{V}_{AIR}$ system in Figure 14.

Figure 14 shows the effect on rms throttle activity and velocity error due to wind shear of varying the complementary filter time constant (τ), for both of the systems previously discussed. It can be seen that these two systems are almost identical.

The overall performance of the different control laws is shown in Table 1. The significant difference in performance is the effect of vertical turbulence where noise levels on height, throttle and elevator are significantly reduced, although velocity error increases by 250%.

A wind shear detector (WSD) was incorporated with the design (figs. 15 and 16) to complete the analysis of wind shear and turbulence. The purpose of this design is to command a new thrust level to offset accelerations due to wind. The details of the design are given in Appendix A.

The rms results (shown in Table 1) for the system with WSD are very similar except for increased throttle and elevator activity due to vertical turbulence. However, these results were calculated for a different time constant (τ). Plotting rms throttle against wind shear for both system shows the characteristic is essentially the same, although for a different value of time constant (i.e., the second system with τ = 10 gives similar results to the third system with τ = 30). (See fig. 17.)

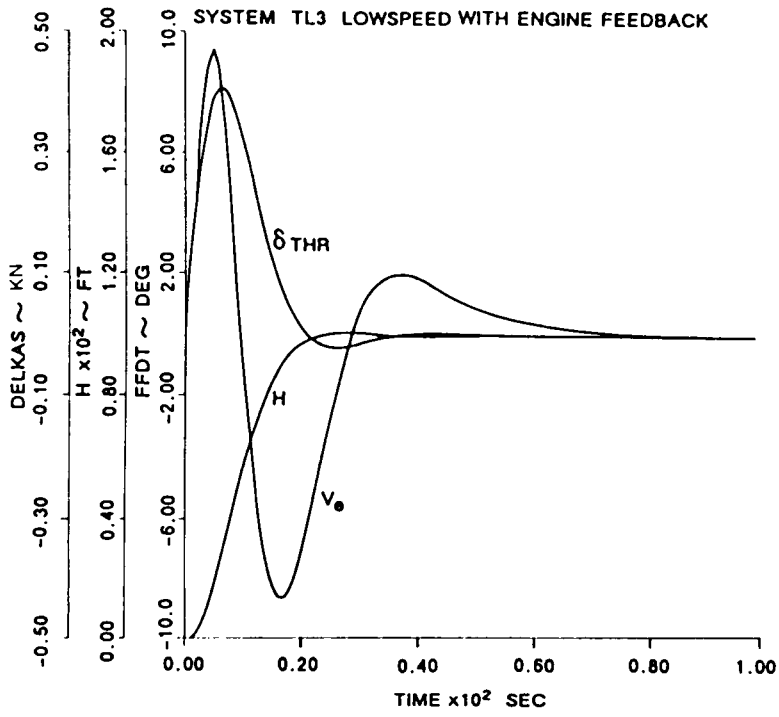

Figure 13. 100-ft Altitude Command

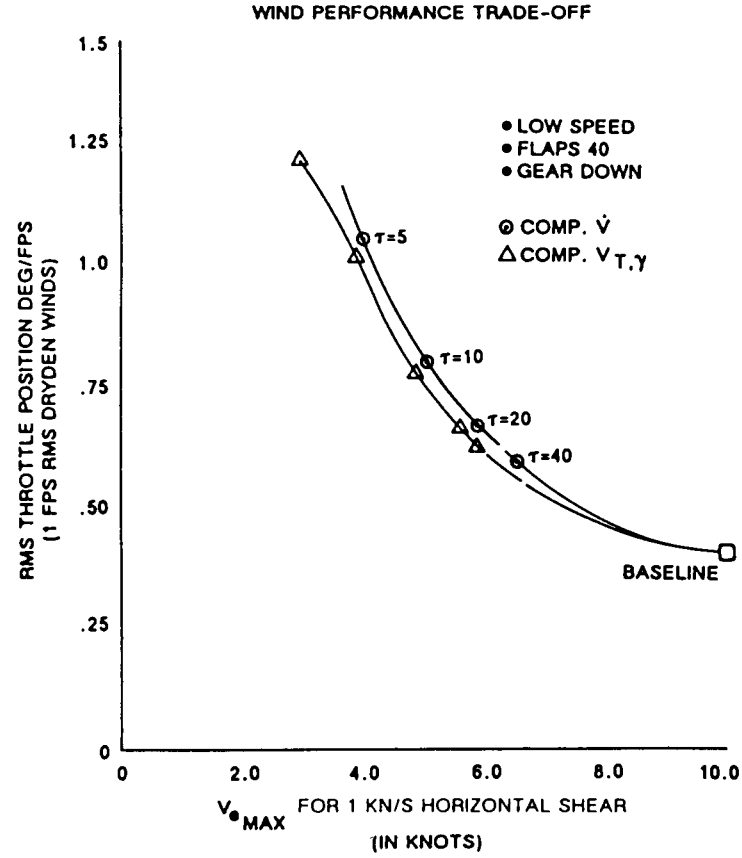

Figure 14. Wind Performance Trade-Off

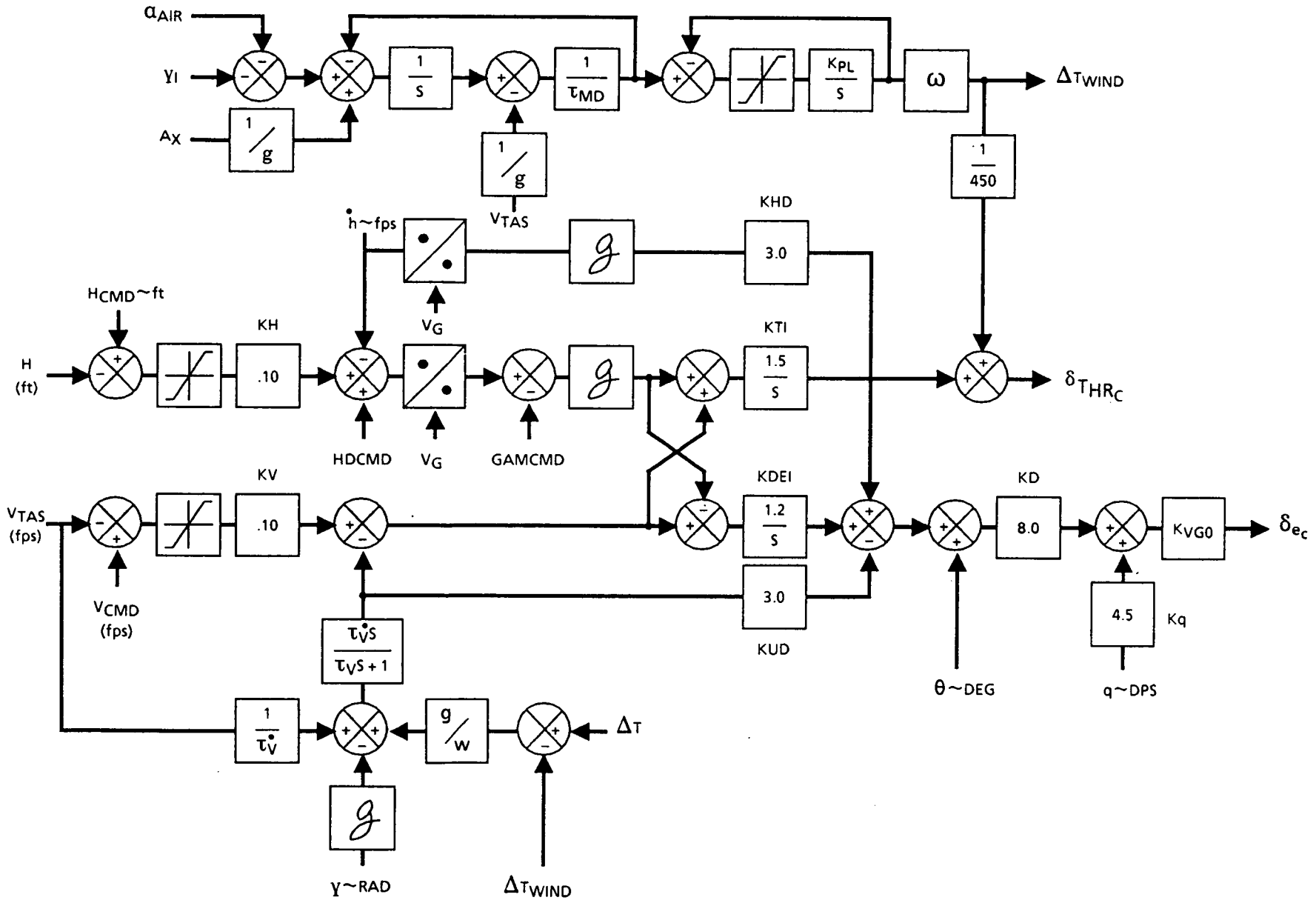

Figure 15. System with $\dot{V}_{eng}$ and Wind Shear Detector

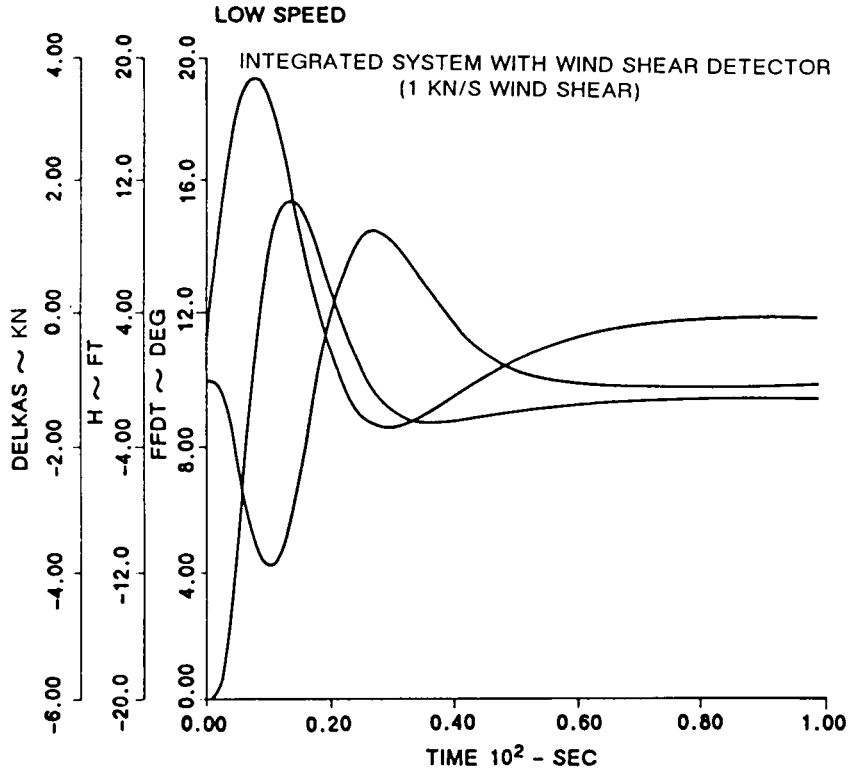

Figure 16. Integrated System With Wind Shear Detector

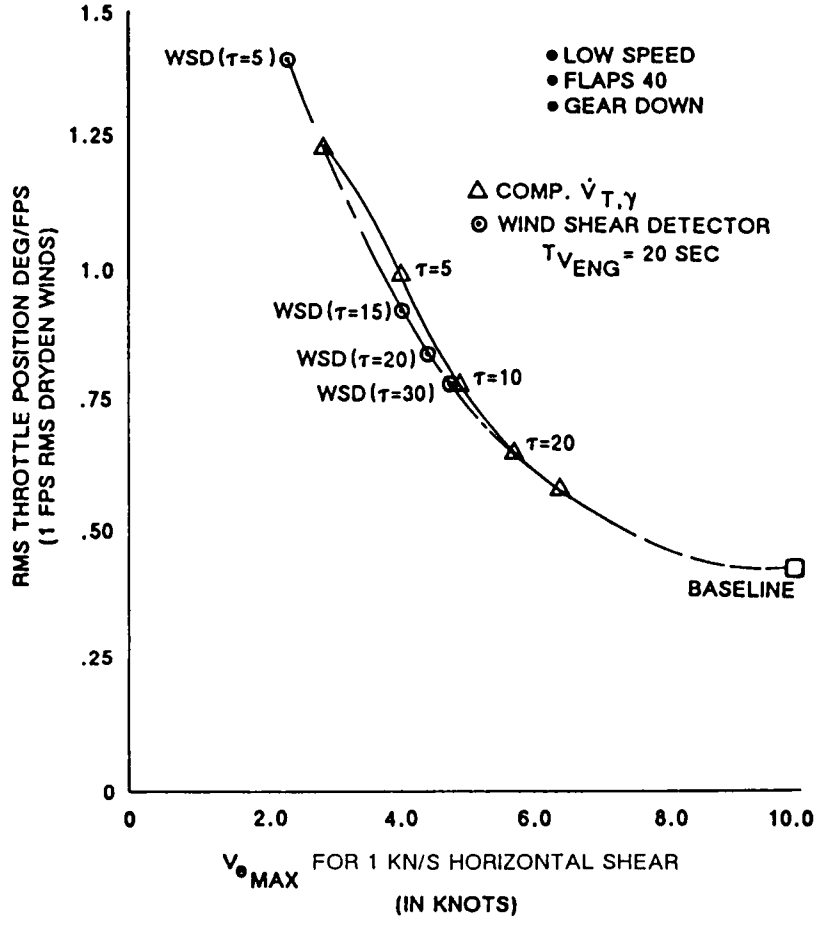

Figure 17. Wind Performance Trade-Off (Wind Shear Detector)

5.5 INNER LOOP DESIGN

Though consideration has been given to the performance of this system in wind shear and turbulence, it was not considered optimum in terms of stability or path tracking capability. Hence, further root locus analysis was carried out to improve stability with the resultant gain configuration presented in Figure 18 along with the bandwidth and damping of the dominant modes. The performance of this system in turbulence was compared with the previous system and found to have lower elevator activity due to the lower gain in the proportional $\dot{h}$ and $\dot{h}$ paths. However, the revised system gave poorer altitude tracking.

Previous research work on TSRV auto/and flare control laws had established that $\ddot{h}$ feedback in the inner elevator control loop exhibited better path tracking than the conventional θ/θ systems. Therefore, an $\ddot{h}/\theta$ system was derived (see Appendix B). The h/θ system is shown in Figure 19 together with the damping and bandwidth of the dominant modes. Altitude and airspeed decoupling were not significantly affected by the different inner loop, although wind shear performance was improved slightly (0.7kn for 1 kn/s wind shear input). Table 3 shows the effect of turbulence (for 1 fps rms input). The h/θ showed improved height tracking compared with the θ/θ loop, although this was achieved at the expense of elevator activity, with throttle activity not being significantly affected.

The performance of the inner loops were compared in the frequency domain (fig. 20a-h). The $\ddot{h}/\theta$ system showed better low frequency performance for altitude tracking but worse high frequency elevator response. In order to take advantage of the preferred characteristics of each system, the two inner loop techniques were combined through a complementary filter. The low frequency component of the $\ddot{h}/\theta$ loop was combined with the θ/θ high frequency component to achieve the complementation. This was an approximate complementation since some of the less significant outer loop terms were omitted to give a system consistent with the total energy control law concept. The system diagram and stability characteristics are shown in Figure 21. Figures 22 and 23 show the time response of the system to a 100-ft altitude command and 10-kn speed command respectively. The altitude and speed decoupling were excellent in both cases. In addition, elevator activity had been significantly reduced (e.g., .81° rms to .16° rms for vertical turbulence of 1 kn/s rms) without penalizing velocity or path tracking.

The final inner loop considered for implementation was an angle of attack inner loop. The motivation for considering this design was the possibility of providing a simple and effective angle of attack limiting capability.

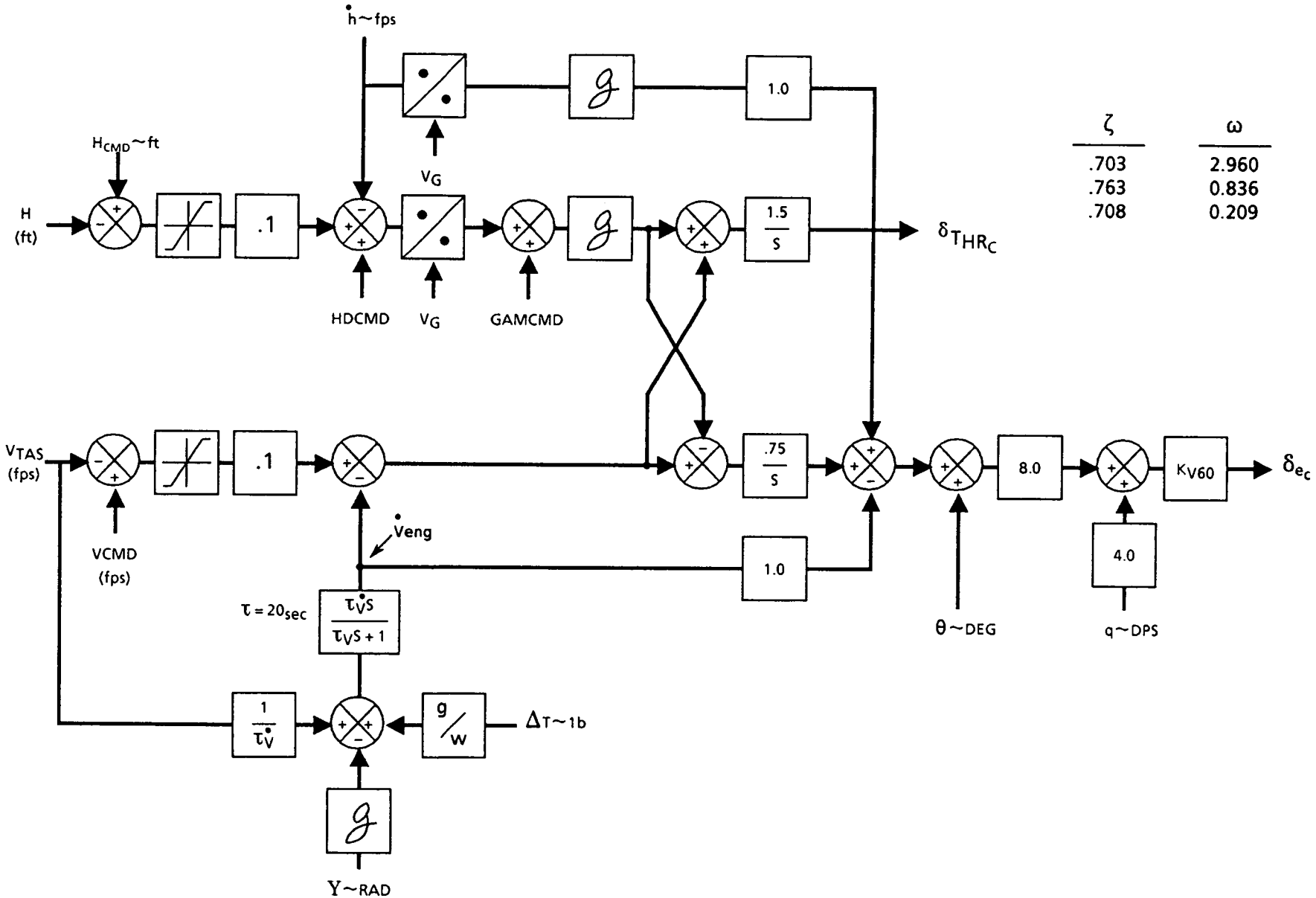

Figure 18. Control Law with Improved Stability

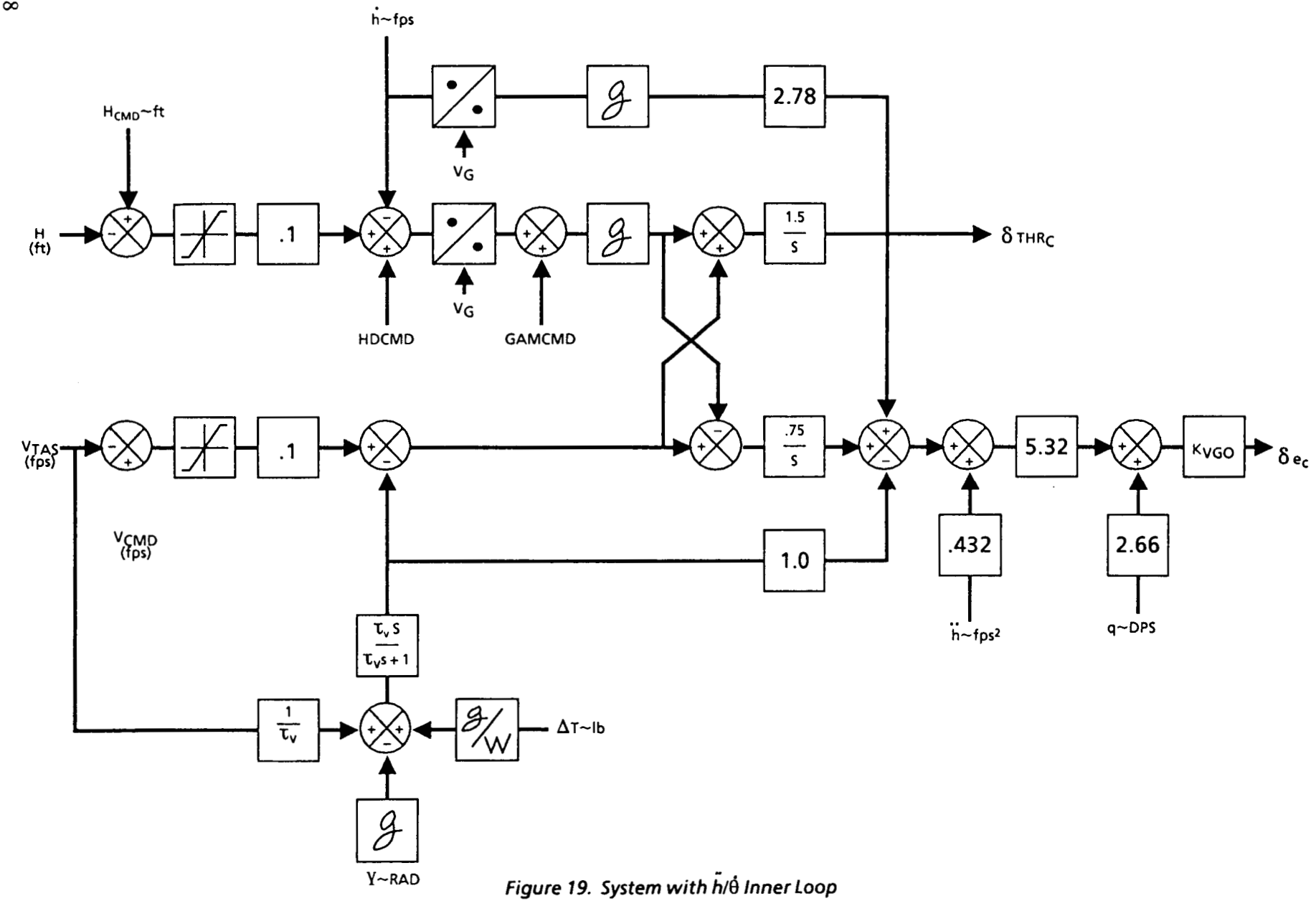

Figure 19. System with $\tilde{h}/\dot{\theta}$ Inner Loop

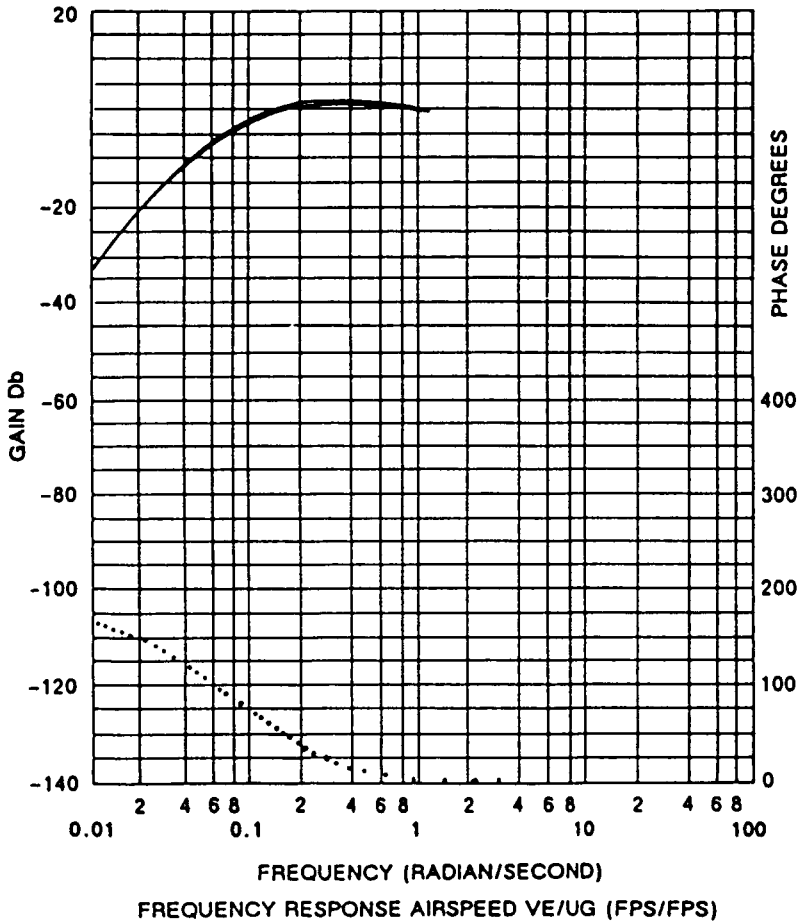

Figure 20a. Frequency Response of Inner Loops

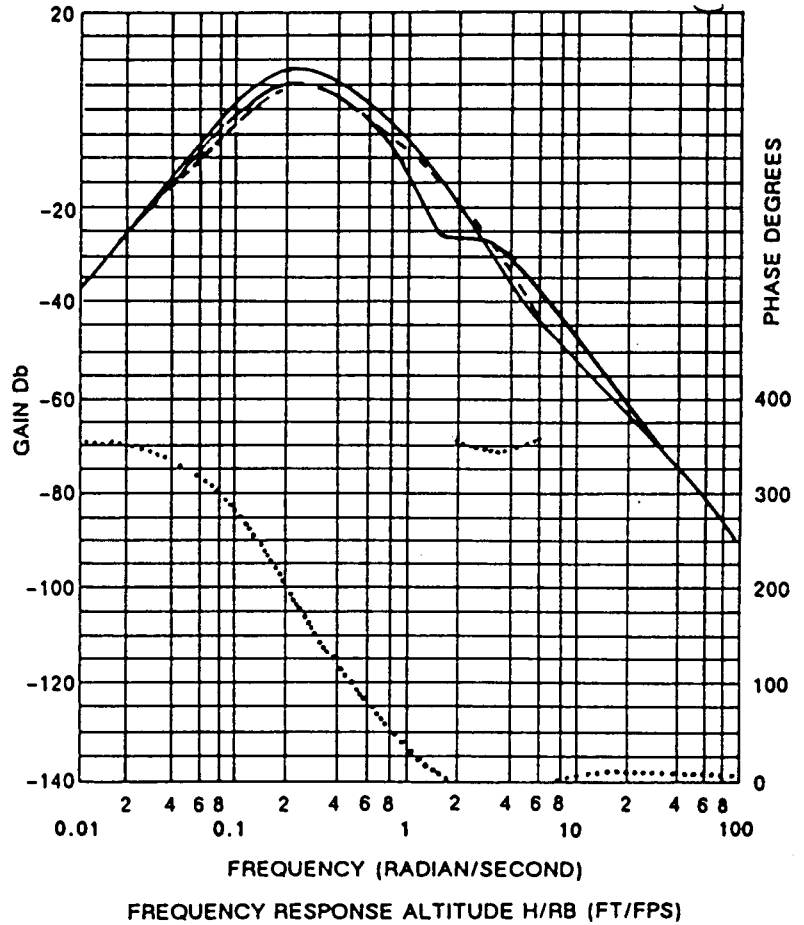

Figure 20b. Frequency Response of Inner Loops

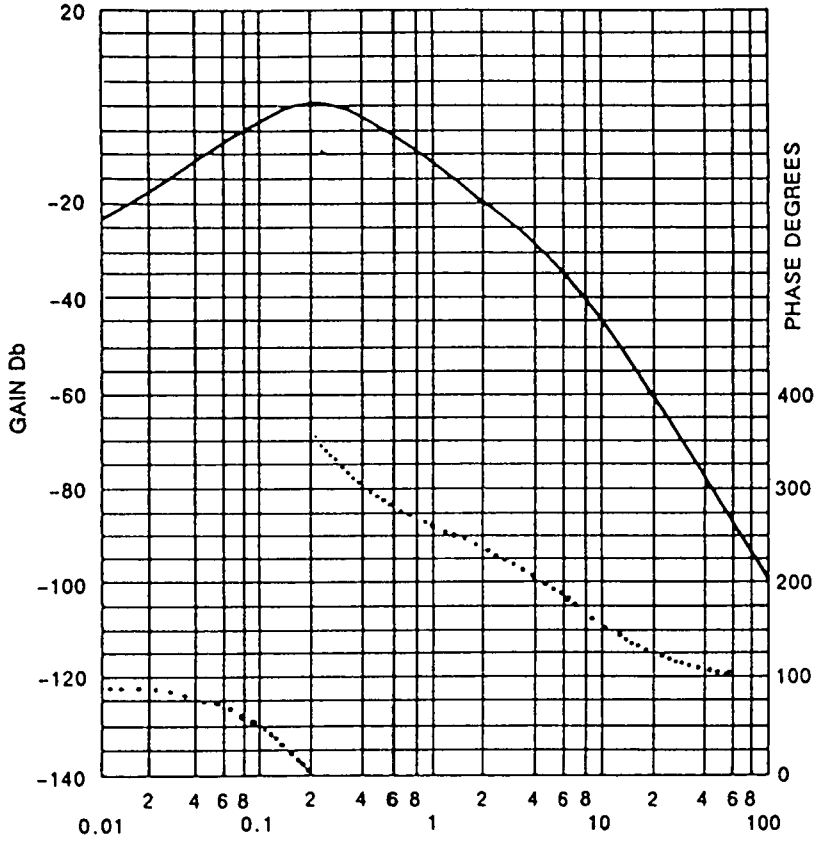

FREQUENCY RESPONSE THROTTLE DELT/WG (DEG/FPS)

Figure 20c. Frequency Response of Inner Loops

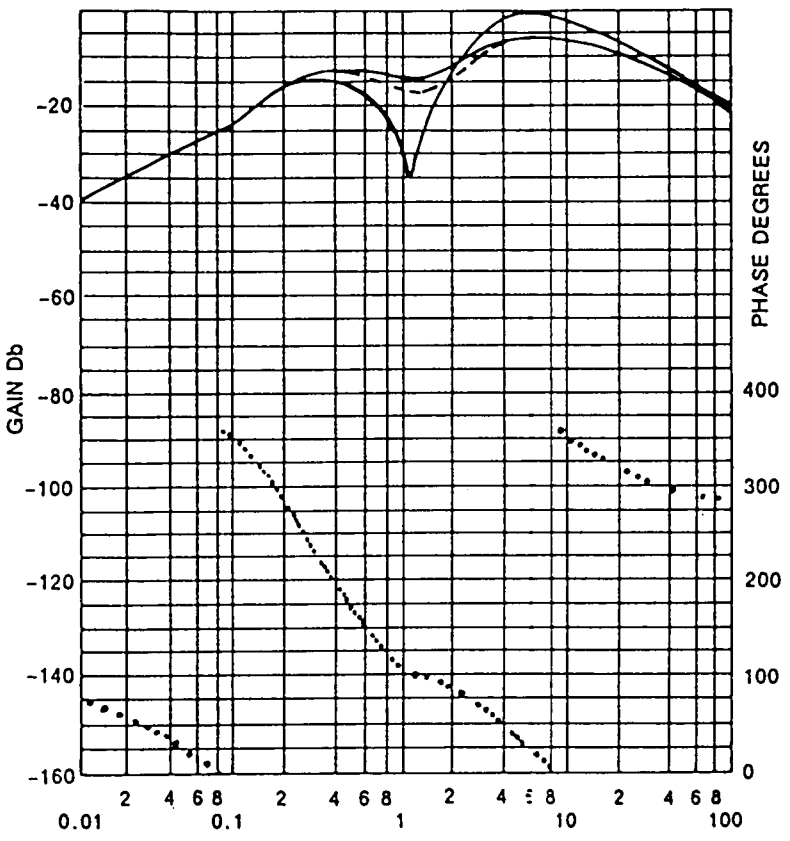

FREQUENCY RESPONSE ELEVATOR DE_/WG (DEG/FPS)

Figure 20d. Frequency Response of Inner Loops

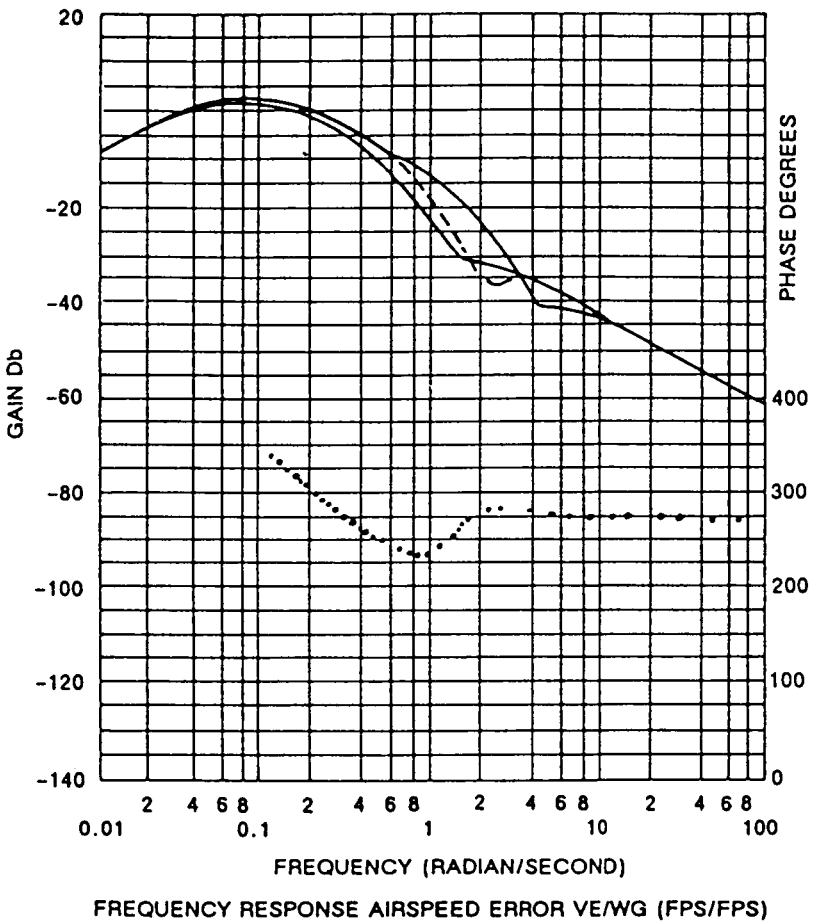

Figure 20e. Frequency Response of Inner Loops

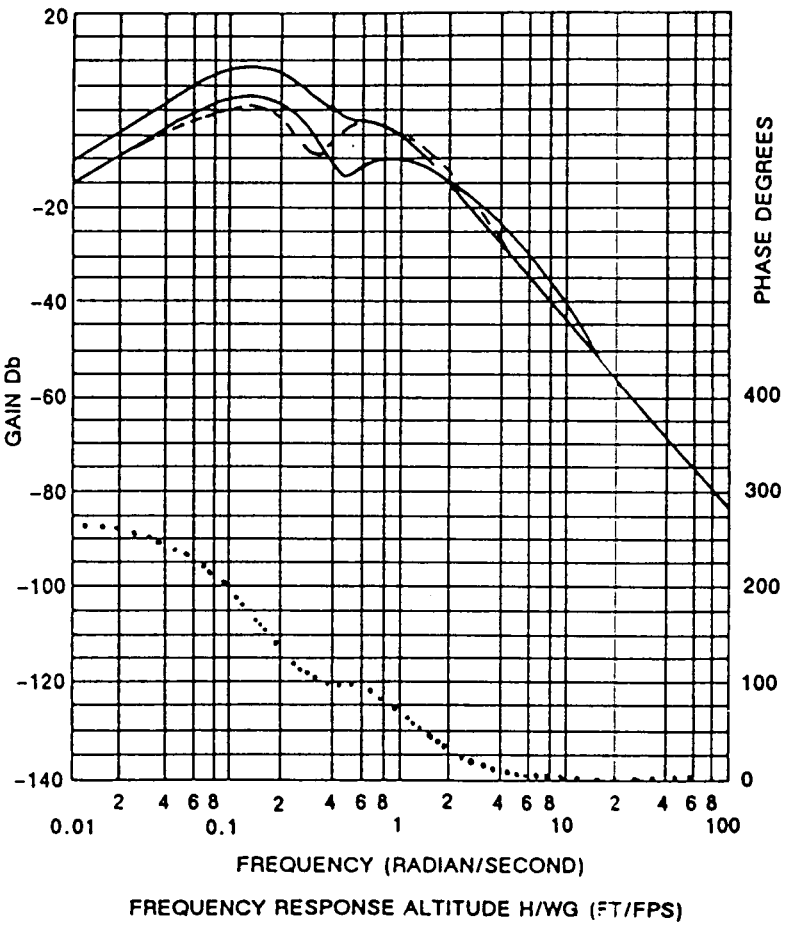

Figure 20f. Frequency Response of Inner Loops

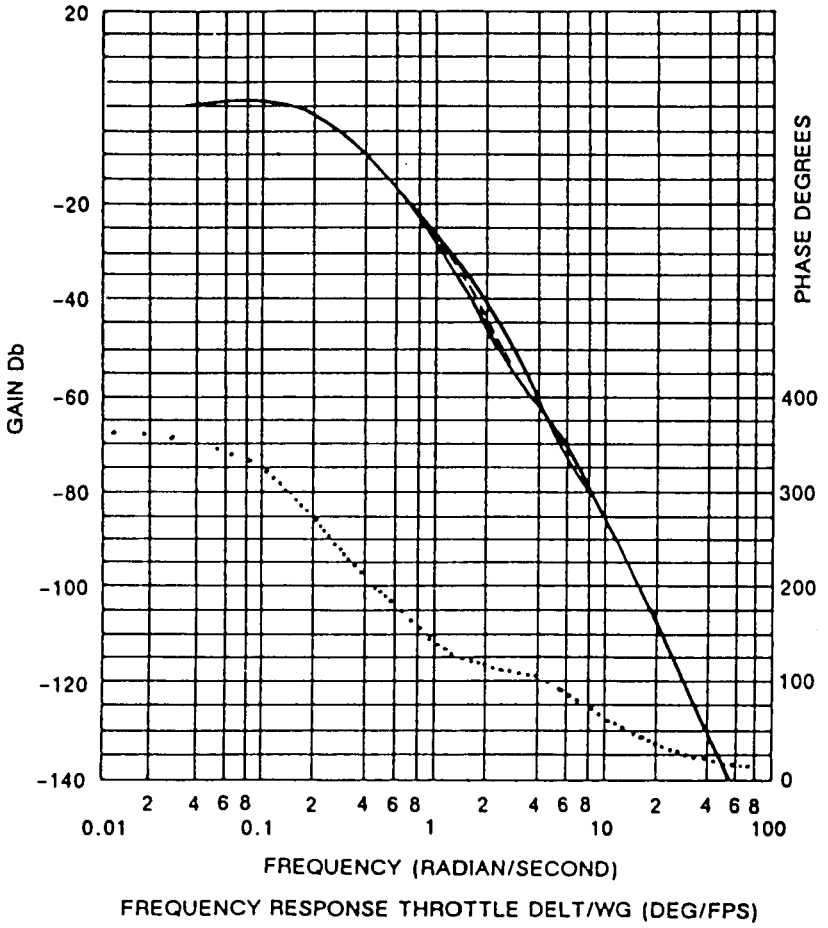

FREQUENCY RESPONSE THROTTLE DELT/WG (DEG/FPS)

Figure 20g. .Frequency Response of Inner Loops

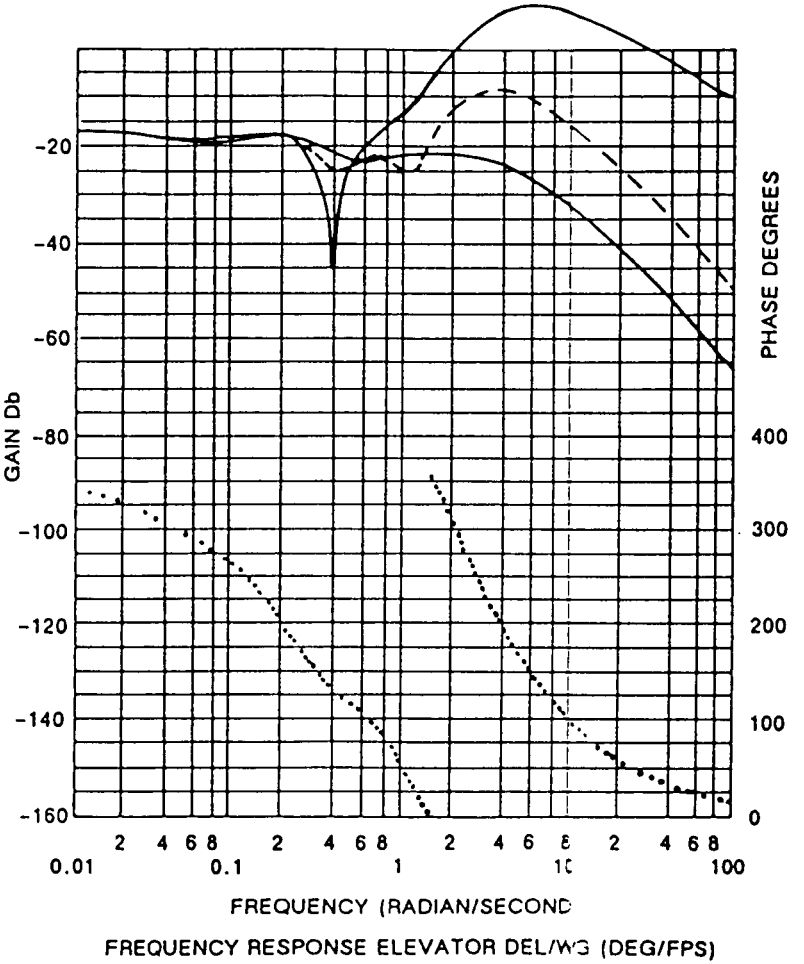

FREQUENCY RESPONSE ELEVATOR DEL/WG (DEG/FPS)

Figure 20h. Frequency Response of Inner Loops

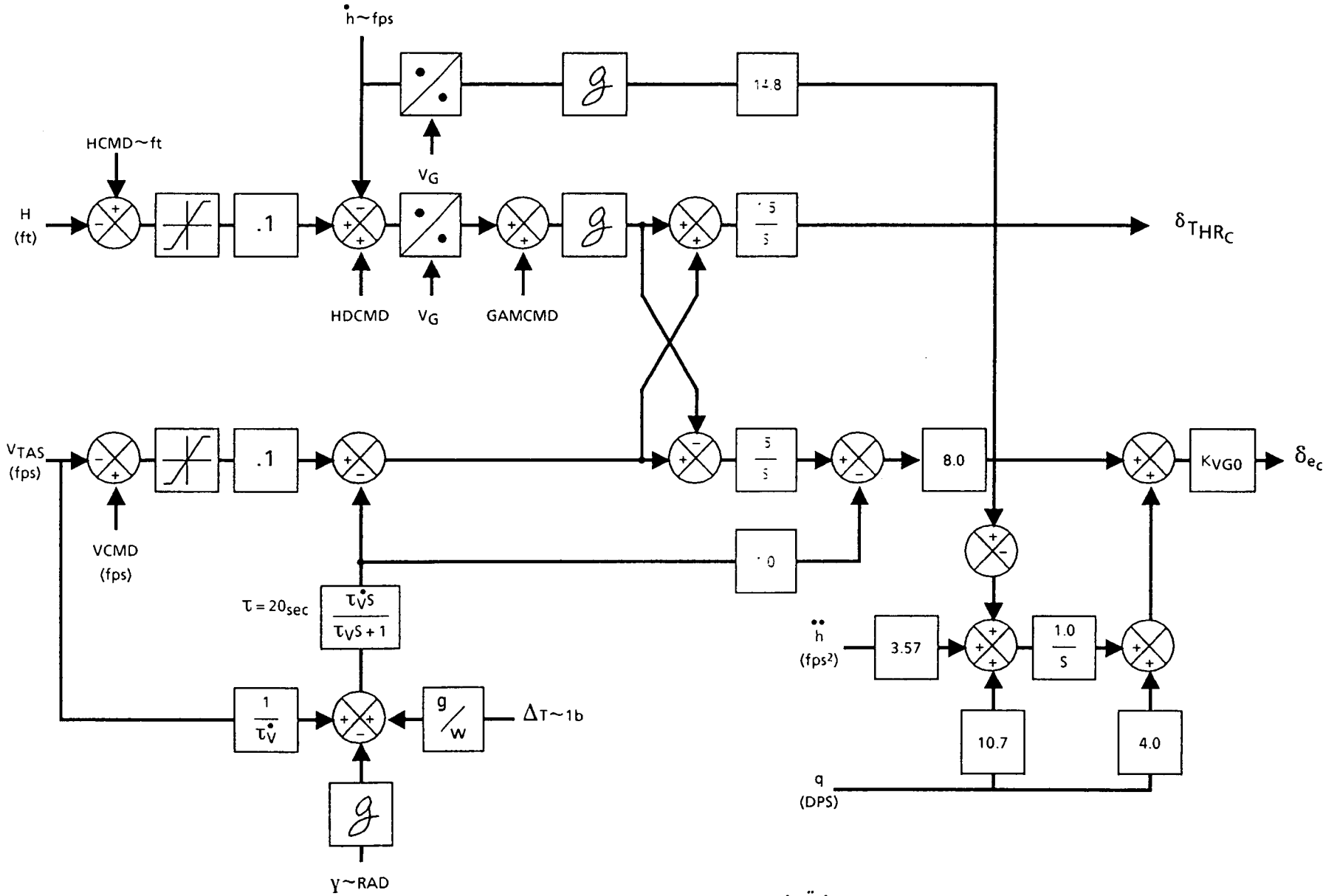

Figure 21. System with Complementary θ/θ̇, ḧ/θ̇ Inner Loop

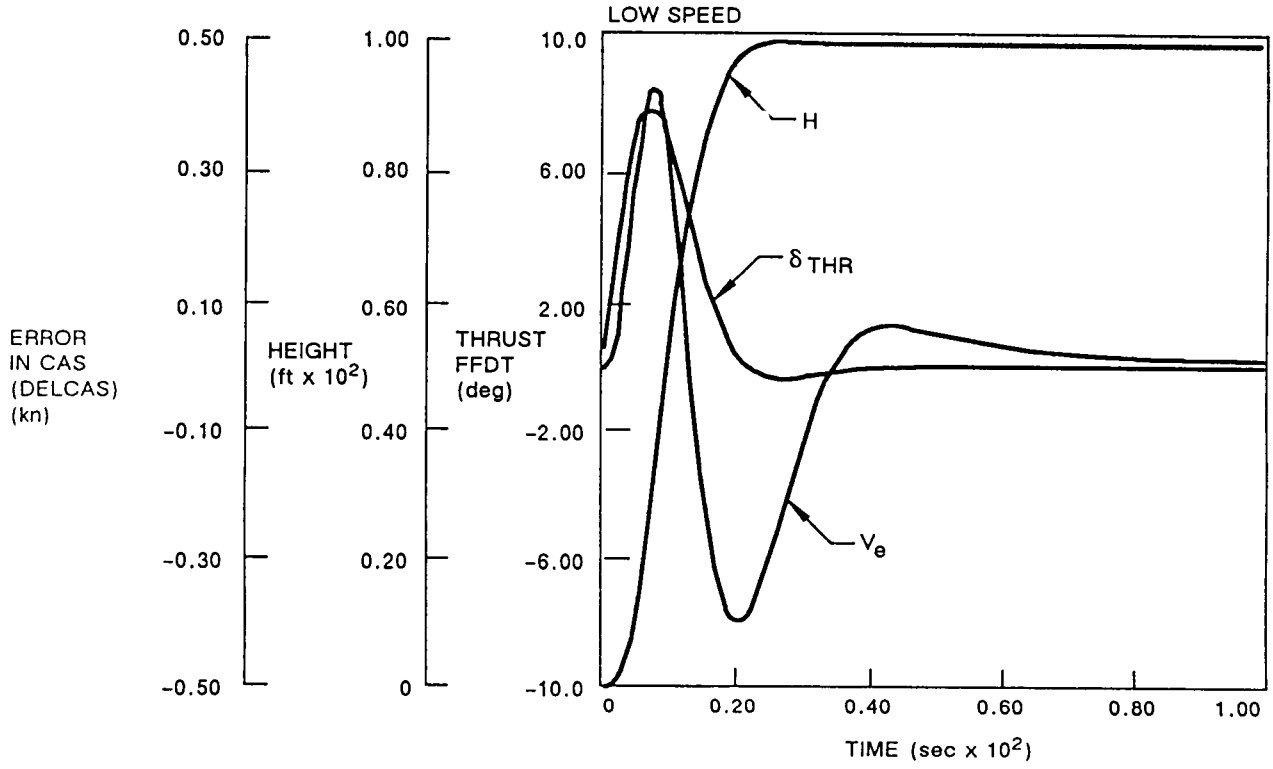

Figure 22. Time Response to 100-ft Altitude Command

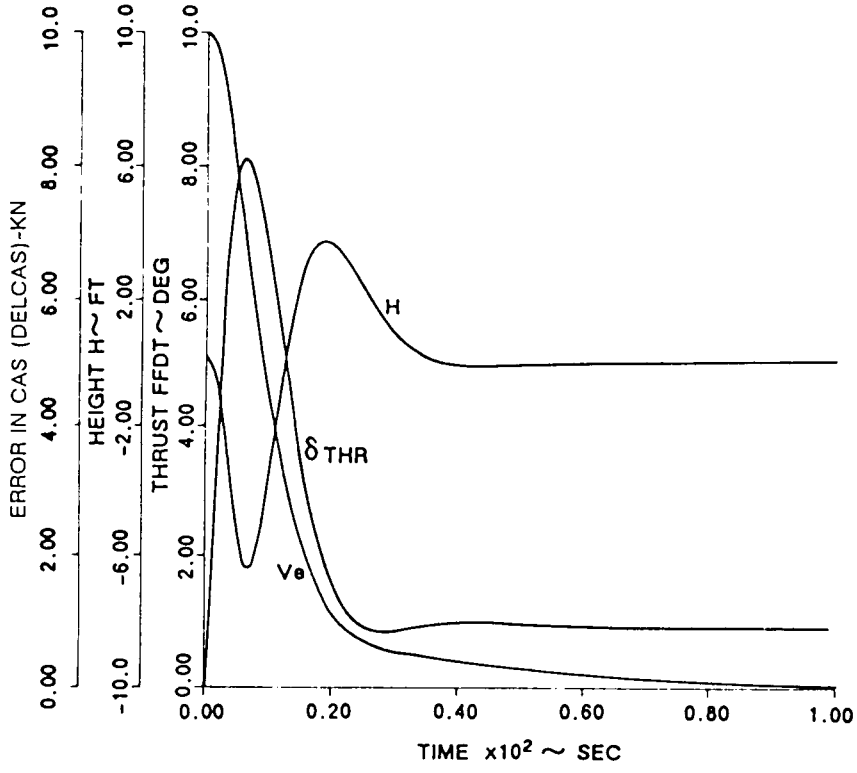

Figure 23. Time Response to 10-kn Speed Command

Table 3. RMS Turbulence Levels (for 1 fps rms Dryden Winds)

TRANSFER INPUT	FUNCTION OUTPUT	$\theta/\dot{\theta}$ (α AIR)	$\ddot{h}/\dot{\theta}$	COMPLEMENTARY FILTER $\ddot{h}/\theta/\dot{\theta}$	α AIR
U_g	V_e	.9663	1.013	.9999	.9663
U_g	H	1.493	1.063	1.0262	1.494
U_g	δ_{THR}	0.6344	.633	.6362	.6344
U_g	δ_{ELEV}	0.1965	.2143	.1787	.1965
W_g	V_e	0.5038	.7199	.6139	.5610
W_g	H	1.3974	.6587	.6394	.9031
W_g	δ_{THR}	0.5312	.5121	.5174	.5154
W_g	δ_{ELEV}	.0972	.8084	.1597	.7964

The total energy control system has a proportional flight path angle signal to the elevator, and is easily converted to an angle of attack inner loop. The practicality of this depends on the feasibility of accurately measuring the angle of attack. The conversion of the α inner loop can be accomplished by substituting $\theta = \gamma + \alpha$ for θ in the inner loop of the $\theta/\dot{\theta}$ system, $\theta = 57.3 \frac{\dot{h}}{V_G} + \alpha$ and for small angles. This system is shown in Figure-24.

The two formulations for angle of attack (i.e., inertial referenced $\alpha(\alpha_{IN})$ and air referenced $\alpha(\alpha_{AIR})$) were investigated for the analysis. In the linear analysis, the low frequency signal (α_{IN}) was not directly affected by longitudinal gust. In addition, the α_{AIR} was linearized in such a manner that it was dependent only on vertical gusts.

The stability characteristics (for both α_{IN} and α_{AIR}) are the same as that of original $\theta/\dot{\theta}$ system, except for the vertical turbulence results for the air system were different to the $\theta/\dot{\theta}$. The α_{IN} system results were identical with the $\theta/\dot{\theta}$ system. These results show that a α_{AIR} feedback system improves path tracking but at the expense of elevator activity. Elevator activity increased to 0.79° rms for the α_{AIR} system compared with 0.097° rms for the α_{IN} system.

Although the $\ddot{h}/\dot{\theta}$ inner loop offered the best overall performance (i.e., low throttle activity with minimum elevator activity) it was decided to proceed with the α inner loop. The primary criterion for this decision being the possibility of providing a simple, effective α limiting capability. This concept is reported in the Section 6.

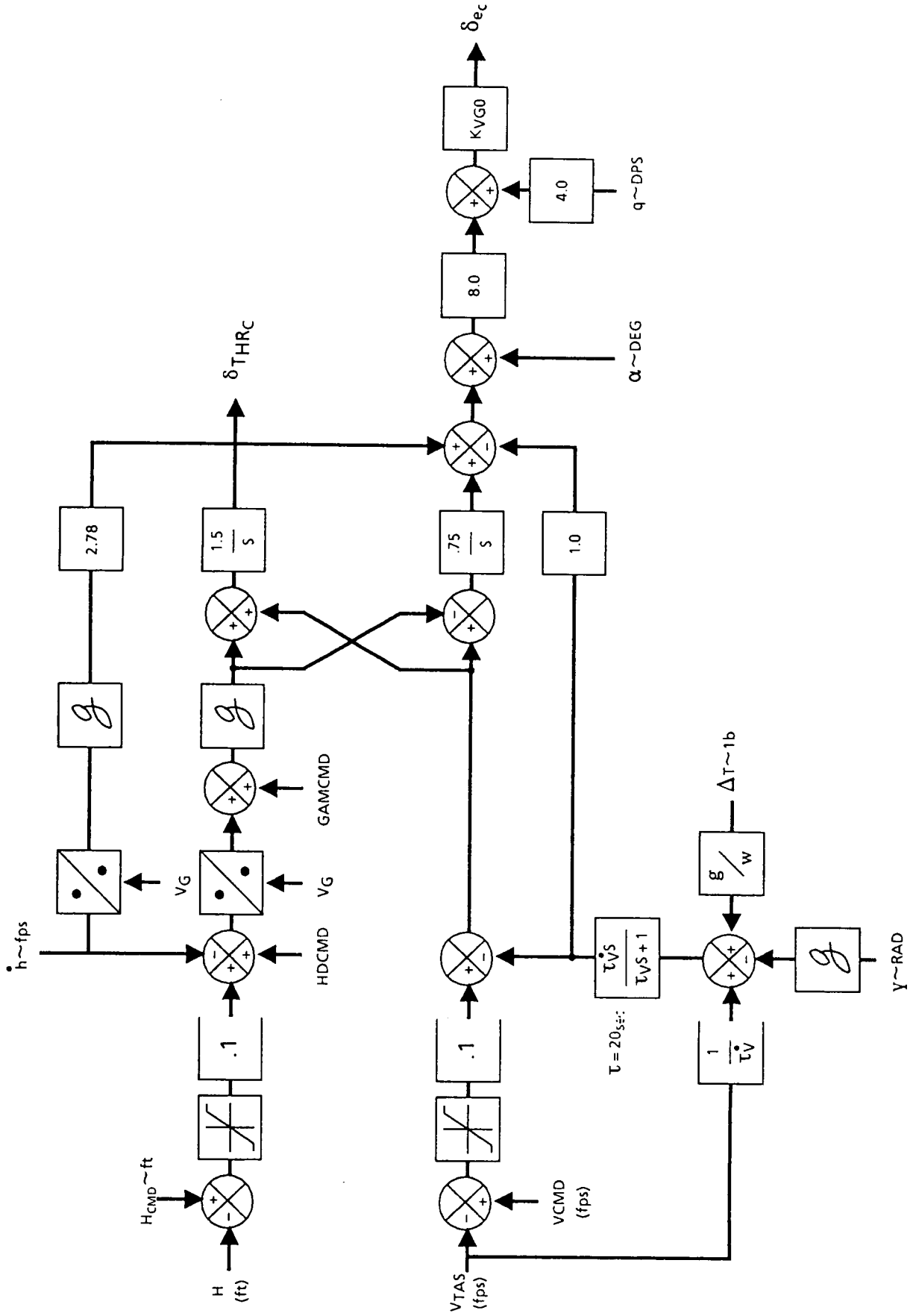

Figure 24. System with α Inner Loop

6.0 DESIGN CONFIGURATION IN NON LINEAR OPERATION

In a situation which demands a large decrease in velocity, the angle of attack can reach unacceptable values and must be limited to prevent stall. Similarly, in response to a command for a large increase in flight path angle, the throttle or EPR can limit. In order to cope with these situations, it was necessary to modify the linear design.

6.1 THROTTLE OR EPR LIMITING

The command cannot be satisfied when the throttle or EPR reaches its limit in response to a large flight path angle (γ) command. Because of the crossfeed A (fig. 25), the error in flight path angle is tied to the inner elevator loop causing a bias signal in speed control. Figure 26 shows the result of a 10° flight path command from the trimmed condition. In this case, the throttle limited and only achieved about 6°. The bias signal ($\gamma_{CMD} - \gamma$) was fed to the elevator inner loop and acted as a V_{cmd} signal causing an increasing error in airspeed.

The obvious solution to prevent the problem of bias in speed for throttle limiting was to cut crossfeed A. However, simply switching out the crossfeed caused undesirable transients. Therefore a high pass filter (washout filter) was added (fig. 27) to eliminate these transients. The action of the filter can be seen in a demand in flight path angle (fig. 28). Whenever the throttle limited, switch 1 closed and the crossfeed signal tended to zero. In situations when the throttle came off the limit, switch 1 opened and the system returned to linear operation without severe transients (fig. 29).

6.2 ANGLE OF ATTACK LIMITING

There was a requirement to restrict angle of attack to a suitable small angle to prevent stall. One solution was to limit the inner loop command. However, it was found that in response to a large step decrease in velocity, the maximum angle of attack limit was reached but the speed command was not satisfied. Consequently, a bias was supplied to the engine via crossfeed B (fig. 25) which prevented the control of flight path angle.

The simple solution used in paragraph 6.1 cannot be applied to the case of limiting. Simply switching out the crossfeed B resulted in a system where altitude is controlled with thrust. This system was unstable with the configuration shown in Figure 25 for realistic values of gain KH. Figure 30 shows the effect on airspeed of switching out crossfeed B and holding the system at an α limit of 4°.

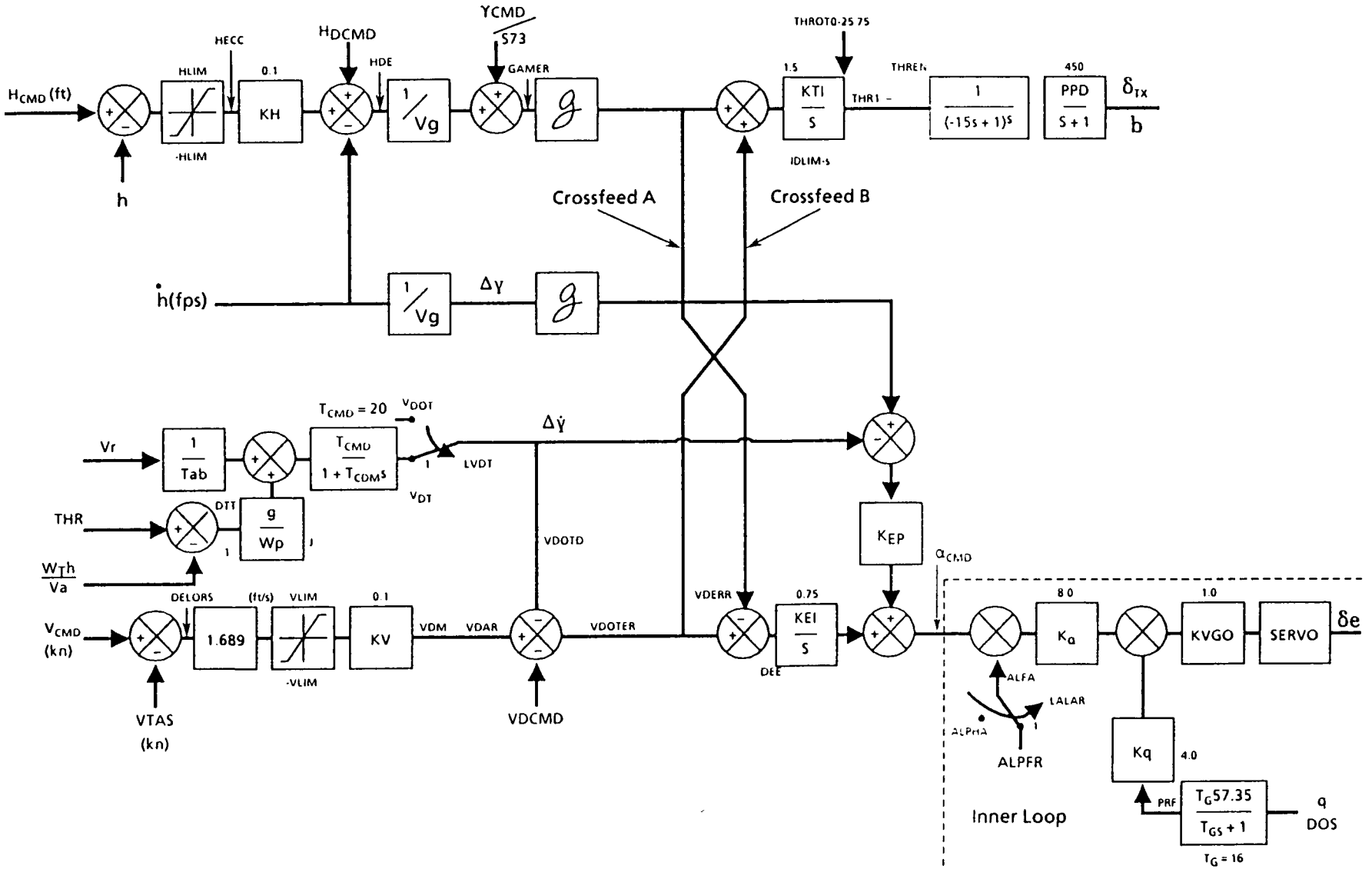

Figure 25. Tecs Linear Crossfeed Model

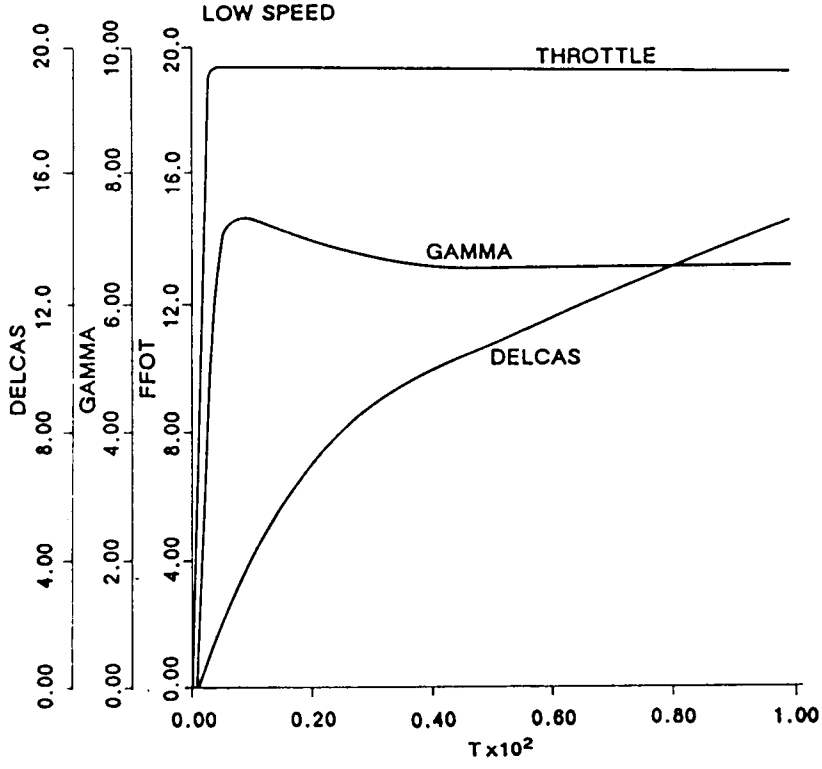

Figure 26. Throttle Limiting-Linear Crossfeed Model

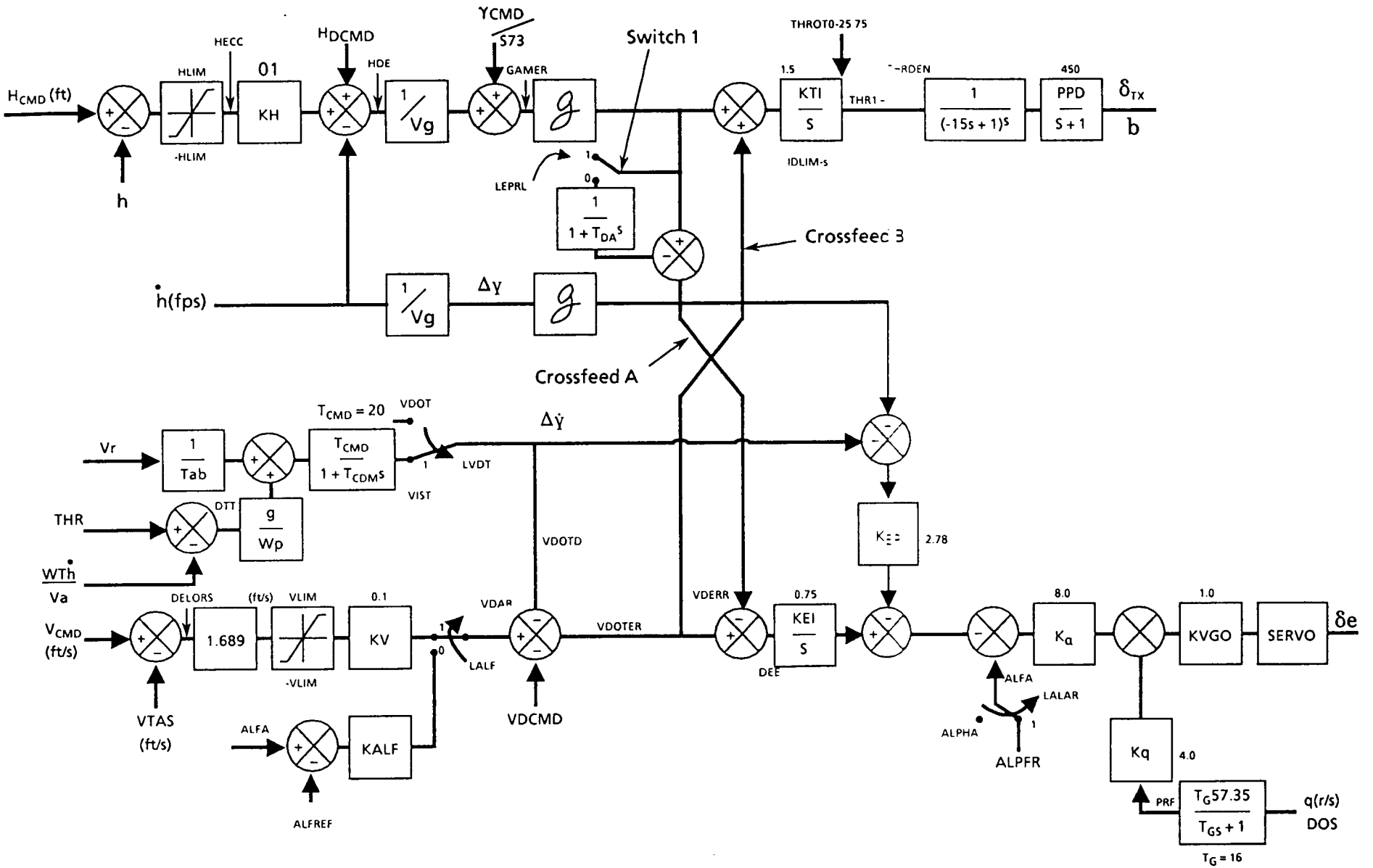

Figure 27. Addition of Washout Filter in Crossfeed A

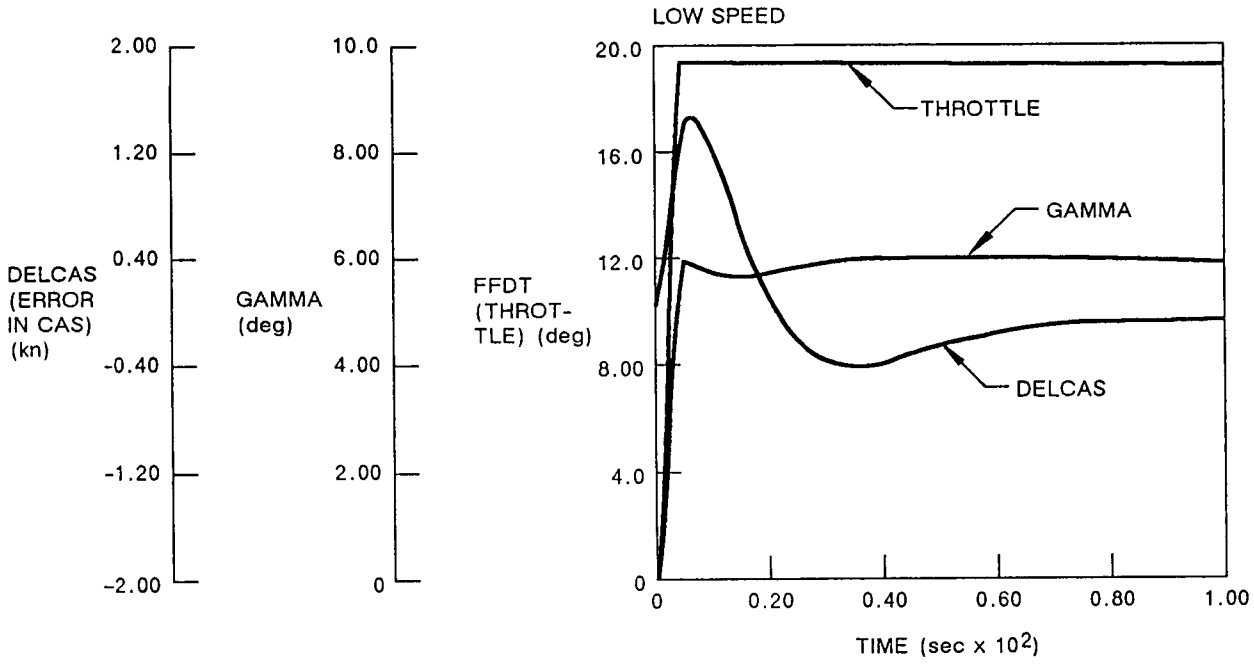

Figure 28. Effect of Washout Filter—Throttle Limiting Due to Y_{CMD}

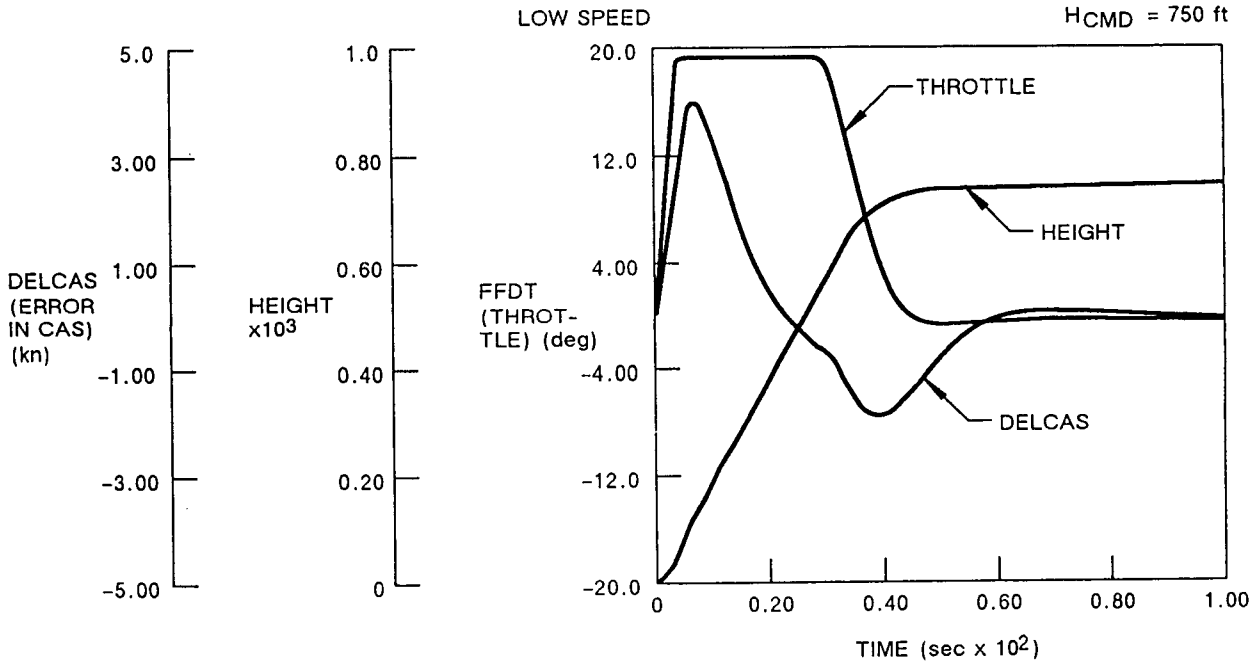

Figure 29. Throttle Limiting Due to H_{cmd}

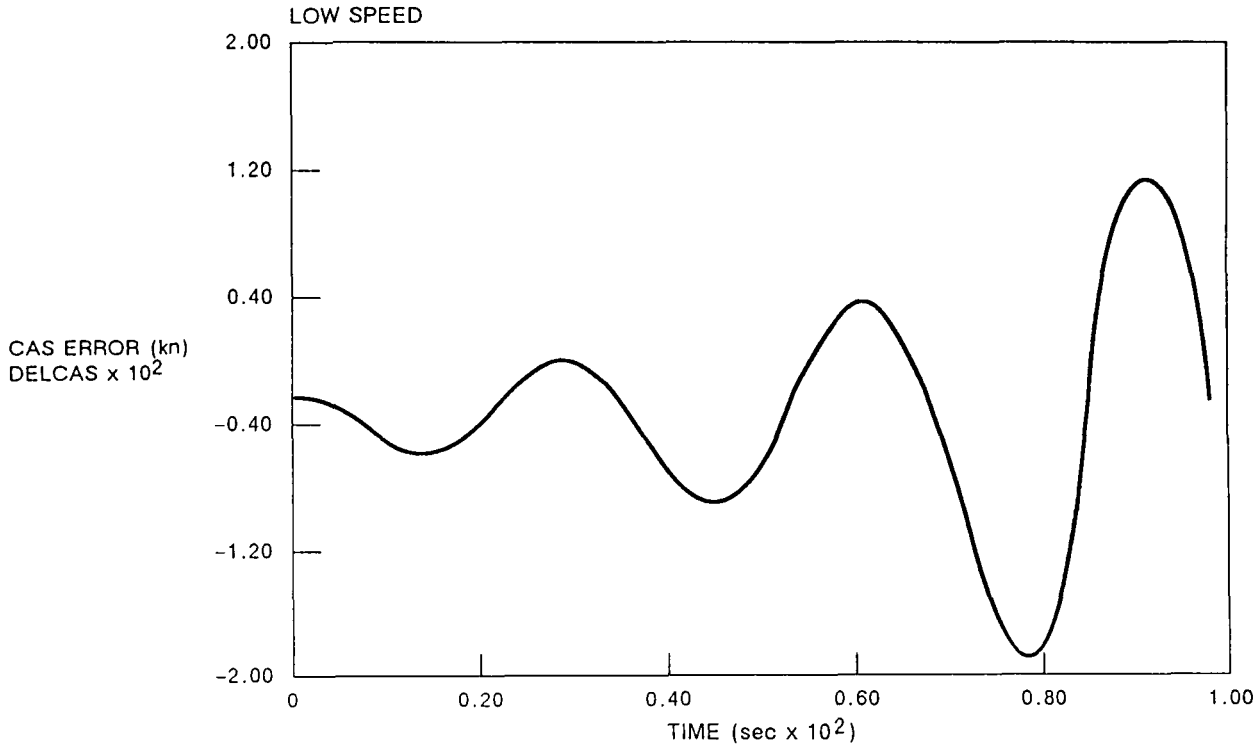

Figure 30. Instability Due to Alpha Limiting

The problem was solved by switching the outer control loop, when limiting occurs, from speed control to α control. Figure 31 shows the control configuration. When signal A was greater than B, the system switched in a transient free manner and the outer loop became an α control system.

$$\frac{K\alpha}{K_V} = \frac{dV}{d\alpha}$$

Where

$$\frac{dV}{d\alpha} = \frac{\text{Rate of change of V}}{\text{W.R.T.}\alpha}$$

This ensured that the velocity and α loops would produce an equivalent inner loop signal.

Figures 32 and 33 show the results achieved using the nonlinear system. For a 20-kn decrease in true airspeed from 120 kn (fig. 32), the system limits at 4° (fig. 33), and a steady state error of 4 kn remains in airspeed.

6.3 ENGINE CONTROL LOOP

A control system was developed to satisfy the thrust response requirements of the autothrottle functions. This system incorporated a proportional feedback control loop designed to improve the dynamic and steady state performance of the 737 engine. In addition, EPR and throttle limiting circuitry was added. A simplified block diagram of the control system is shown in Figure 34.

The JT8D-9 turbofan provided the basic engine for the simulation. The model was adapted from the 737-200 model available on the Harris Flight Simulator (Reference 1) and developed into an ACSL simulation.

The input to the engine model was throttle lever angle. The throttle was driven by a servomotor modelled by a lag having a time constant (τ_δ) of 0.15s and rate limit of 10°/s. In addition, hysteresis was added to simulate cable backlash in the linkage. The magnitude of the hysteresis was obtained from Reference 2.

The proportional feedback control loop was designed using a linear engine model consisting of a gain and a simple lag τe = 1s. Figure 35 shows that the control loop consisted of a second order system comprising of engine model and throttle servo. Assuming that the steady state gain should be unity and a damping ratio (ζ) of 1, then values were calculated for KEPRP (112.5) and KFB (.55).

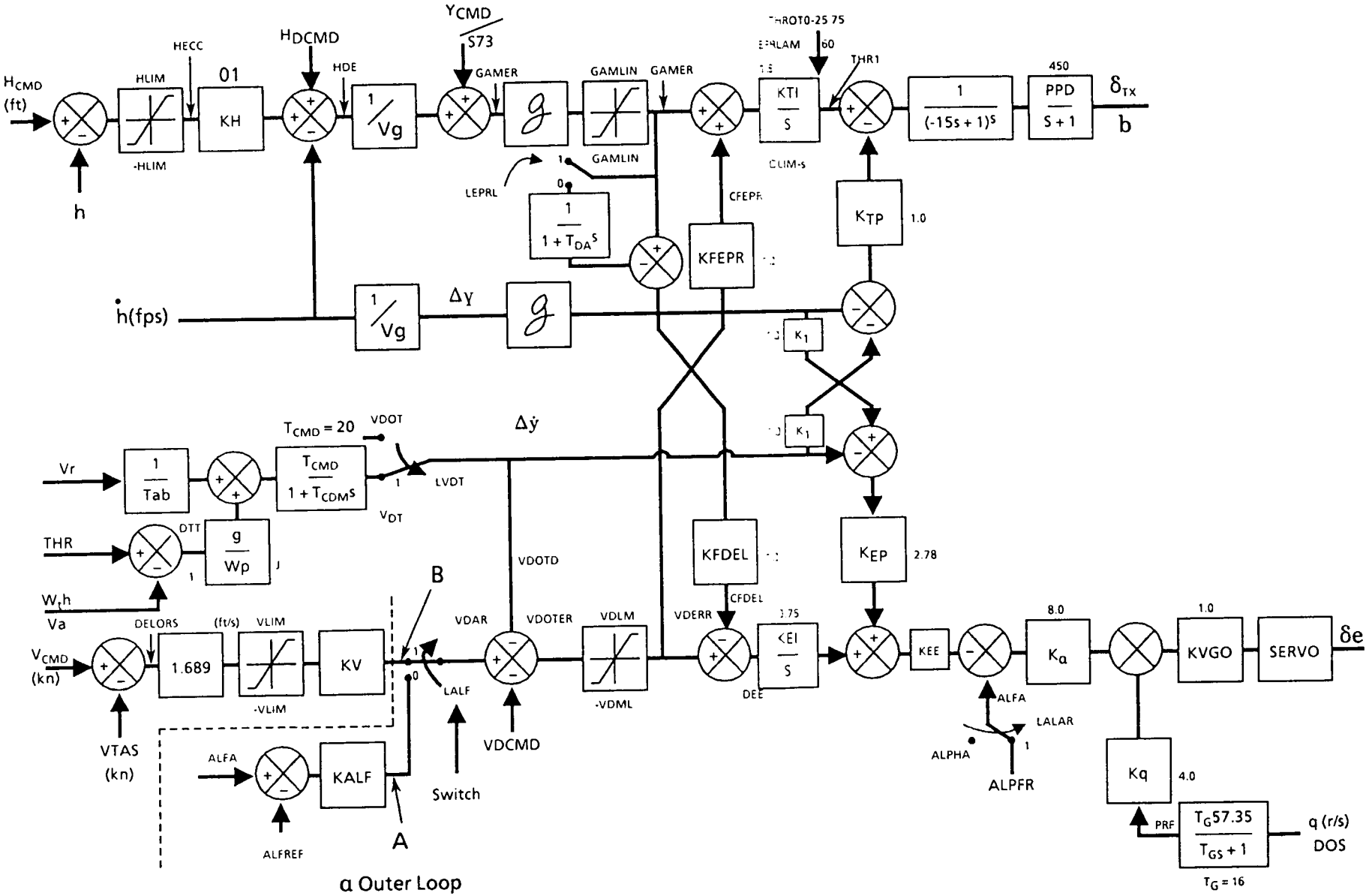

Figure 31. System Configuration Including α Outer Loop

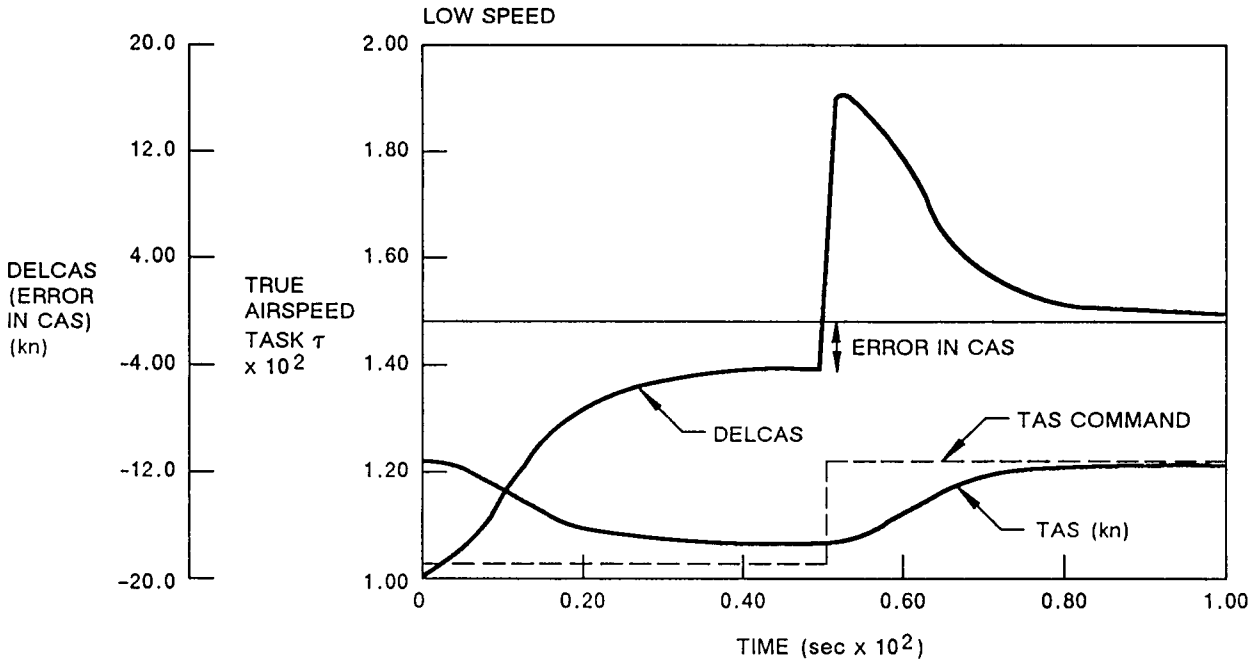

Figure 32. Effect on Airspeed—α Limiting

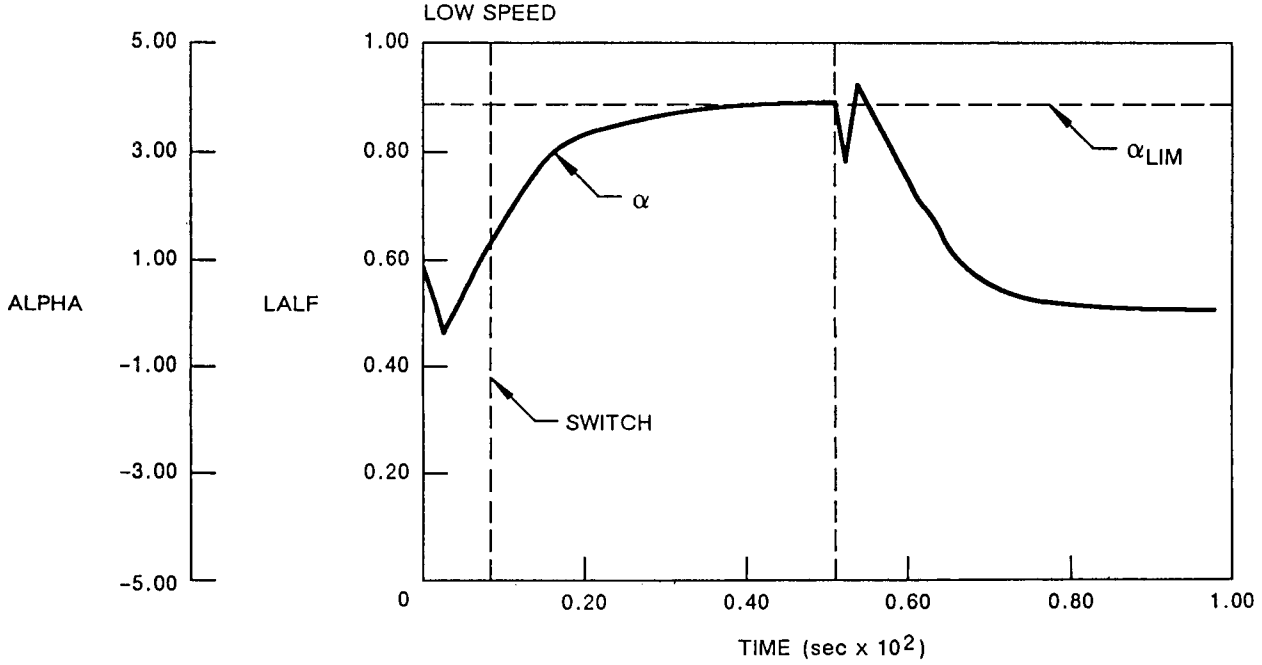

Figure 33. Plot of α Against Time

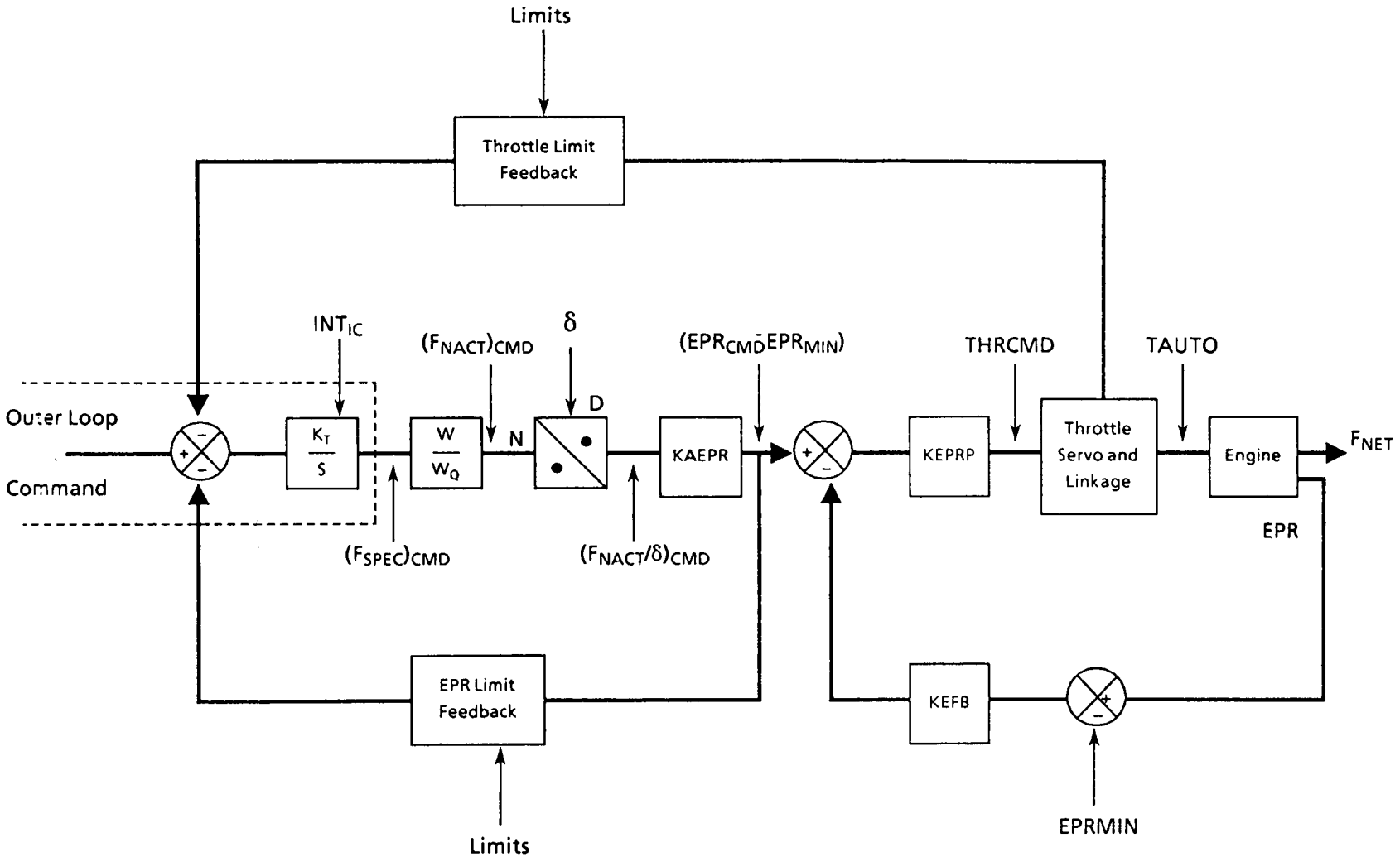

Figure 34. Engine Control System

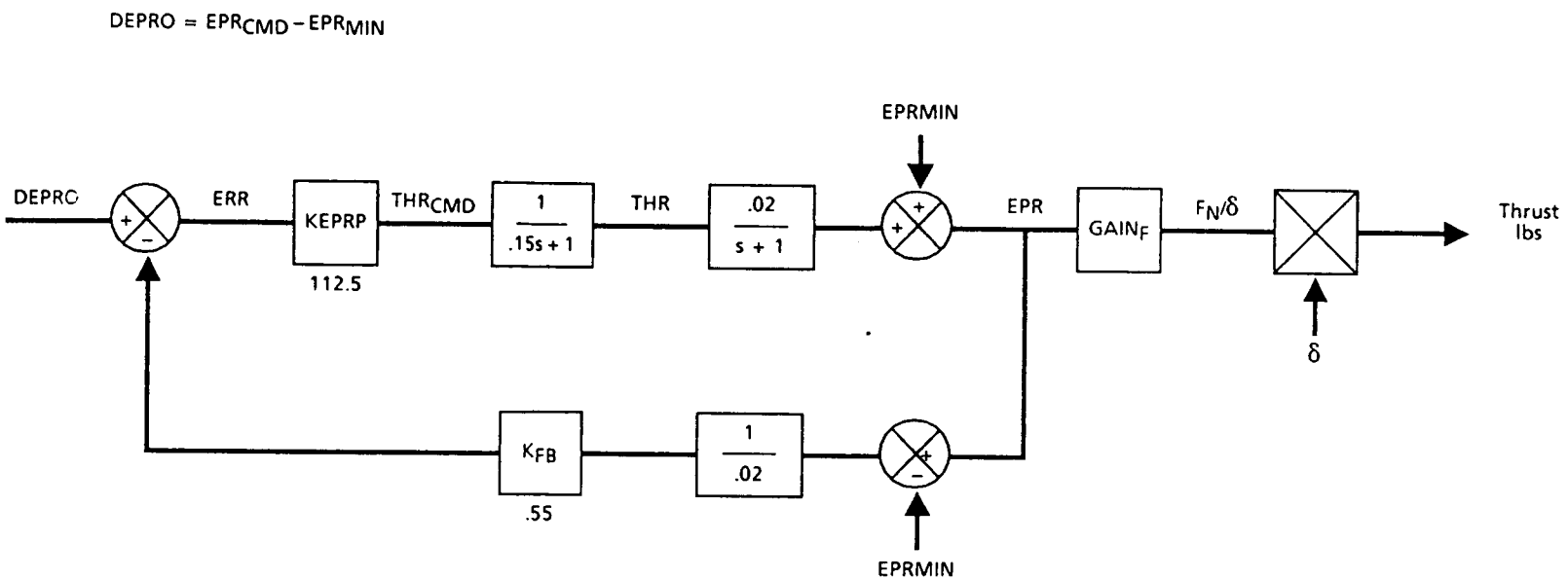

Figure 35. EPR Demand Engine Loop (Linear Design)

The simulation results obtained using these gain values are shown in Figure 36 for the initial conditions of:

Alt = 20000 ft

Mach = 0.69

EPR_{IC} = 1.55

The commanded change in EPR is 0.5. Owing to backlash (of 2.17), the actual EPR started below the commanded level. It can be seen that the rate limit within the throttle of 10°/s greatly modified the input command to the engine (TAUTO) when compared with throttle command (THR CMD). The purpose of the engine control loop is to provide the required thrust in response to the outer loop command signal. However, it is not possible to feedback thrust measurements and EPR feedback (normally employed with Pratt and Whitney engines). A linear relationship between EPR and thrust exists provided atmospheric conditions remain constant. Nevertheless, variation in altitude will change this relationship. In this system an attempt has been made to correct this change by modifying the outer loop command via δ (ratio of P/Po). Furthermore, during flight the aircraft weight will decrease due to fuel consumption modifying the required thrust command. Figure 34 shows a time varying gain (W/Wo) has been introduced to compensate the EPR command for weight variation.

Two important features of the overall engine control systems are the throttle limit and EPR limit feedbacks (fig. 37). If either the EPR command or throttle command exceed the 737 engine limits, then a scaled signal is fed back to reduce the integrator input and prevent further saturation of the integrator. The action of the limits is demonstrated in Figure 38 for a step change in engine outerloop command (not shown in Figure 38). The output of the integrator (ICTI) ramps up until the throttle limit is reached (65°), at which point a signal (DELTA) is fed back to reduce the integrator input. It can be seen that the throttle command (THCM) and throttle output (TAUTO) are held at the 65° limit.

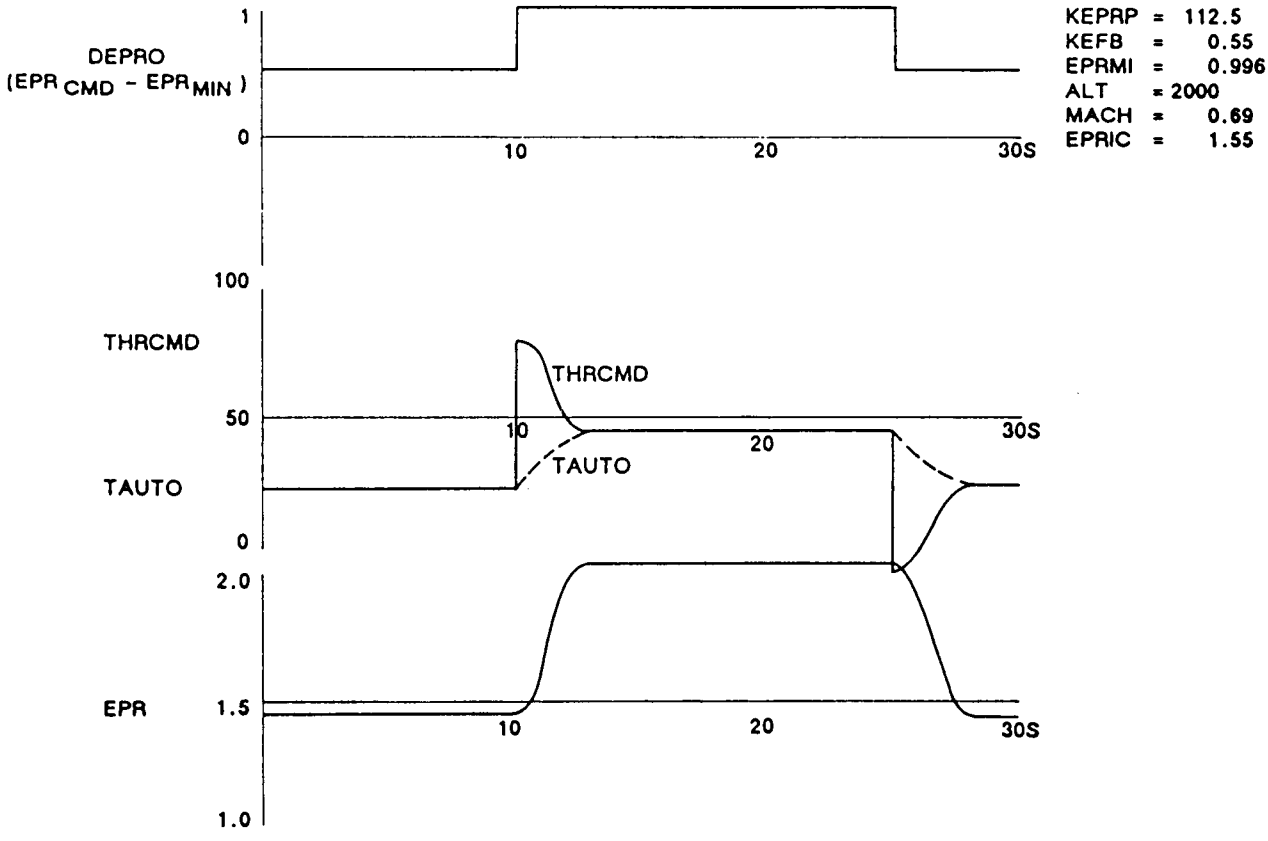

Figure 36. ACSL Engine Simulation Results

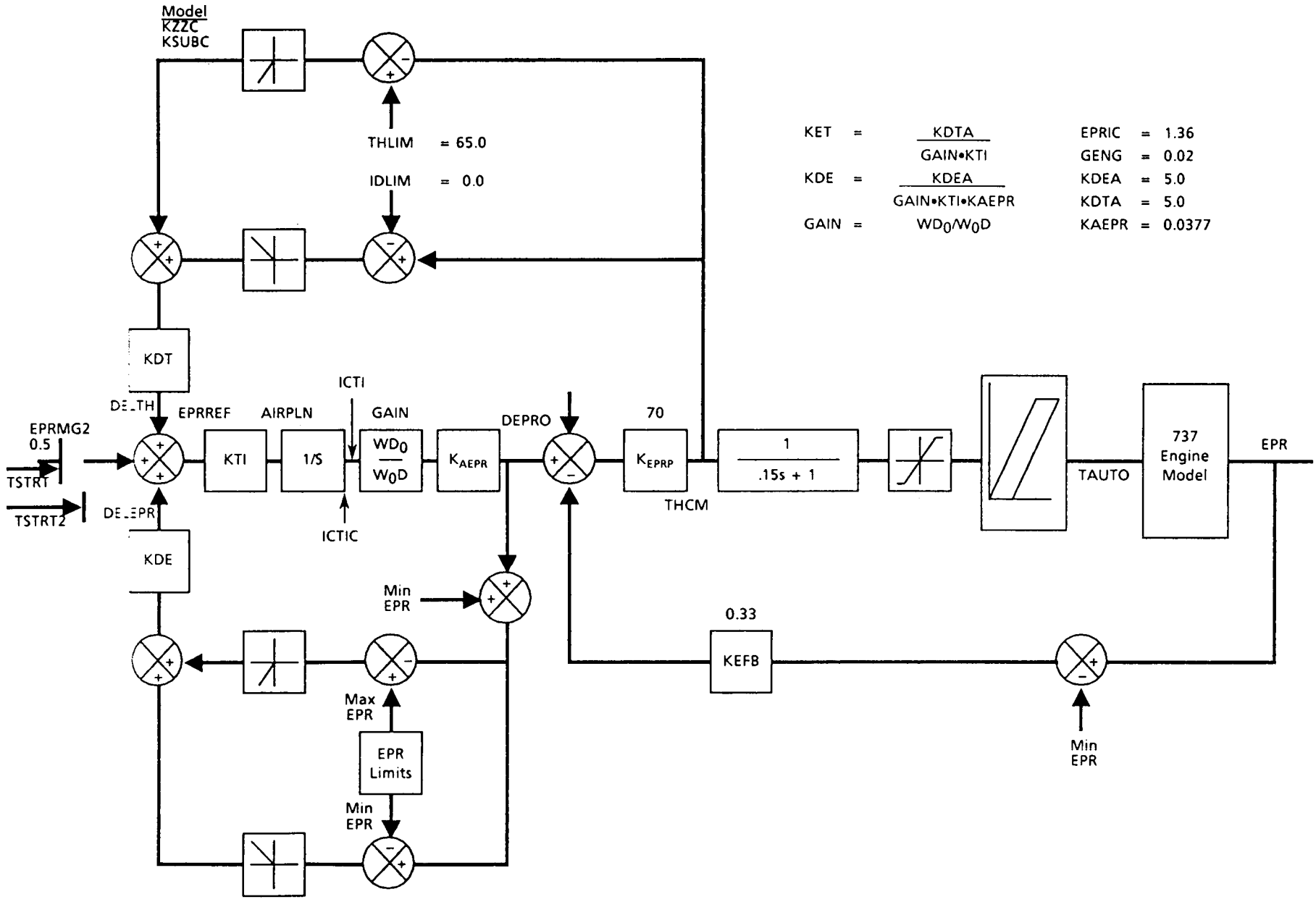

Figure 37. Detailed Engine Loop (ASCL Simulation)

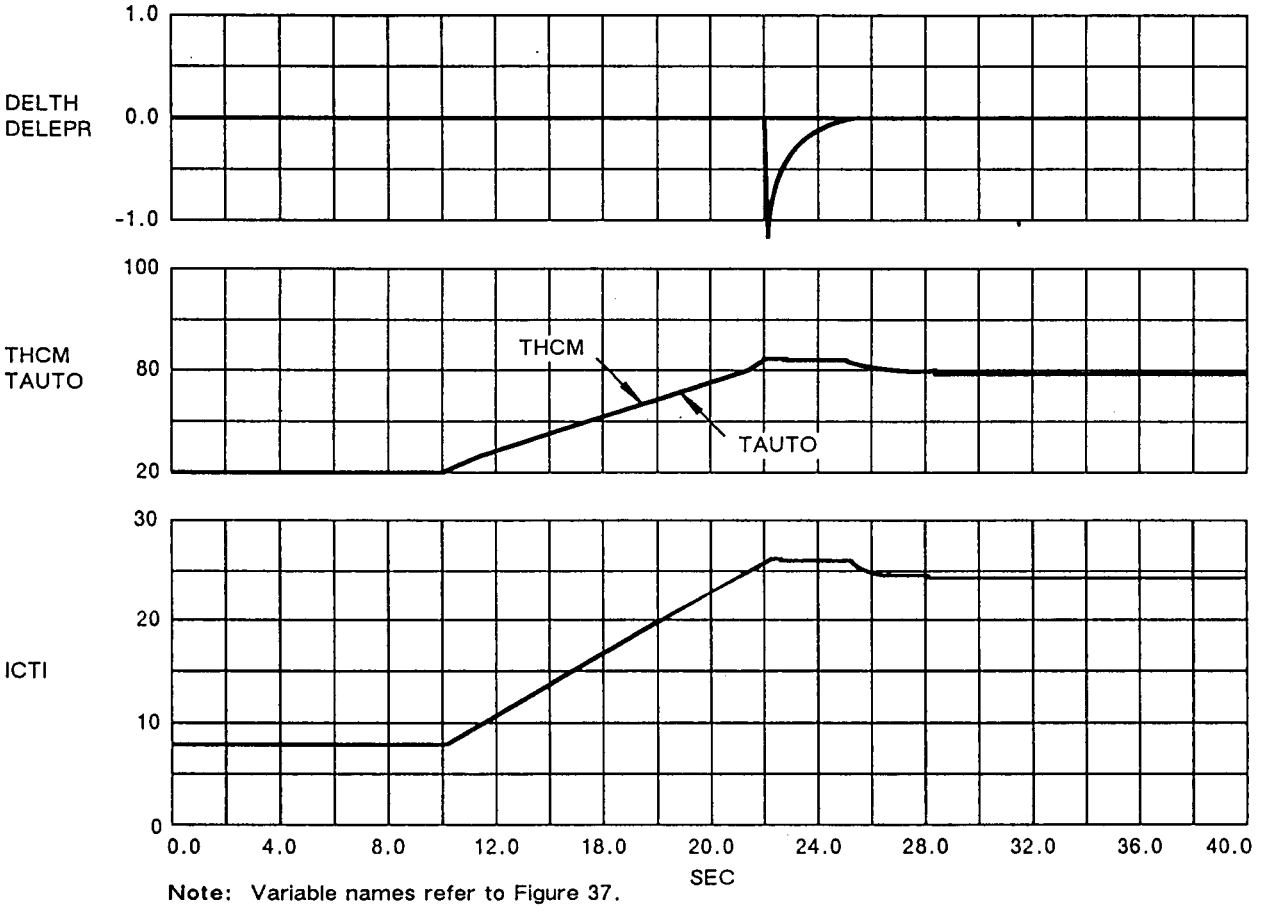

Note: Variable names refer to Figure 37.

Figure 38. Engine Response in Limiting Condition

7.0 ADDITIONAL CONTROL MODES

The integrated autopilot/autothrottle design, discussed in previous sections, was configured to control height (h), true airspeed (V_{TAS}) and flight path angle (FPA, γ). However, the basic design philosophy was such that the inner loops are driven by FPA error (γ_ε) and longitudinal acceleration ($\dot{V}$). It is therefore relatively simple to incorporate additional control modes by designing these modes to generate the appropriate γ_ε and $\dot{V}$ signals.

7.1 GROUND SPEED MODE

Control of ground speed was the simplest additional mode to implement. Implementation consisted of providing a ground speed command, and feedback of ground speed V_G and ground speed rate $\dot{V}_G$ in place of the true air speed signals (fig. 39).

7.2 MACH AND CAS SPEED MODES

The Mach and CAS speed control modes are required to facilitate profile descent procedures. One preferred procedure is to descend at constant Mach to some preselected altitude at which point switch to descend at constant CAS. Conversely, during ascent one procedure is to fly at constant CAS then switch to constant Mach.

The means of implementing the Mach/CAS control loop (fig. 40) is documented in Reference 3. This implementation consists of converting the MACH or CAS signal to a TAS signal which drives the velocity control loop.

In the case of the Mach control law, the Mach command signal is converted to V_{TCMD} by computing the current speed of sound and using this as the conversion factor. In the case of CAS, the V_{CAS} error signal is formed prior to converting to V_{TAS}. This technique allows an approximate conversion factor (derived from speed conversion tables) to be used (i.e., $V_{CAS} = V_1 (1 - .12 \times 10^{-4} h)$.

It can be seen that as $V_{T\varepsilon}$ is controlled to zero $V_{CAS\varepsilon}$ must go to zero, and that an exact measurement of height is not critical to accurately controlling V_{CAS}. During the first portion of descent, the control system is designed to hold the airplane at constant Mach. When CAS equals a preselected CAS, then the system automatically switches to CAS hold and continues the descent by maintaining constant LAS. On ascent the reverse is true.

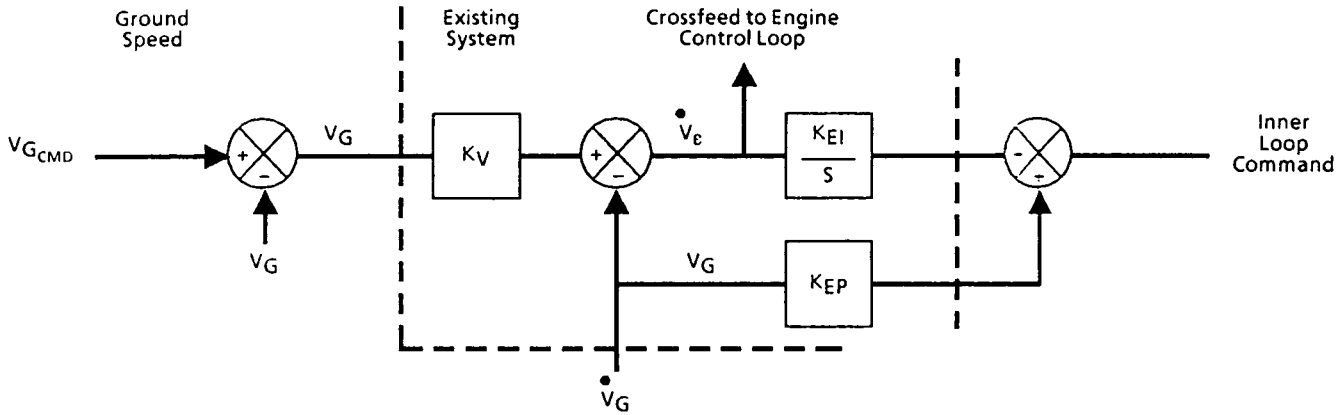

Figure 39. Implementation of Ground Speed Mode

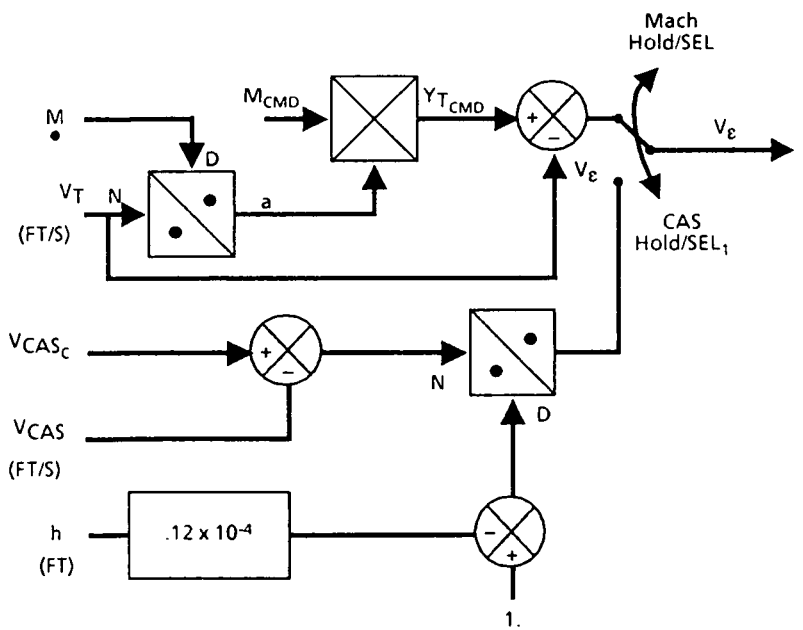

Figure 40. Implementation of Mach/CAS Hold

7.3 GLIDE SLOPE AND VERTICAL PATH MODES

An additional control loop has been added to the basic configuration to allow a transient free captive exponential of the glide slope during landing approach. Figure 41 shows the geometry of the engagement. The airplane is approaching from beneath the glide slope at a current height error h_e(ft) off the glide slope. An exponential capture law dictates that the airplane follow a trajectory defined by

$$\dot{h}_{derived} = K_h h_e$$

where

$\dot{h}_{derived}$ = $\dot{h}$ with respect to glide slope

This law was accomplished by forming an $\dot{h}_{derived}$ signal by complementing the low frequency component of h_e rate with the high frequency component of $\dot{h}_I$ using the appropriate filtering (fig. 42). For an h_e that is positive and decreasing (i.e., the airplane is approaching beneath the glide slope), the error rate $\dot{h}_{derived}$ measured with respect to the glide slope is positive (fig. 42). The effect of this signal is that the output of glide slope mode (γ_c) is 'biased' such that it changes sign and commands a negative flight path angle prior to the glide slope. Obviously the distance h_e at which V change sign is a function of $\dot{h}$ derived and forward gain (for constant airspeed) as given by the previous equation:

$$\dot{h} = \frac{\text{derived}}{K}$$

$$D \times \frac{h_{derived}}{K_h}$$

Therefore engagement of glide slope mode will occur earlier for high $\dot{h}$ derived or low K_h.

Vertical path mode has been designed to function in a similar manner to glide slope (fig. 43), however, the control input is generated by the flight control computer in the form of a desired height profile. Additional software has been added so that several vertical paths can be flown consecutively with transient free switching being achieved between each leg.

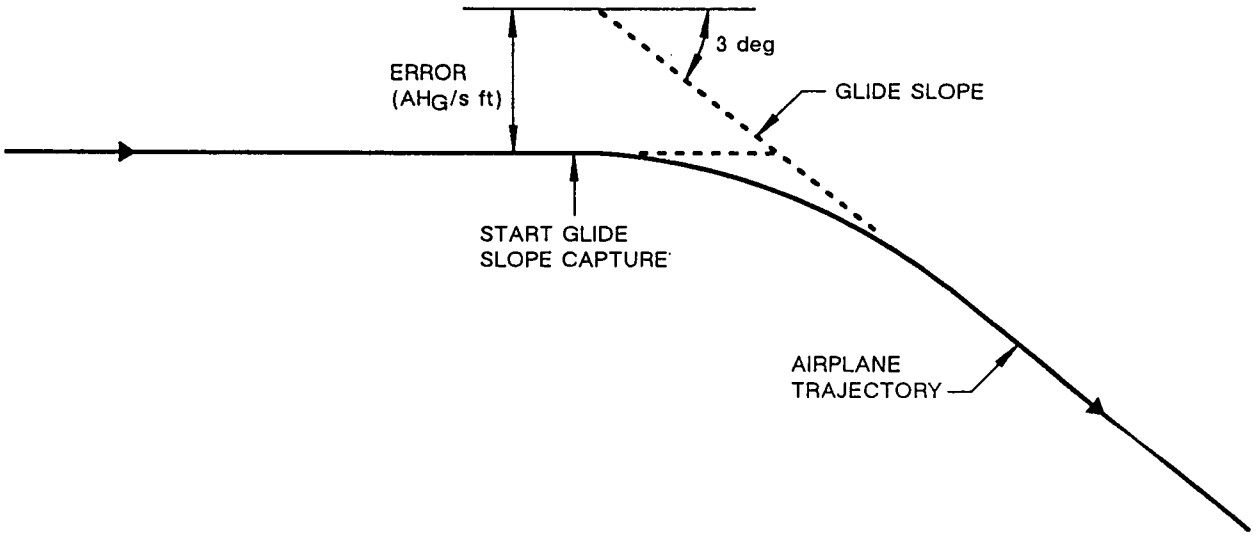

Figure 41. Geometry of Glide Slope Engagement

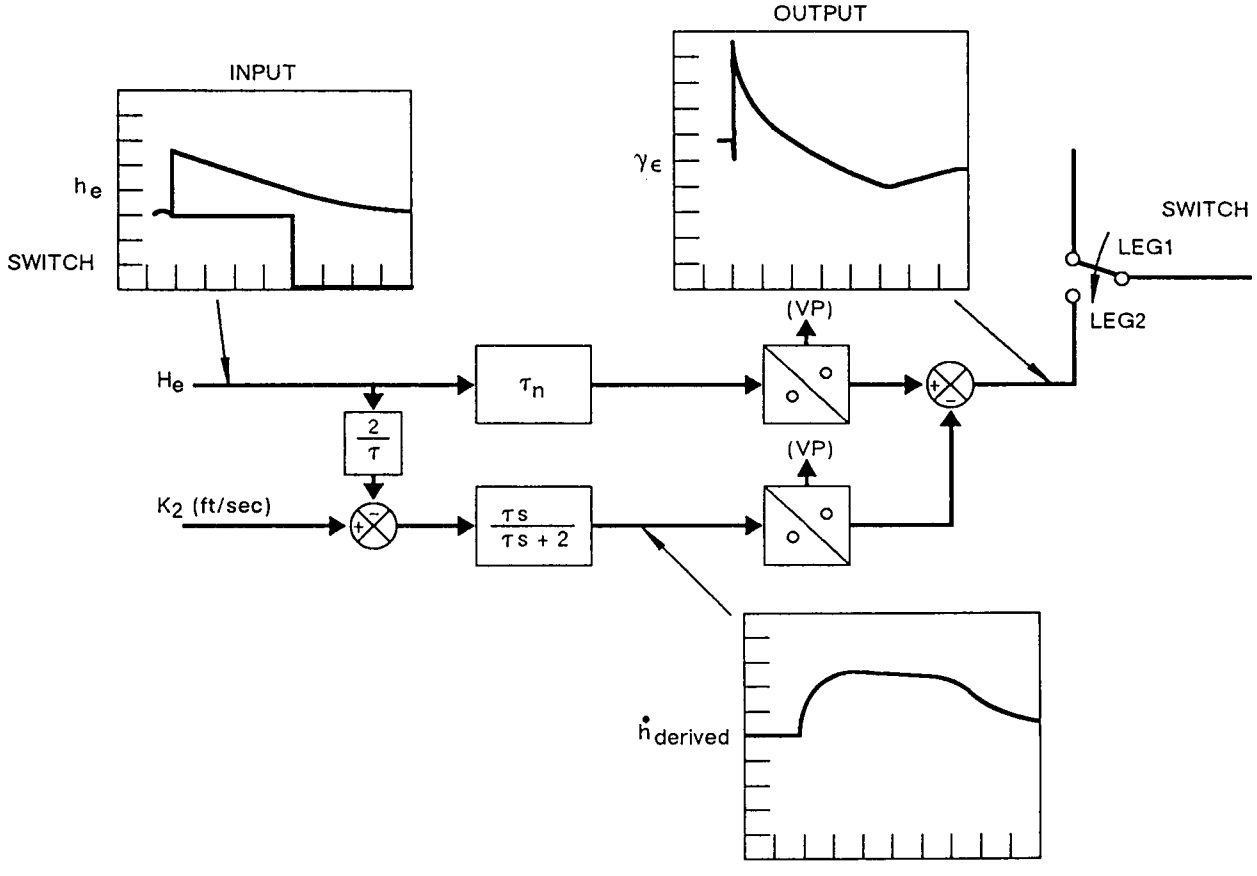

Figure 42. Transient Free Switching—Glide Slope Mode

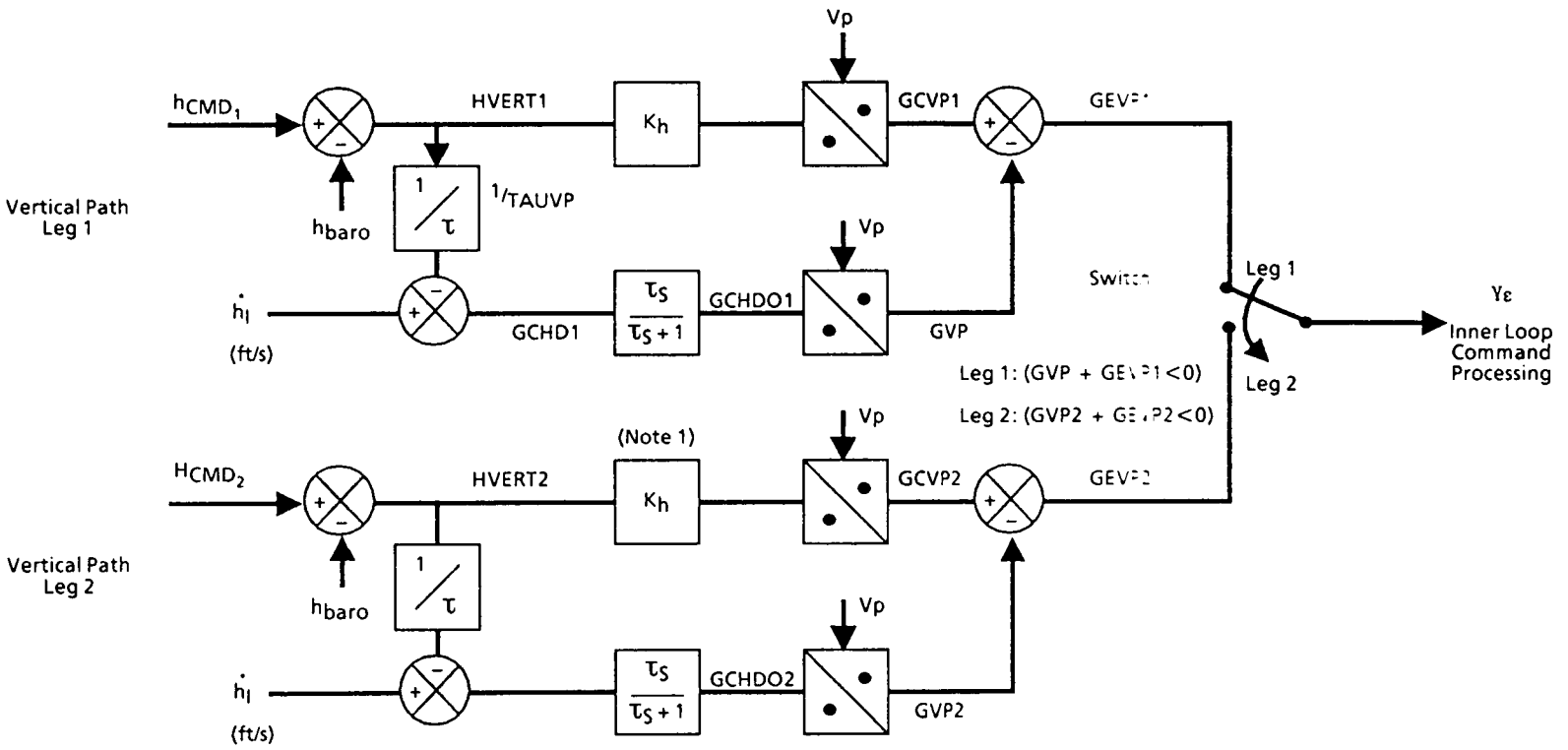

Figure 43. Vertical Path Mode

8.0 MODE CONTROL PANEL

In addition to developing the integrated autopilot/autothrottle algorithm, consideration has been given to the hardware necessary for a pilot to select the various autopilot modes and the software necessary to control the arming, engagement and switching between the various modes of operation. Figure 44 shows the mode control panel designed for the system.

Figure 44 shows that the panel is split into four sections: longitudinal modes, lateral modes, speed modes and system status. At present the lateral modes (i.e., longitudinal V-CWS) and PROFL (speed profile) modes have not been designed. However, both are intended to be included at a future date. Pushing the appropriate mode control button changes or arms the modes. A longitudinal mode must be selected in addition to a speed mode. Engagement of a mode causes the corresponding mode button to light up green, whereas arming a mode causes automatic engagement to occur once certain criteria have been satisfied. In this case the mode control button lights up amber when armed and turns green when engagement occurs. The operation of the individual control modes is discussed in the following paragraphs.

8.1 LONGITUDINAL MODES

8.1.1 Flight Path Angle

The flight path angle control mode is engaged without prior arming. (Engagement causes tracking of commanded FPA.) When disengaged, the FPA display shows actual FPA. However, when engaged the actual FPA is taken to be the command and the display. Once engaged, the command can be adjusted using the adjust knob.

8.1.2 Velocity Control Wheel Steering (CWS)

Velocity CWS is a computer augmented manual control mode in which the rate of change of commanded FPA is proportional to control column deflection. The mode is engaged directly and is compatible with any of the speed modes.

8.1.3 Glide Slope (GS) and Vertical Path (V-Path)

GS mode is armed by pushing the GS mode button with engagement occurring automatically as described in paragraph 7.3. The mode will not arm without detection of a valid GS signal. V-PATH mode operates in a similar manner to GS. However, in this case, the mode will not arm unless a vertical path is stored in the flight control computer.

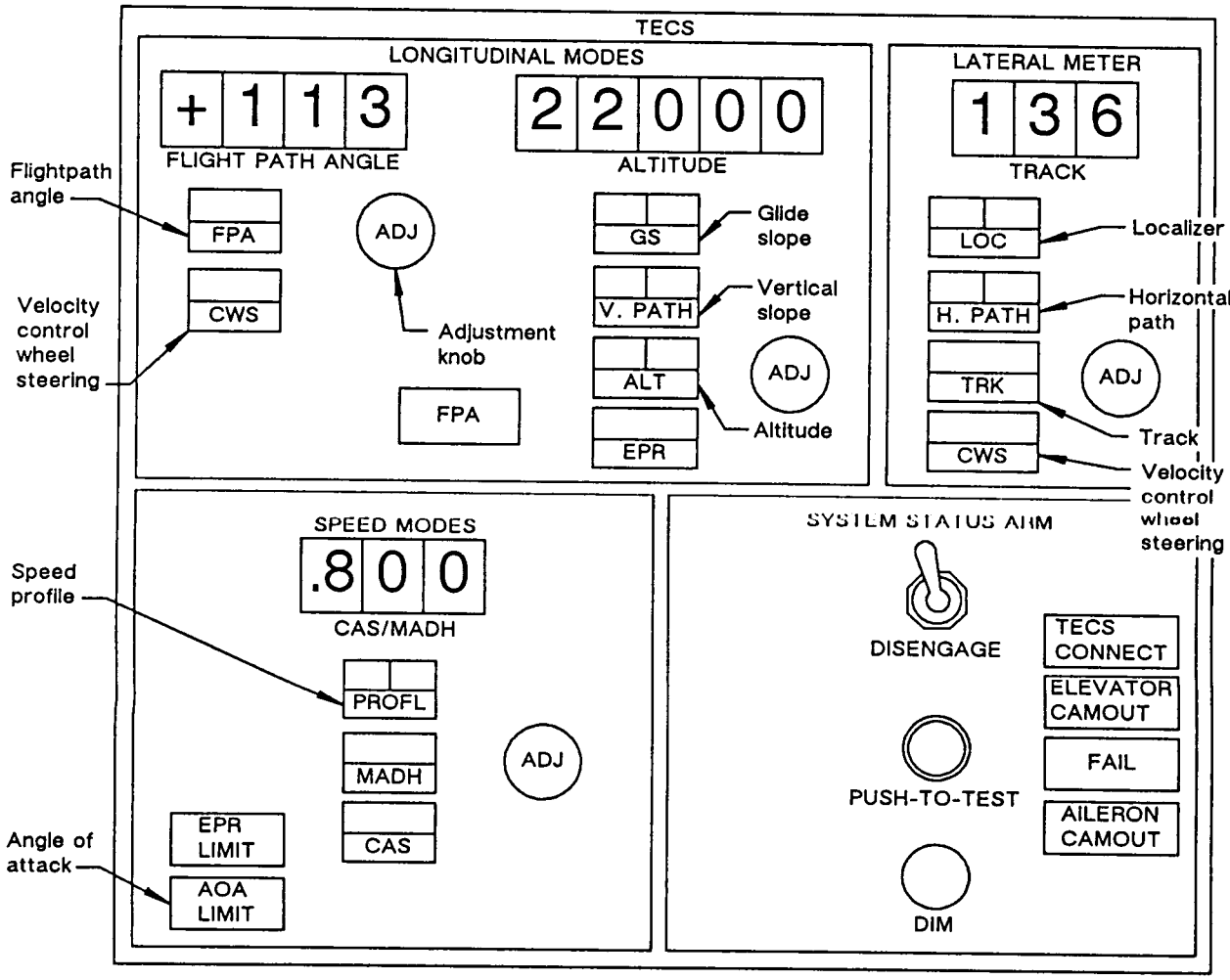

Figure 44. Diagram of Mode Control Panel

7-U80109-35

8.1.4 Altitude

The altitude hold mode can either be engaged directly or armed by preselecting a desired altitude. When the mode is not engaged or armed the display shows the current altitude in feet. Engagement causes the actual altitude to be fixed on the display and to be taken as the command signal. The display can be altered using the altitude adjust knob.

The adjust knob can also be used to establish the altitude preselect mode by dialing the adjust knob when the mode is disengaged. This causes the existing altitude at the time of knob rotation to be stored in memory. The altitude increments are added to the stored altitude to hold the new preselected altitude. The mode is then armed and will automatically engage when the capture criterion is satisfied.

8.1.5 EPR

The EPR mode causes the system to command maximum safe thrust setting while holding speed. This mode can be engaged directly. Selection of another flight path mode while the EPR mode is engaged causes the EPR mode to disengage and the selected FP mode to engage. An additional pushing of the EPR button following engagement, will cause the EPR mode to disengage and the FP mode to engage.

8.2 SPEED MODES

The speed control options on the mode control panel (fig. 44) are: CAS, MACH and PROFL. A speed mode will always operate in conjunction with a longitudinal mode with the default mode being CAS. Switchover between CAS and MACH is designed to occur automatically at certain flight conditions, but may be overridden by pushing the desired mode switch.

The display shows either the commanded CAS or MACH number (depending on mode selected) which is equal to the actual speed at the time of engagement.

The command can be changed by rotating the adjustment knobs. Changing between CAS and MACH causes the equivalent speed command to be displayed, preventing transients on switchover.

The speed profile mode (PROFL) can be armed by pushing the PROFL button. Engagement occurs automatically once the desired criteria are satisfied. For the mode to arm, a speed profile must be stored in the flight control computer.

9.0 PERFORMANCE ASSESSMENT

The control law algorithm was implemented on the Harris non-linear airplane simulator to demonstrate the overall system concept and evaluate the performance using a more complex non-linear simulation. The implemented system is shown in Figures 45–48 with Figure 45 showing a simplified block diagram of the total system and Figures 46–48 showing the detailed system.

9.1 ENGINE CONTROL LOOP

Comparison runs were made with the Harris simulator to confirm that the ACSL simulation (paragraph 6.3), had yielded a realistic engine response. These were made at two aerodynamic conditions (figs. 49 and 50): (1) altitude = 5000 ft, equivalent air speed = 150 kn, and (2) altitude = 20000 ft, equivalent air speed = 310 kn.

Gains predicted by linear analysis resulted in an underdamped response with excessive throttle excursion, and consequently, the forward and feedback gains (fig. 46) were reduced to KEPRP = 75 and KEFB = 0.3. The effect of reducing the system gain did not significantly effect the response time of the engine to the step input (DEPRO = 0.5). The command signal (DEPRO, fig. 49) is defined as:

$$EPR_{cmd} - EPR_{min}$$

where $EPR_{min} = 0.99$

Hence, the output EPR changes from 1.4 to 1.9 for a command from 0.4 to 0.9. Figure 49 also shows the throttle command (THCM) and throttle (TAUTO). It can be seen that a dominant feature of the transient response is the rate limiting of the throttle (10%). Figure 50 shows a 0.5 change in EPR from an initial value of 1.55 at the cruise condition.

9.2 SPEED AND ALTITUDE MODES

The primary operating mode of the system is in altitude and speed hold modes. To demonstrate the system performance with these modes engaged, the response to speed and altitude steps was recorded over a range of aerodynamic conditions:

(1) 120 kn CAS, 1500 ft (figs. 51 and 52)
(2) 150 kn CAS, 5000 ft (figs. 53 - 55)
(3) 200 kn CAS, 10000 ft (figs. 56 and 57)
(4) 250 kn CAS, 15000 ft (figs. 58 and 59)
(5) 320 kn CAS, 20000 ft (figs. 60 - 62).

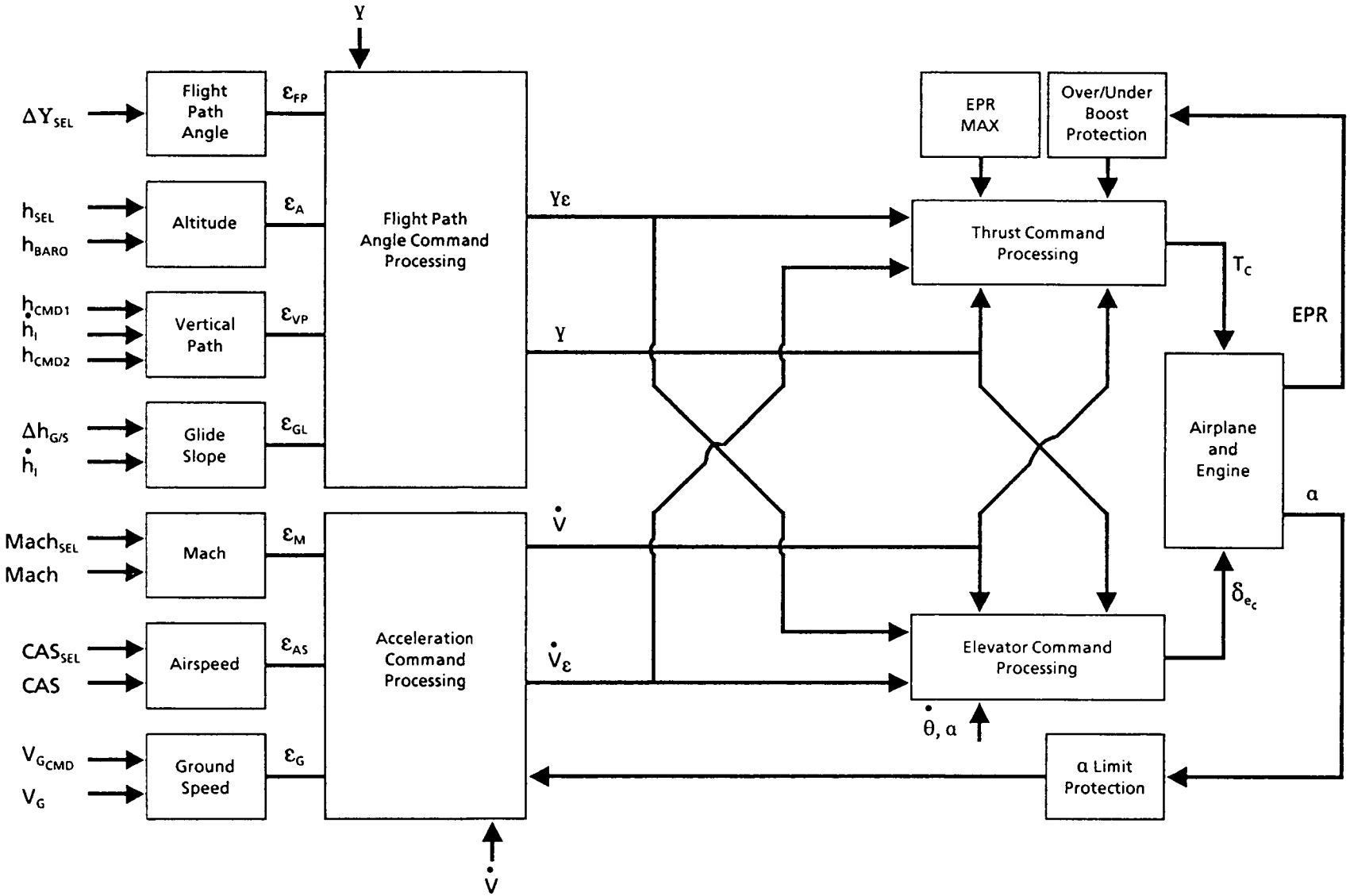

Figure 45. Integrated Elevator/Thrust Control System

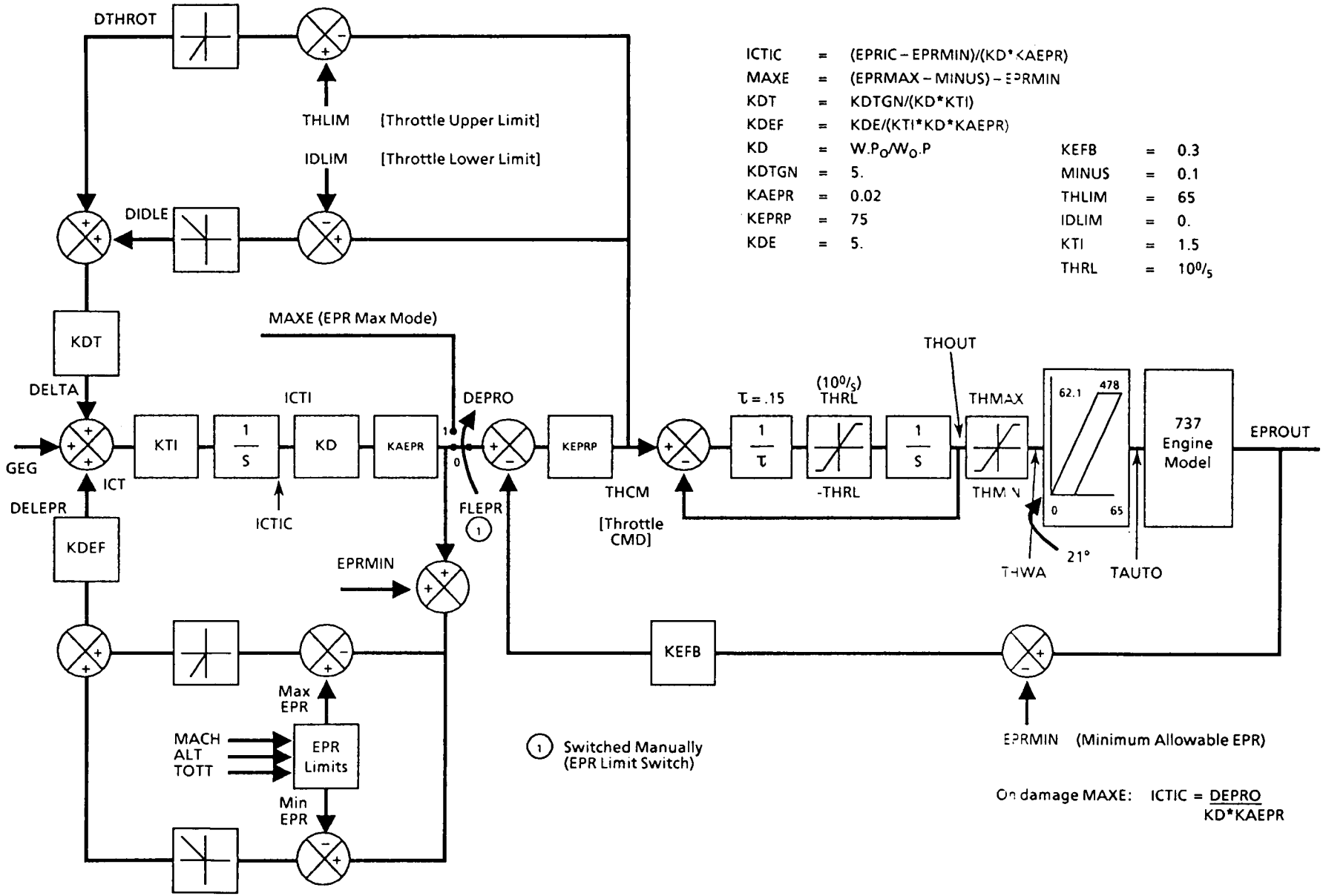

ICTIC = (EPRIC – EPRMIN)/(KD*KAEPR)
MAXE = (EPRMAX – MINUS) – EPRMIN
KDT = KDTGN/(KD*KTI)
KDEF = KDE/(KTI*KD*KAEPR)
KD = $W.P_O/W_O.P$
KDTGN = 5.
KAEPR = 0.02
KEPRP = 75
KDE = 5.

KEFB = 0.3
MINUS = 0.1
THLIM = 65
IDLIM = 0.
KTI = 1.5
THRL = $10^0/_5$

Figure 46. Engine Control Loop

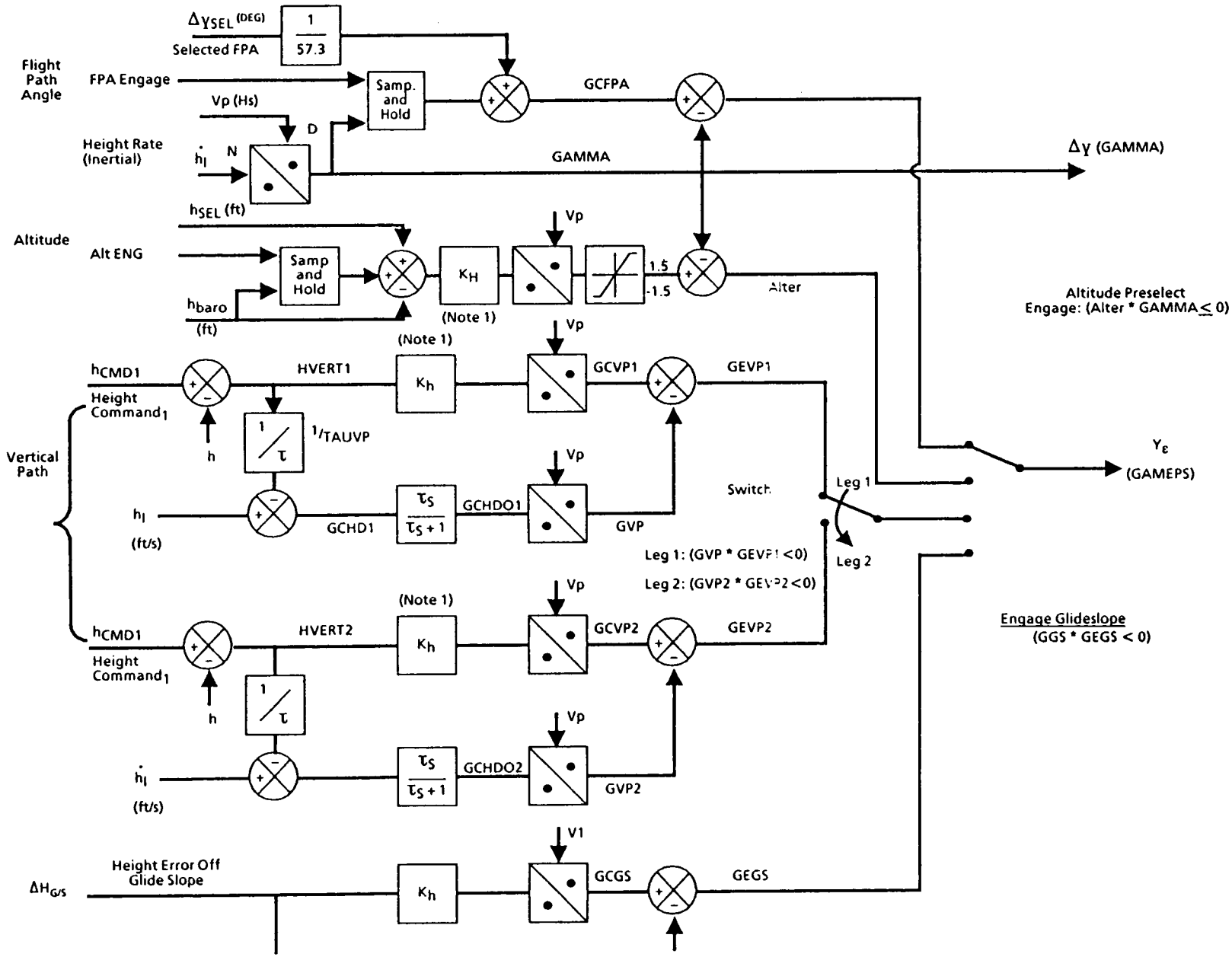

Figure 47. Integrated Autopilot/Autothrottle System Path and Speed Modes

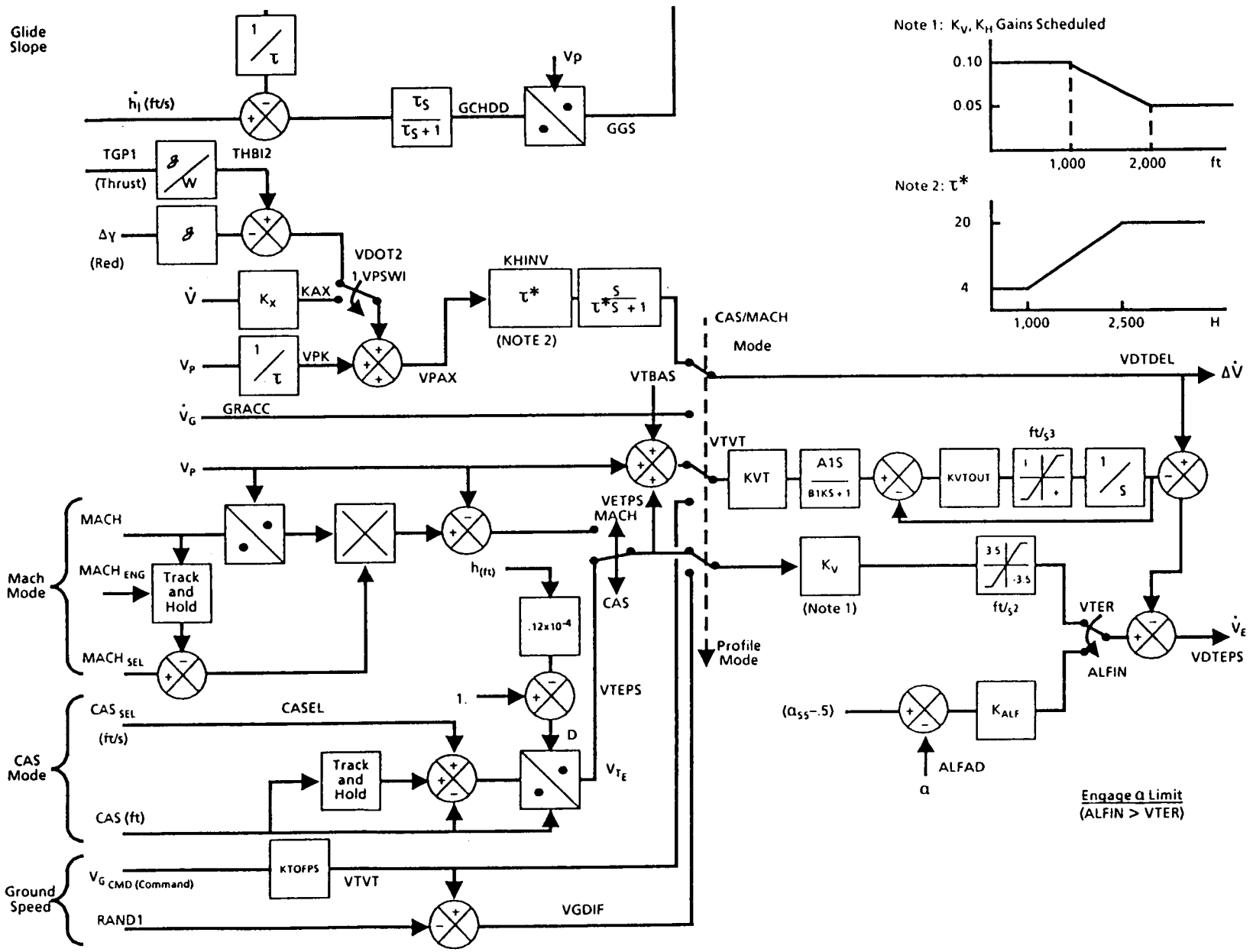

Figure 47. Integrated Autopilot/Autothrottle System Path and Speed Modes (Continued)

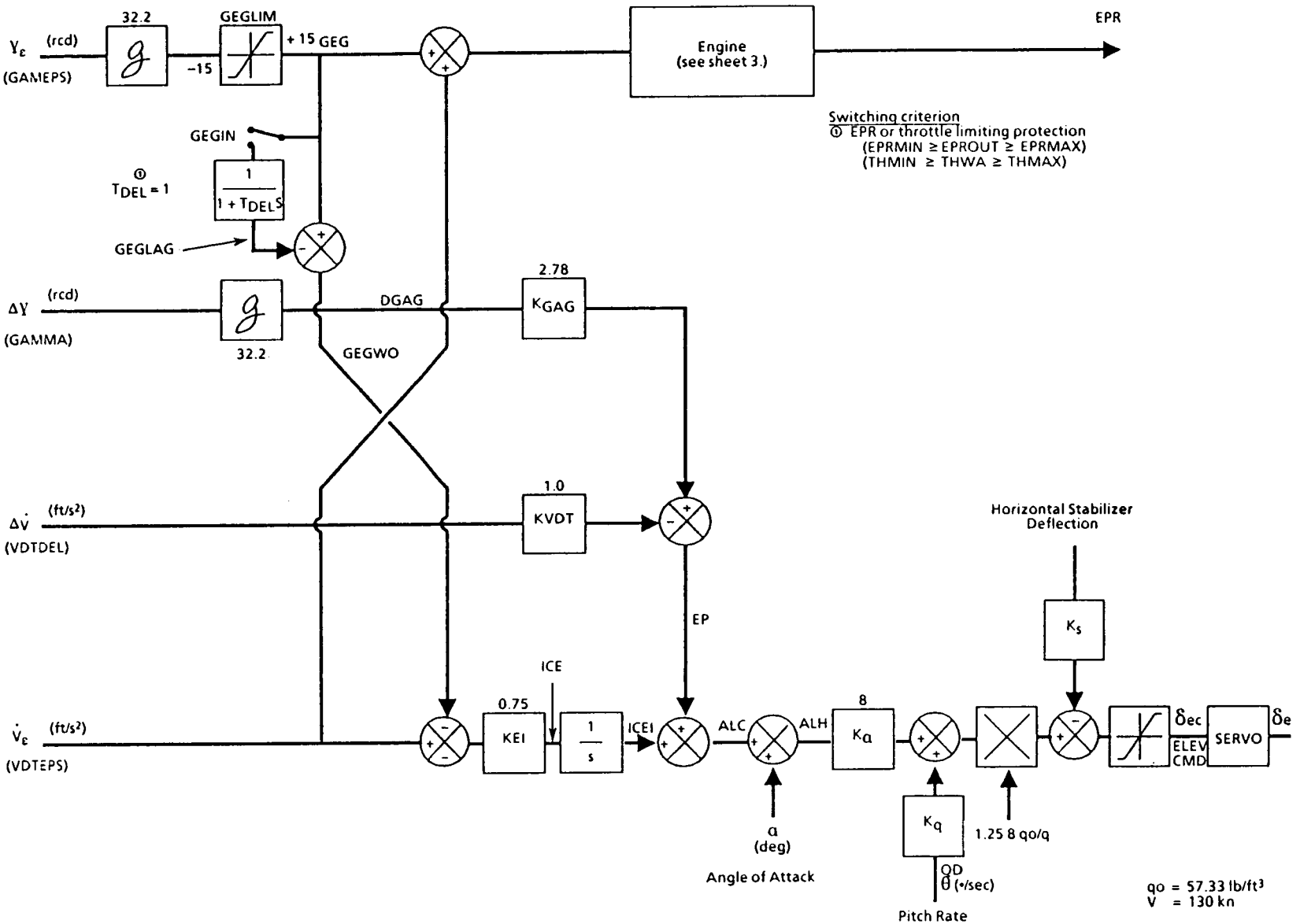

Figure 48. Thrust and Elevator Command Processing

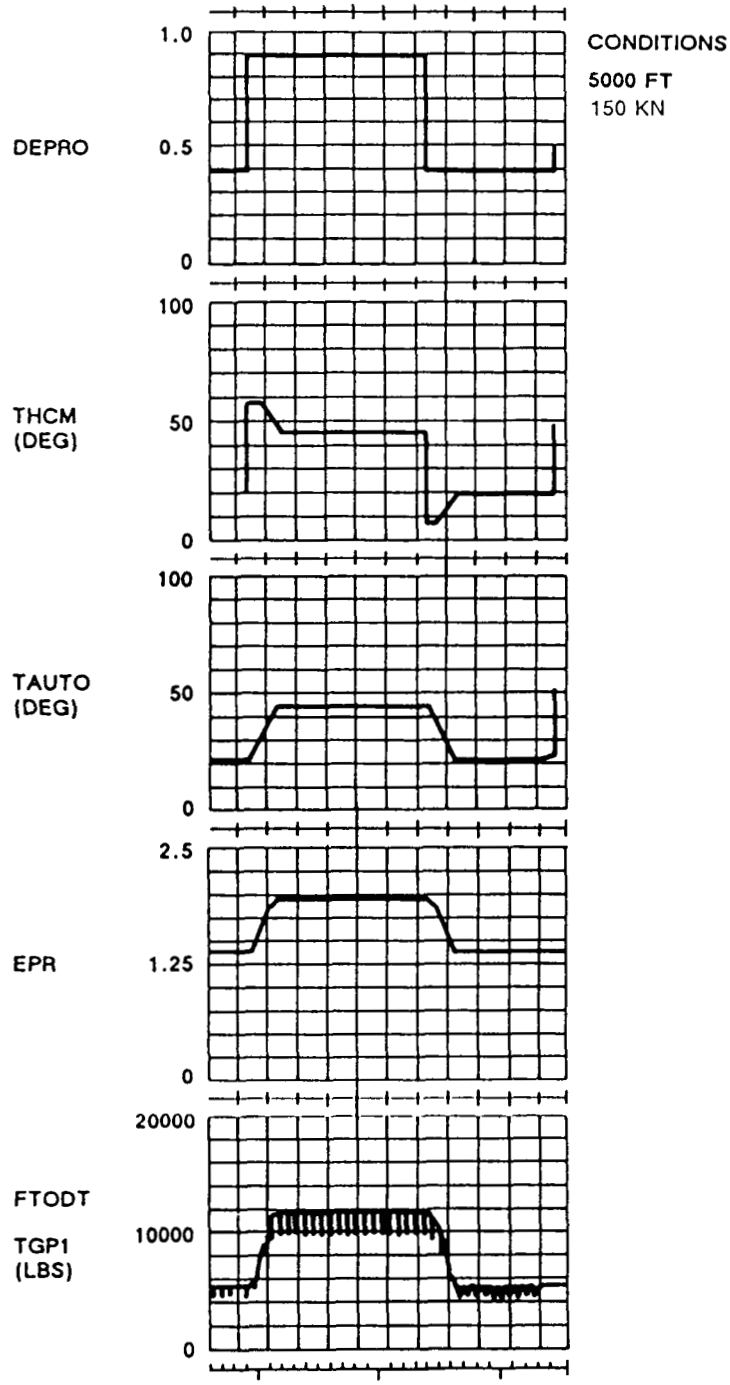

Figure 49. Engine Performance (5000 ft, 150 kn, EAS)

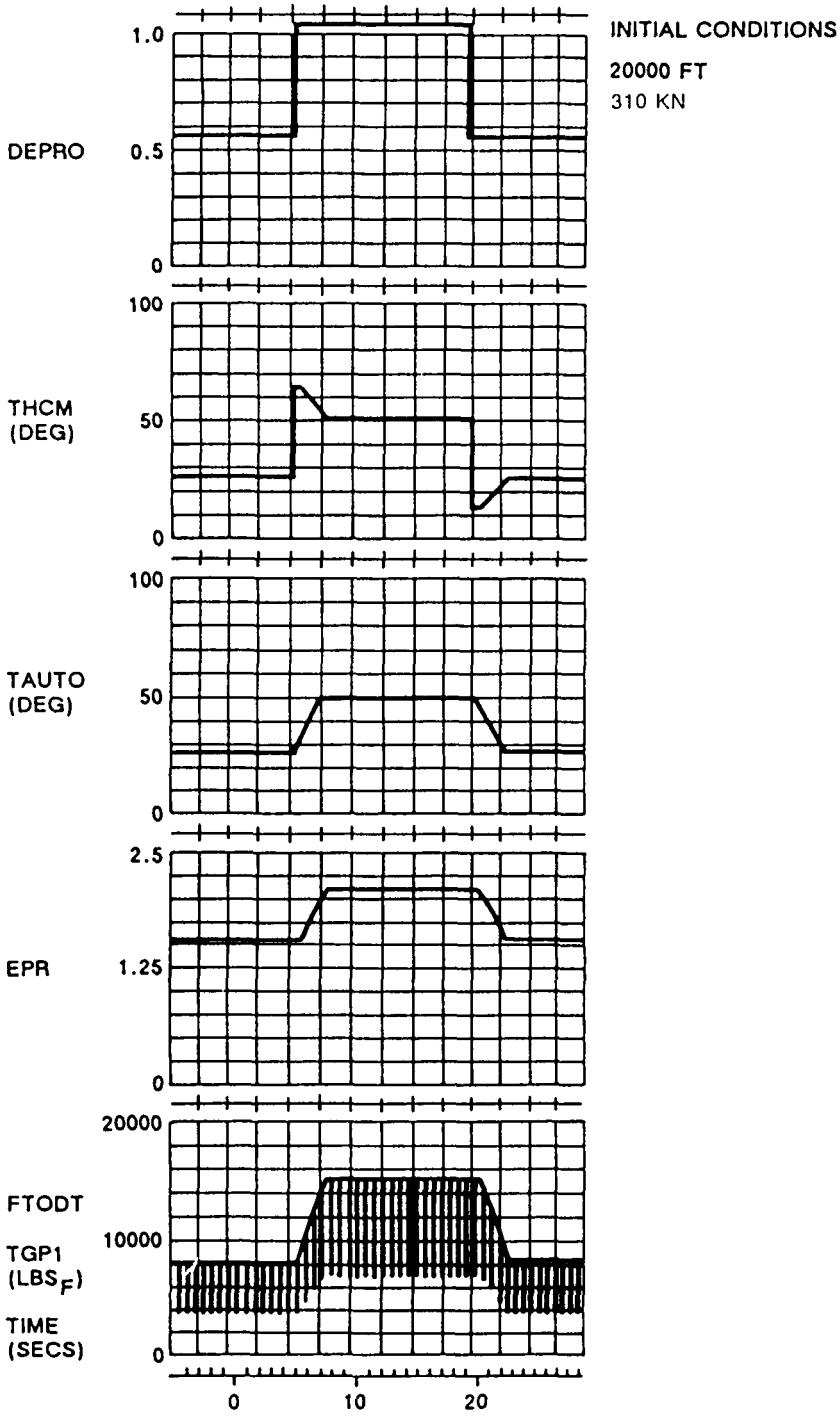

Figure 50. Engine Performance (20000 ft, 310 kn, EAS)

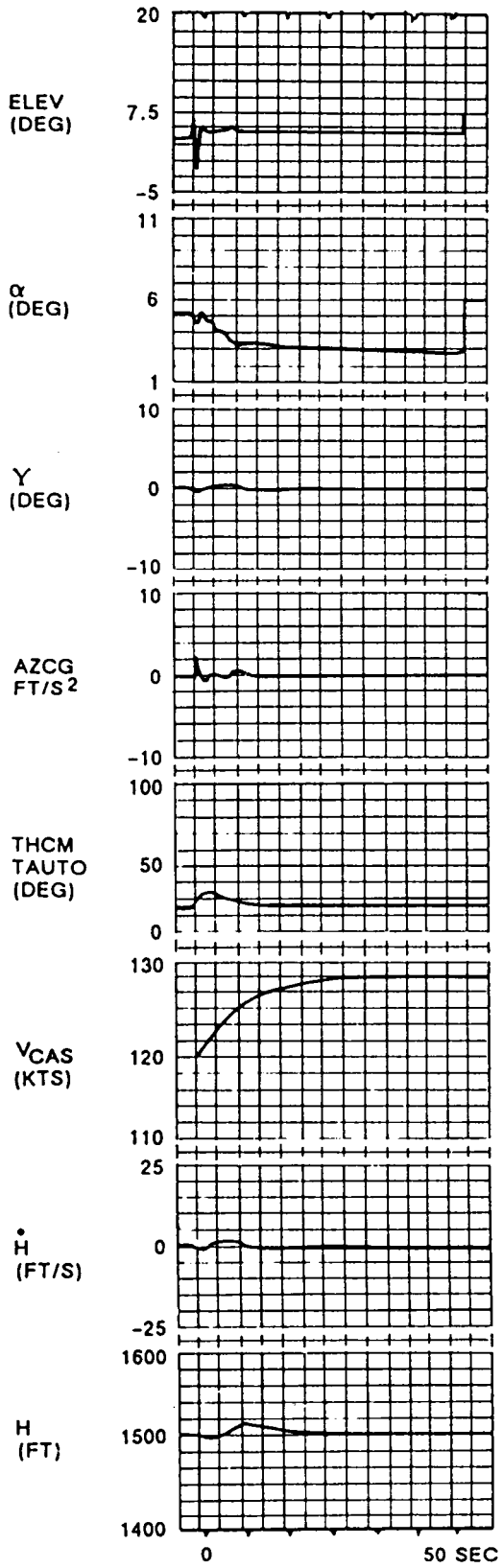

Figuro 51. 10-kn Stop In V_{CAS} (120 kn, 1500 ft)

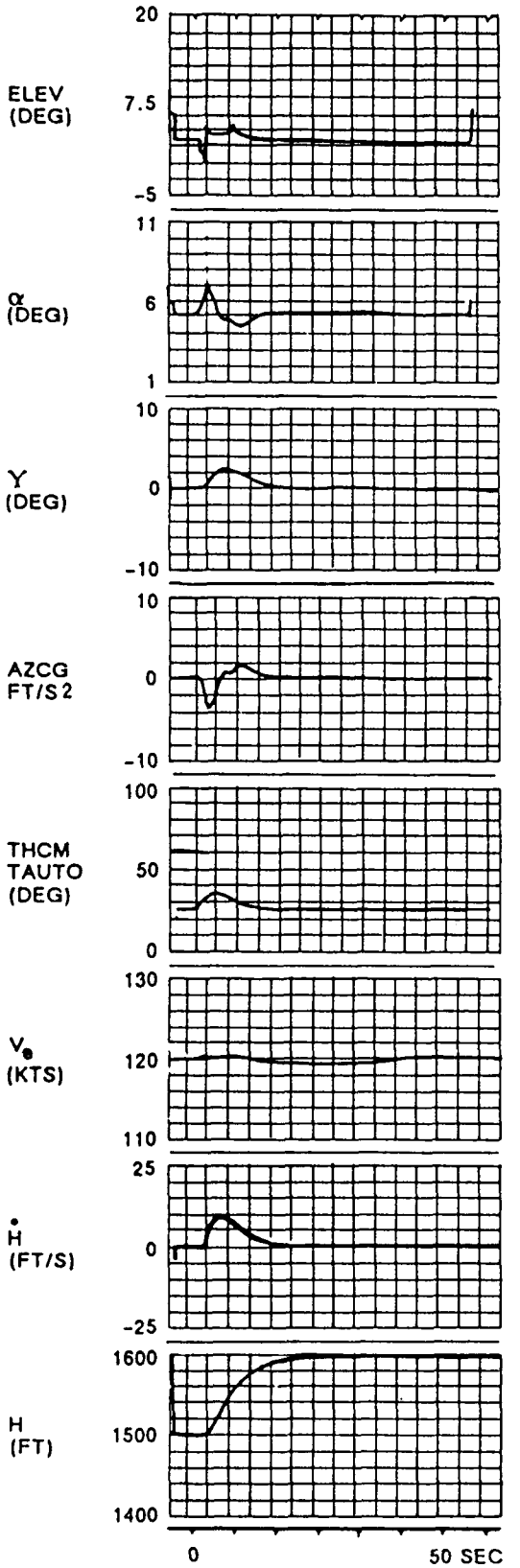

Figure 52. 100-ft Step in Height (120 kn, 1500 ft)

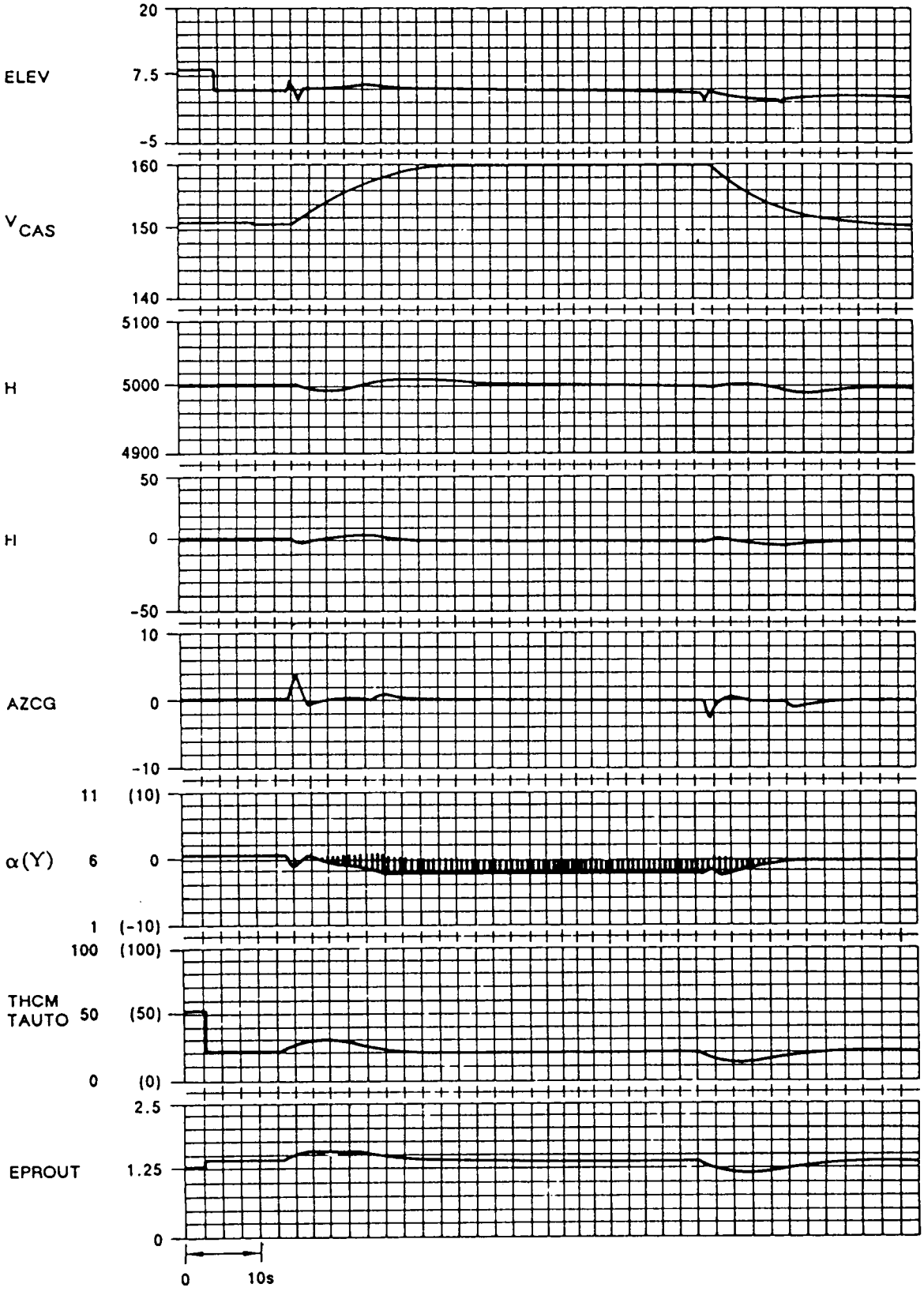

Figure 53. 10-kn Step in V_{CAS} (150 kn, 5000 ft)

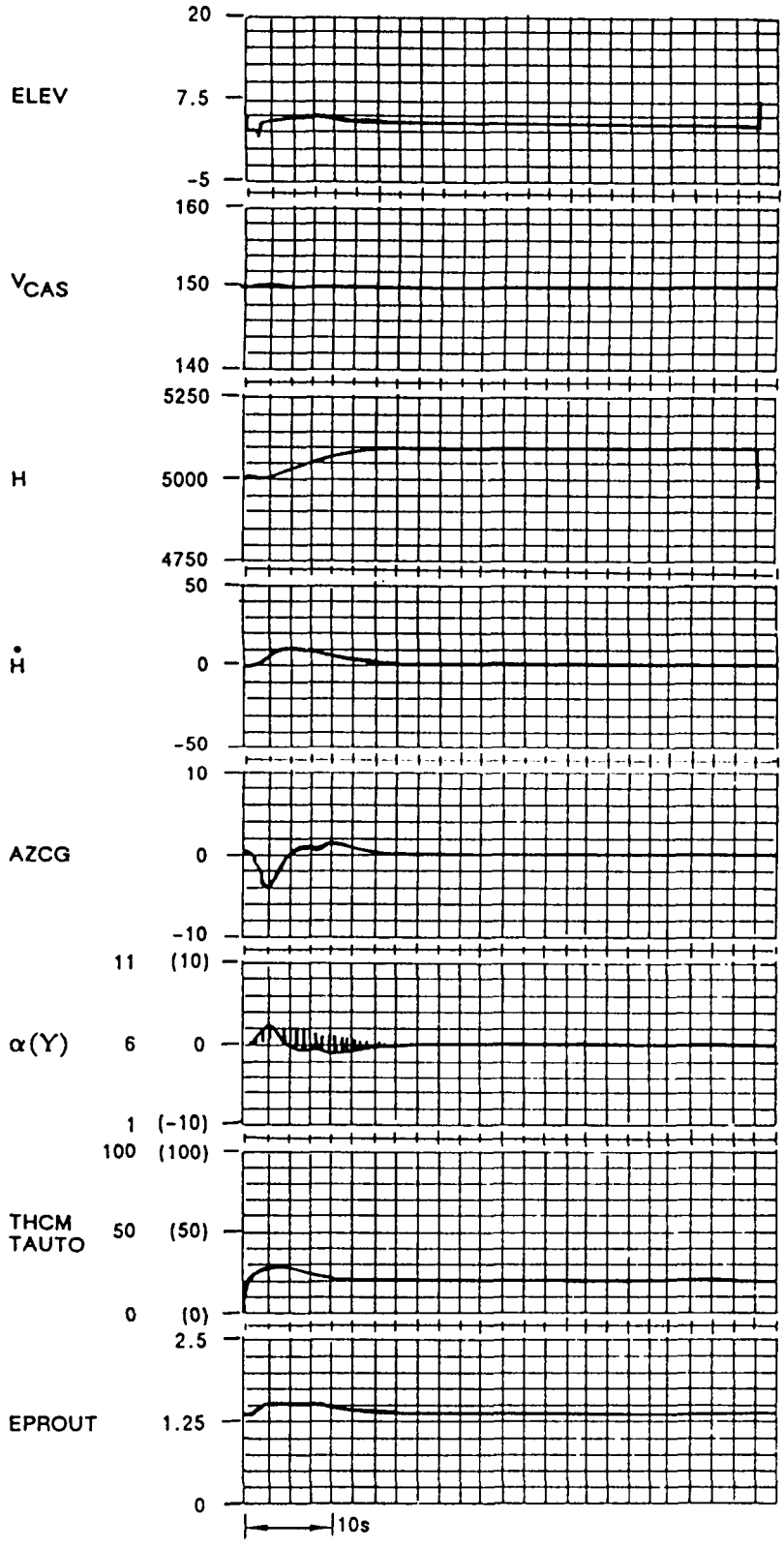

Figure 54. 100-ft Step in Height (150 kn, 5000 ft)

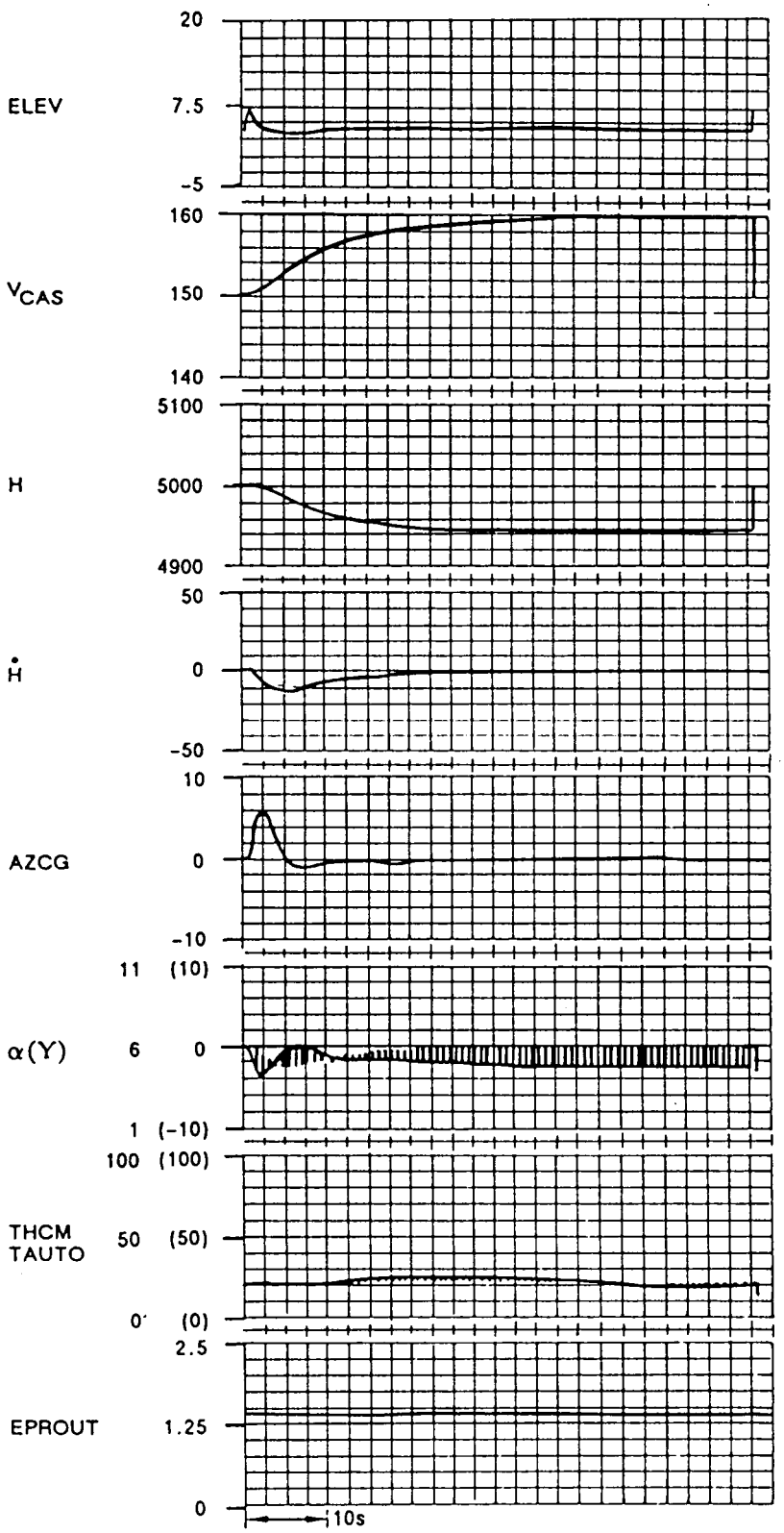

Figure 55. Double Maneuver (ΔV_{CAS} = 10-kn , ΔH = 100 ft)

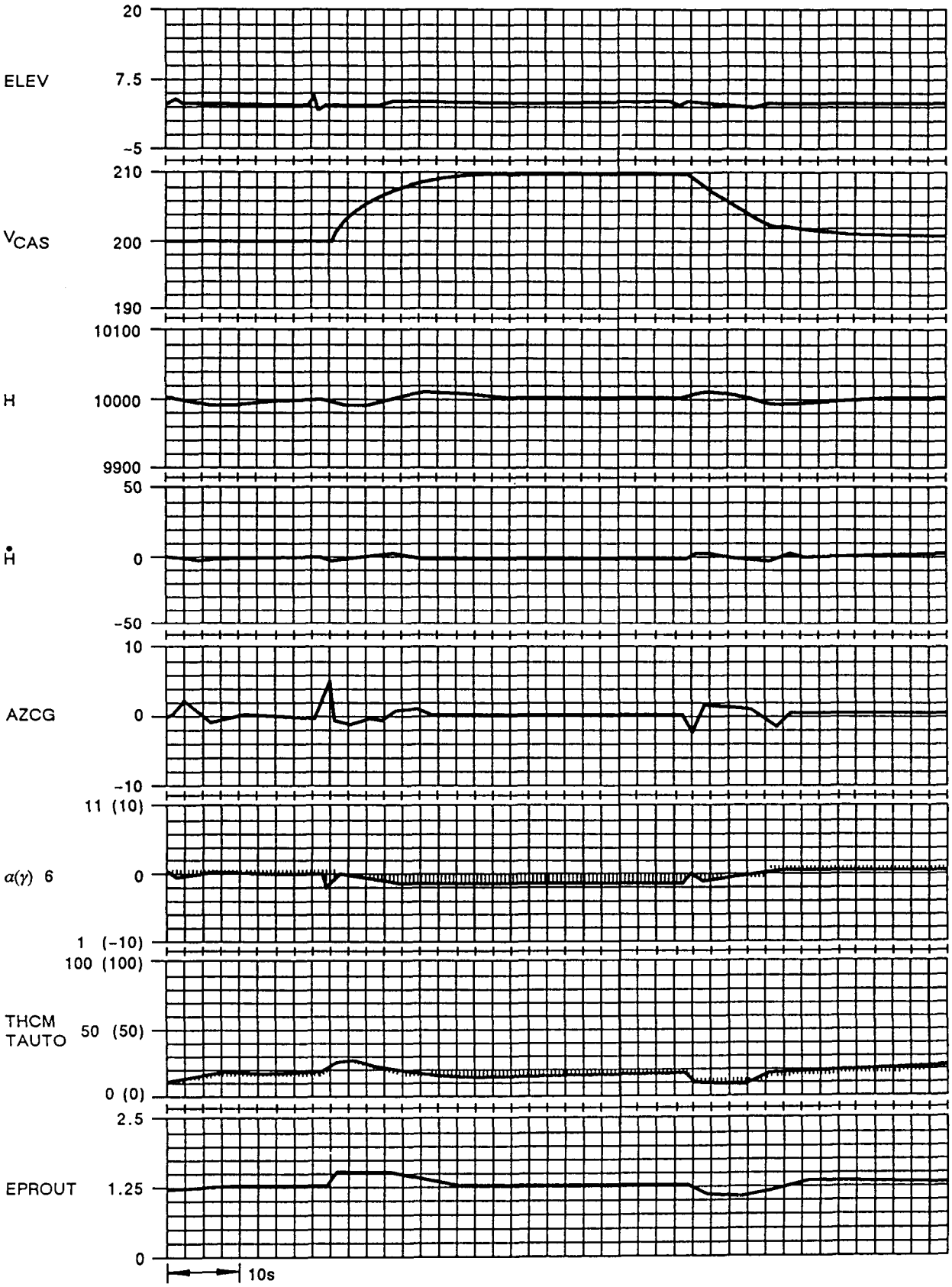

Figure 56. 10-kn Step in V_{CAS} (200 kn, 10000 ft)

6-U80109R1pk7-12

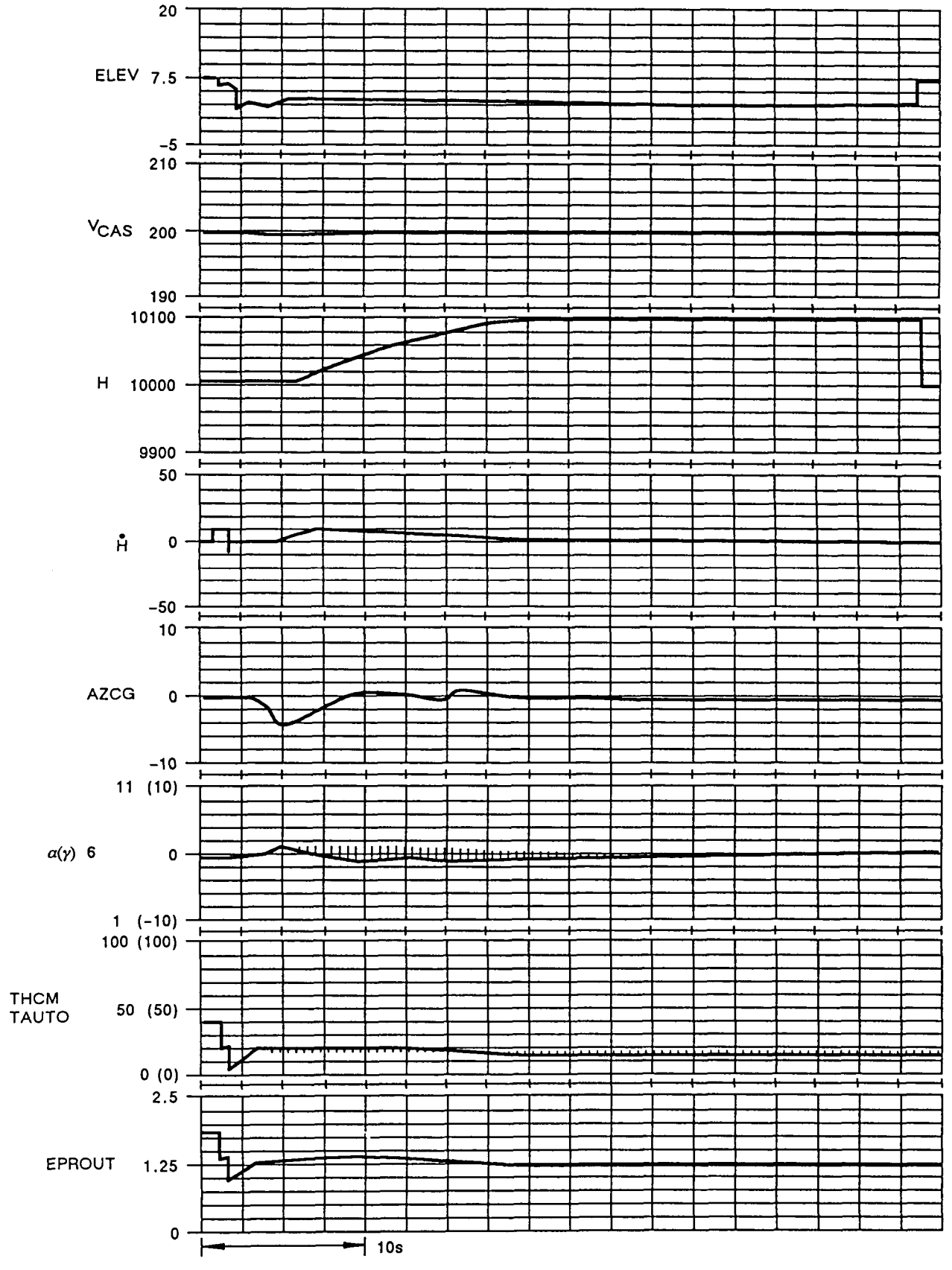

Figure 57. 100-ft Step in Height (200 kn, 10000 ft)

7-U80109R2pk15-13

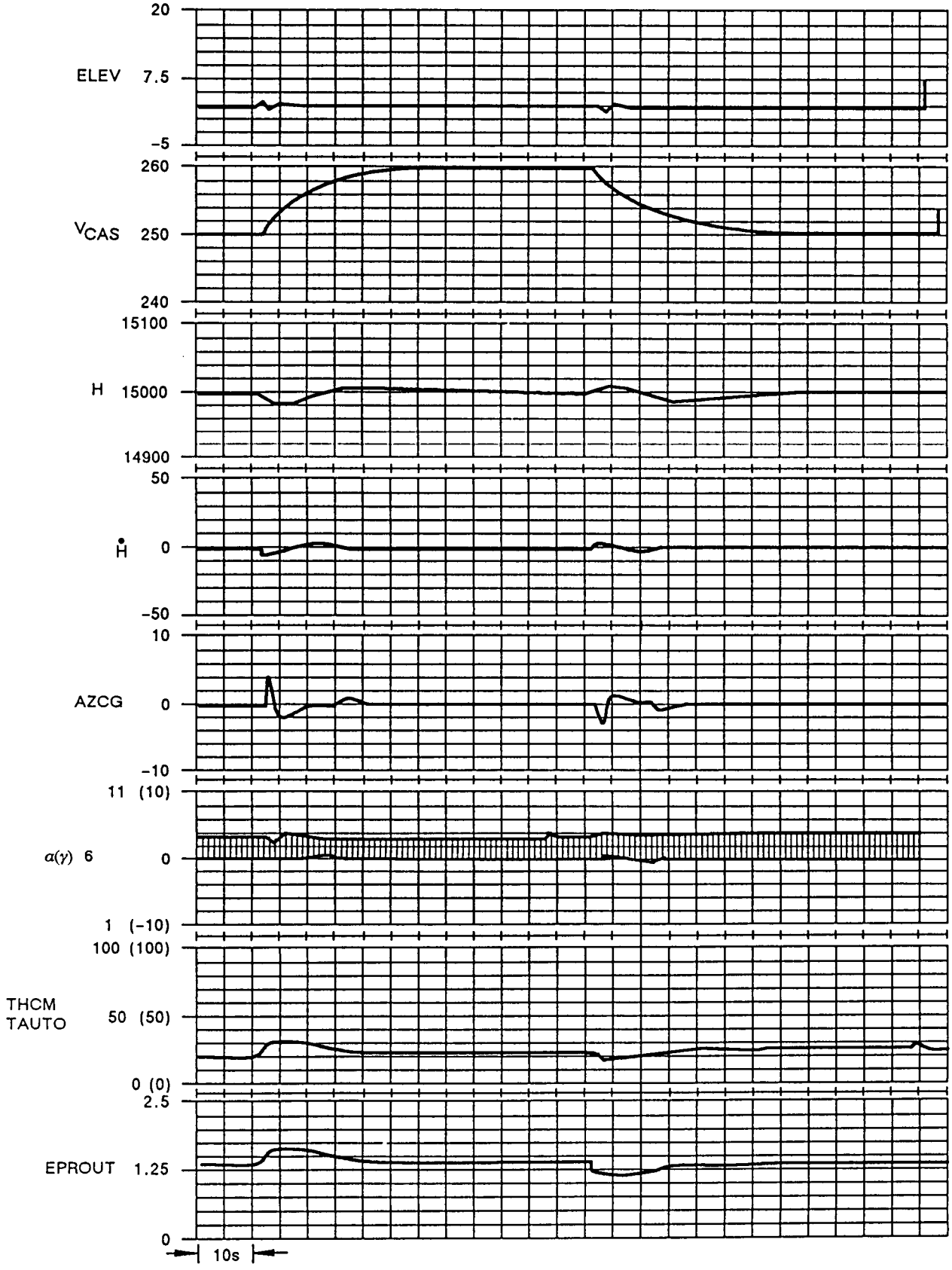

Figure 58. 10-kn Step in V_{CAS} (250 kn, 15000 ft)

7-U80109R2pk14-14

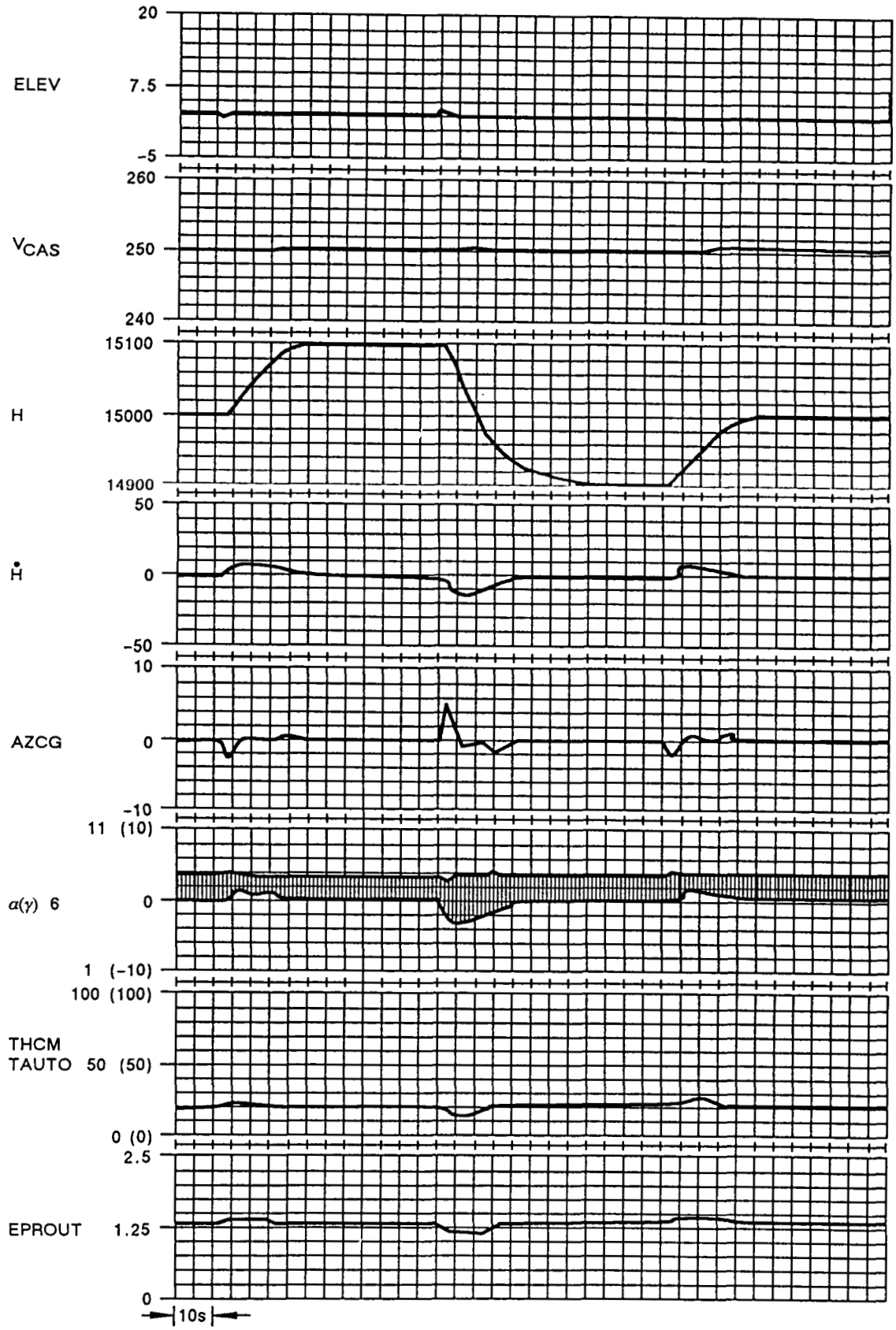

Figure 59. 100-ft Step in Height (250 kn, 15000 ft)

7-U80109R2pk15-15

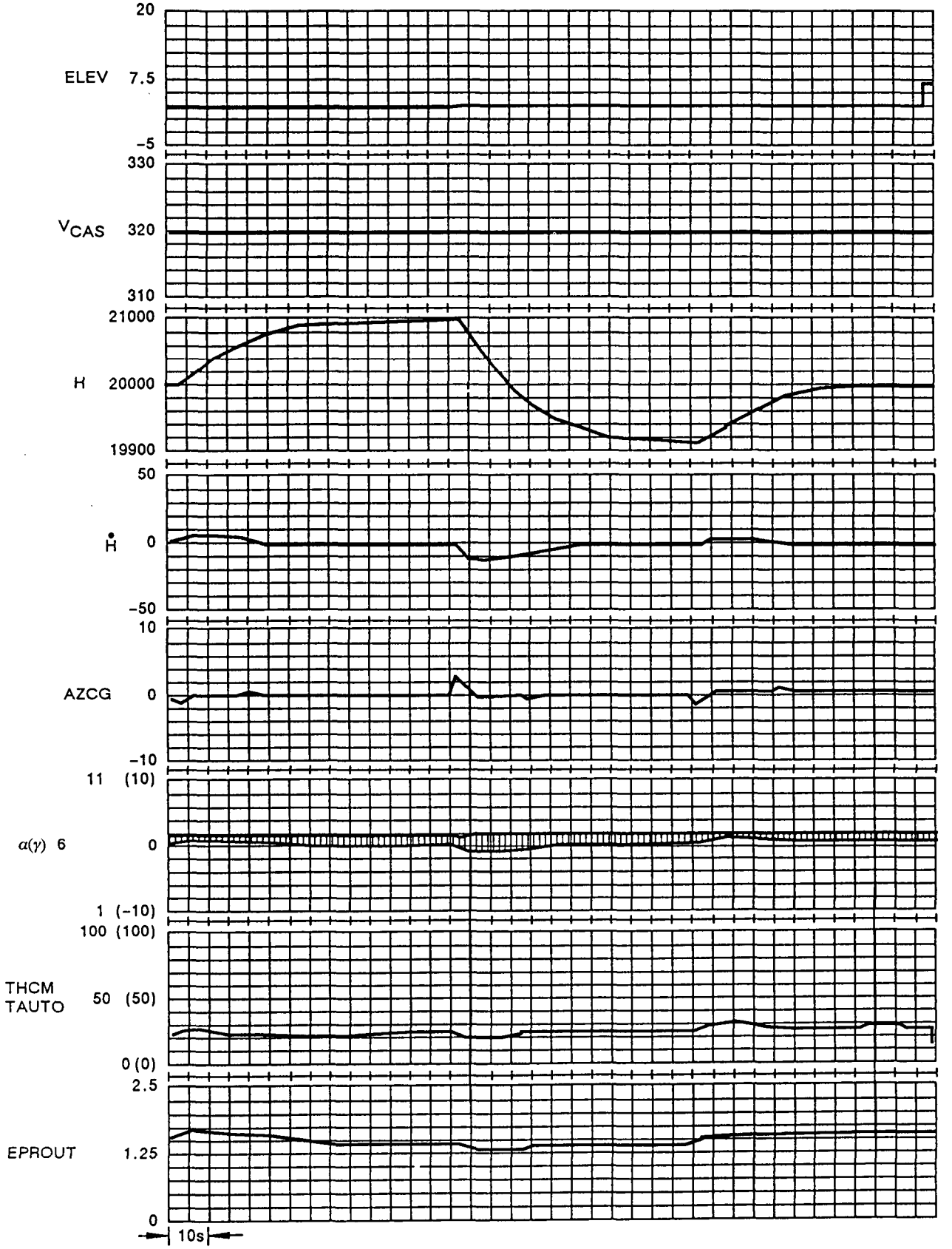

Figure 60. 10-kn Step in V_{CAS} (320 kn, 20000 ft)

7-U80109R2pk15-16

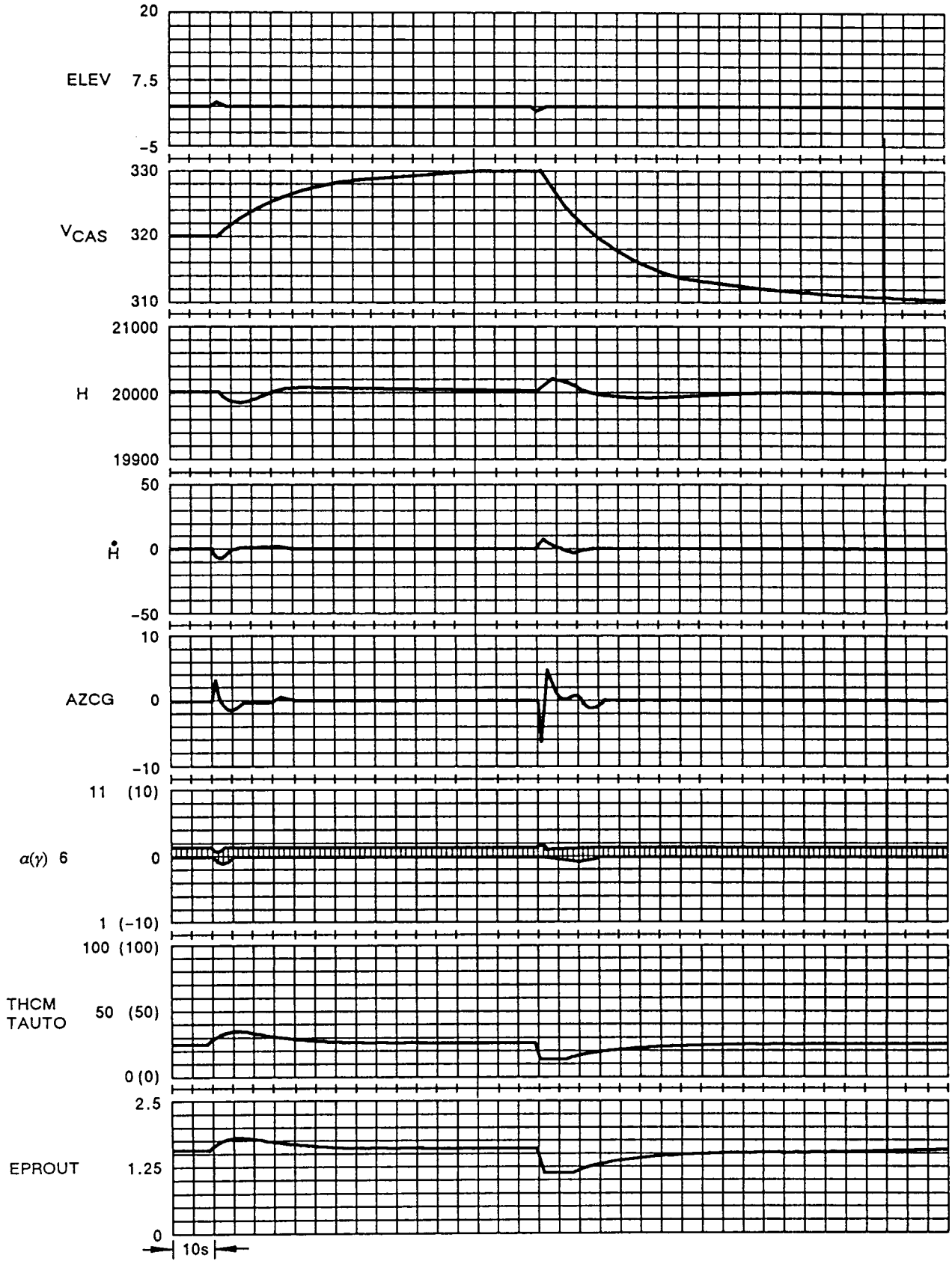

Figure 61. 100-ft Step in Height (320 kn, 20000 ft)

6-U80109R1pk7-17

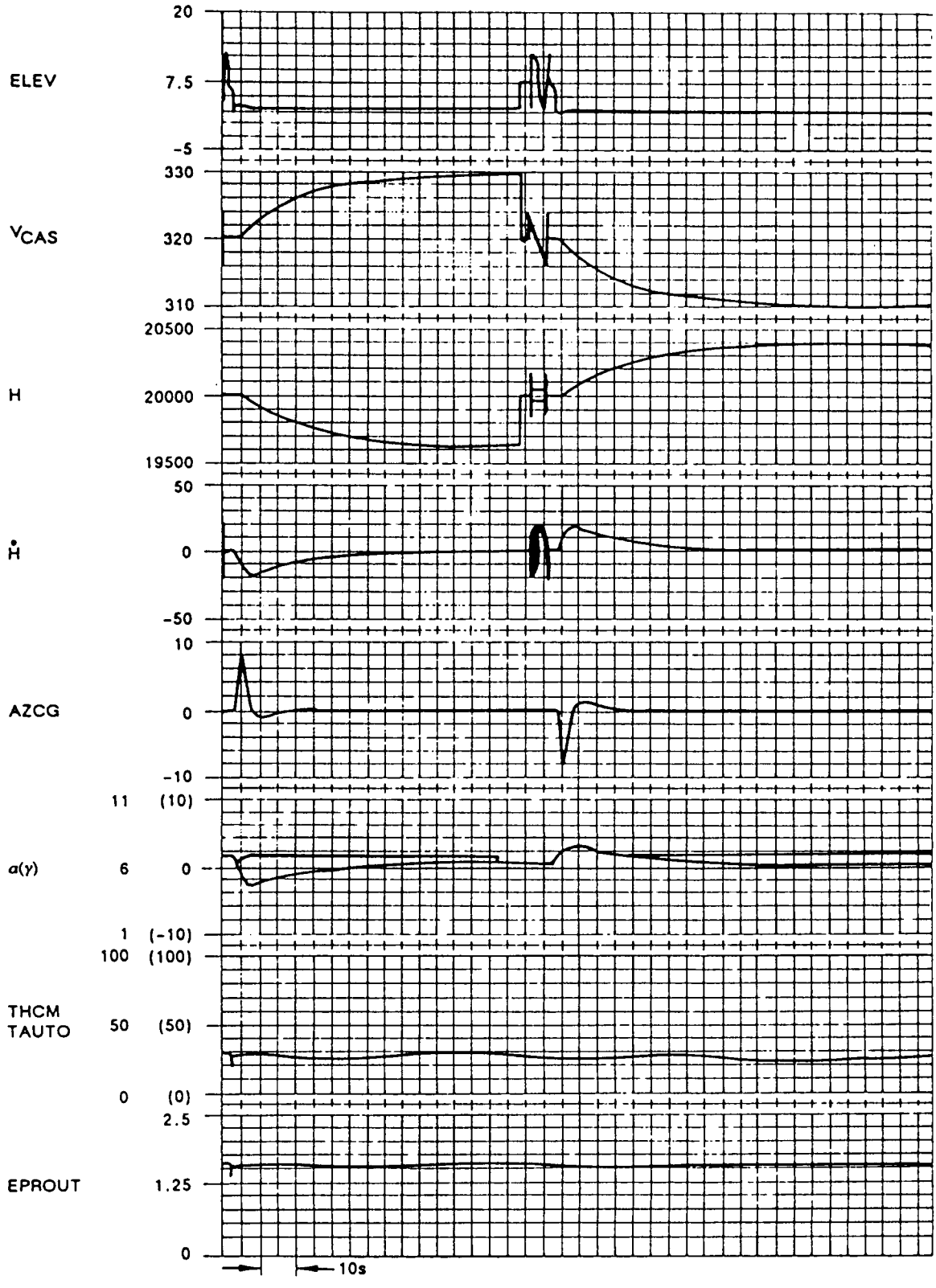

Figure 62. Double Maneuver (ΔV_{CAS} = 10 kn, ΔH = -380 ft)

Height error was less than the design requirement of 20 ft for all the velocity changes shown. A typical height error for 10 kn change in velocity was approximately 10 ft (fig. 53). The transient response in all cases exhibited no overshoot and reached 95% of final value by about 35 s. In all cases the engine response was smooth with no excessive or unnecessary throttle motions. Vertical accelerations peaked at 0.1g for 10 kn changes in V_{CAS}, except at condition (4) (250 kn CAS, 15000 ft) when the 'g' level reached 0.15g.

For all height changes shown, velocity error did not exceed the design requirement of 1 kn and was typically 0.5 kn. As with velocity changes, the transient response exhibited zero overshoot.

In Section 2 is discussed one design feature of the integrated autopilot/autothrottle (i.e., the constant energy concept). In a constant energy maneuver (i.e., one in which the change in potential energy is matched by the change in kinetic energy) the system will use the elevator to retrim the energy in the system and the throttle activity will be negligible. This type of maneuver is demonstrated in Figure 55 where the command inputs are + 10 kn change in velocity coupled with a -138-ft change in height. These command inputs were calculated to be energy equivalent at 150 kn. It can be seen that the elevator immediately responds at the start of the maneuver, whereas throttle activity is negligible. The throttle command (THCM) does show about 2° change over the maneuver, but owing to backlash in the system the throttle lever angle (TAUTO) does not respond with no change in EPR detectable.

A similar energy equivalent maneuver was performed at 20000 ft with a 10-kn change in speed corresponding to a -380-ft change in height. Again the change in throttle command is small ($< 4°$) and the change in EPR and throttle lever angle negligible.

The effects of large changes in command inputs are shown in Figures 63 and 64. Figure 63 shows the response to a 1000-ft change in altitude and demonstrates the action of two of the limiters in the system. These limiters are designed to limit the rate of climb and the acceleration levels experienced during large maneuvers.

The reference to Figure 47 shows a limiter in the altitude command path. The system is designed such that a command for change in altitude generates a flight path angle error (γ_ε) signal which is limited. The result is a height rate limit which varies as a function of velocity from approximately 1800 ft/min at low speed (120 kn) to 6800 ft/min at cruise (310 kn EAS).

In addition to this limit, other limiters exist on γ_ε and V_ε in order to restrict acceleration commands to approximately 0.1g. However, during transients, the normal acceleration will exceed this 0.1g level.

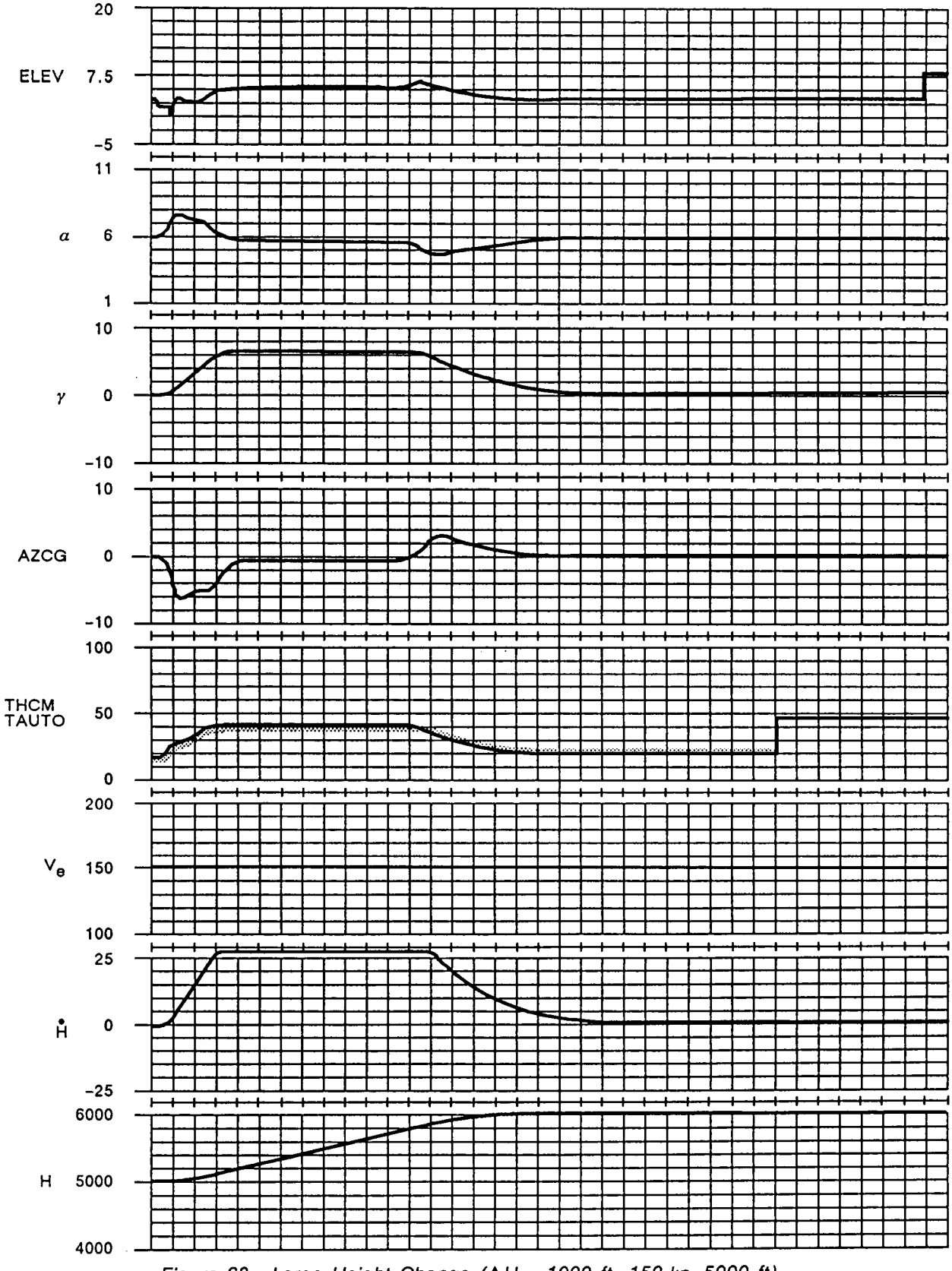

Figure 63. Large Height Change (ΔH = 1000 ft, 150 kn, 5000 ft)

7-U80109R2pk14-19

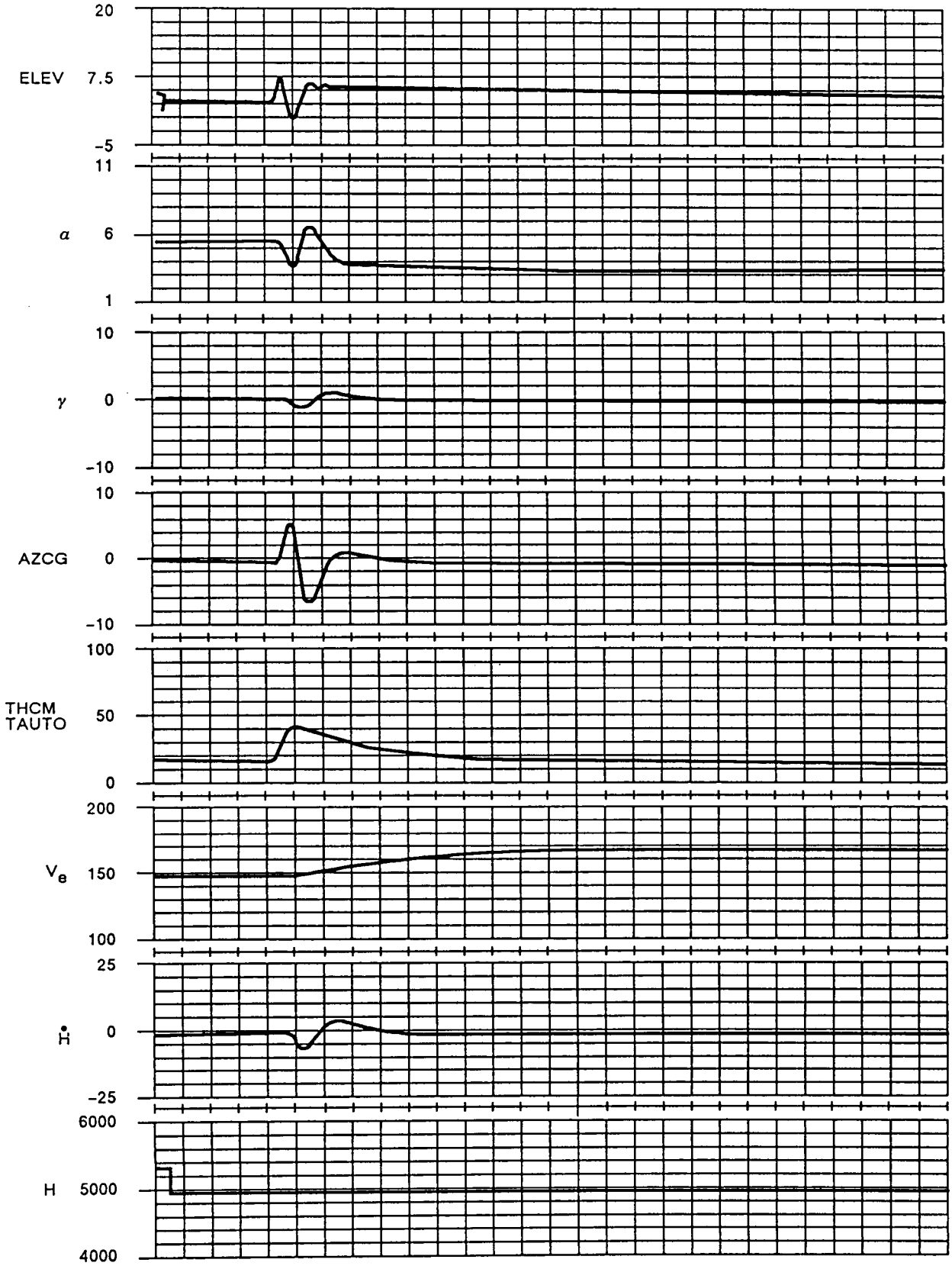

Figure 64. Large Velocity Change (20 kn change 150 kn, 5000 ft)

7-U80109R2pk14-20

Figure 63 shows that during the 1000-ft altitude change, the height rate was limited to approximately 30 ft/s. During the initial phase of the maneuver the normal acceleration peaked at 6 ft/s^2 but settled to 4.4 ft/s^2. Capture of the new altitude was achieved with no overshoot and velocity error was insignificant (<1kn).

The effect of a 20-kn step in CAS (fig. 64) shows negligible height error and smooth velocity captive. Transient peaks in normal acceleration exceeded 0.1g reaching 6 ft/s^2. However, future adjustment of limiters or gains could reduce this figure if necessary.

The speed mode options available with the integrated autopilot/autothrottle are CAS, Mach or ground speed modes. The design and operation of these modes is described in paragraphs 7.1 and 7.2. Considering the CAS/Mach mode operation, a switch over between the modes was designed to occur automatically at preselected speeds. During ascent, the system will switch from CAS to Mach mode whereas during descent the system switches from Mach to CAS.

Figure 65 shows the system operation: initially the airplane is commanded to descend at a flight path angle of -3° but holding Mach 0.7. CAS increases to the preselected switch point of 325 kn, then the system holds CAS constant while Mach decreases. An added feature of the altitude mode is the capability to preselect desired altitude. The system climbs or descends at the required flight path angle until the switching criterion is satisfied then engages altitude mode in a smooth transient free manner (fig. 66).

9.3 FLIGHT PATH ANGLE, GLIDE SLOPE AND VERTICAL PATH MODES

The response to a step change in Flight Path Angle ($\Delta\gamma = 3°$) is shown in Figure 67 (150 kn EAS, 5000 ft) and Figure 68 (310 kn EAS, 20000 ft). Captive was smooth with minimum change in throttle. However, normal acceleration peaked at 8 ft/s^2 in the high speed example.

The design of glide slope and vertical path following mode are described in detail in paragraph 7.3. The aim of the mode is to provide a smooth transient free captive of either the glide slope or some portion of the precalculated vertical path. The operation of both these modes is illustrated in Figures 69 and 70 showing the desired transient response of γ and height with low acceleration (AZCG) and negligible velocity error.

9.4 NONLINEAR OPERATION DUE TO α OR ENGINE LIMITING

The integrated autopilot/autothrottle system has been designed to prevent stall due to excessive α command and to prevent engine overboost due to large throttle commands. The design and implementation of these features is described in Section 6. Figure 71 shows the effect of commanding a

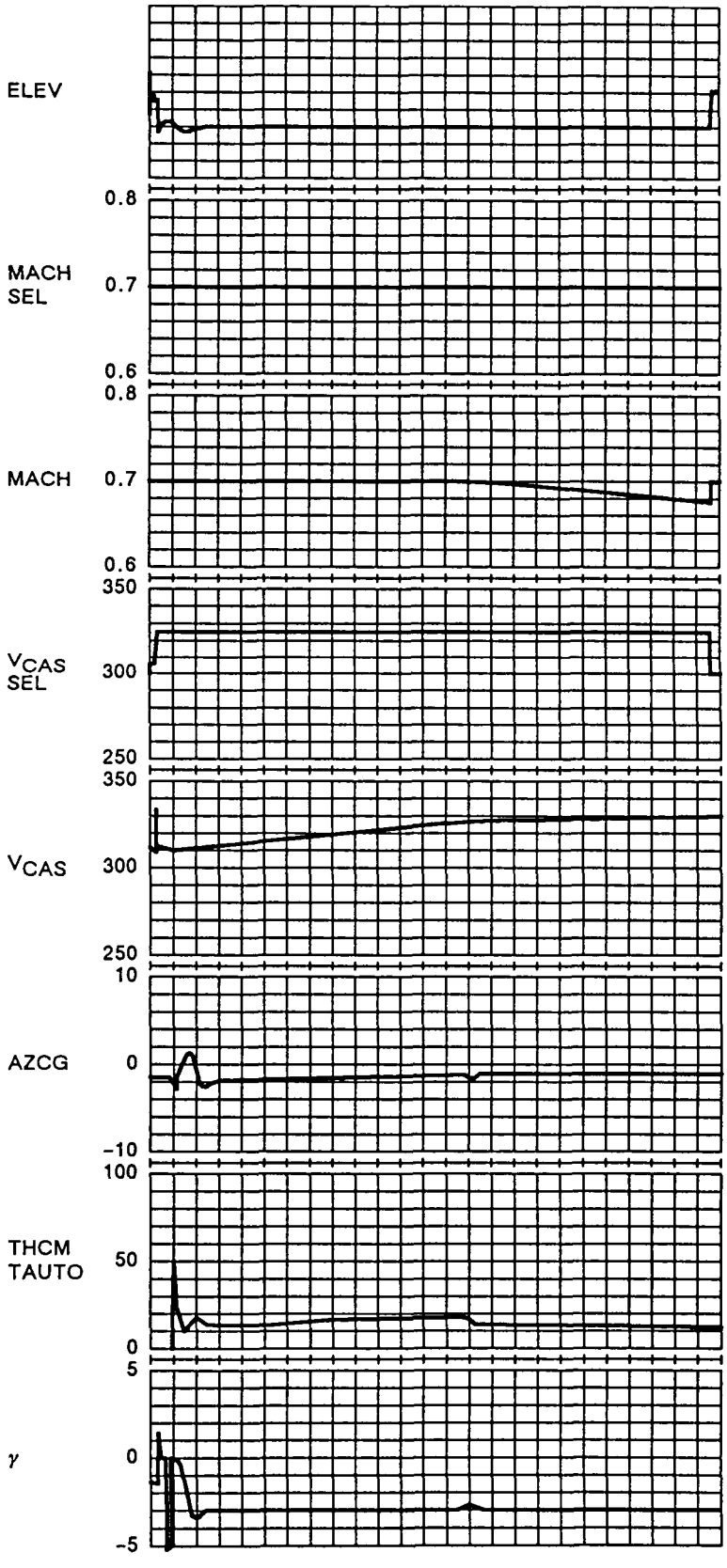

Figure 65. Mach to CAS Switch

7-U80109R2pk14-21

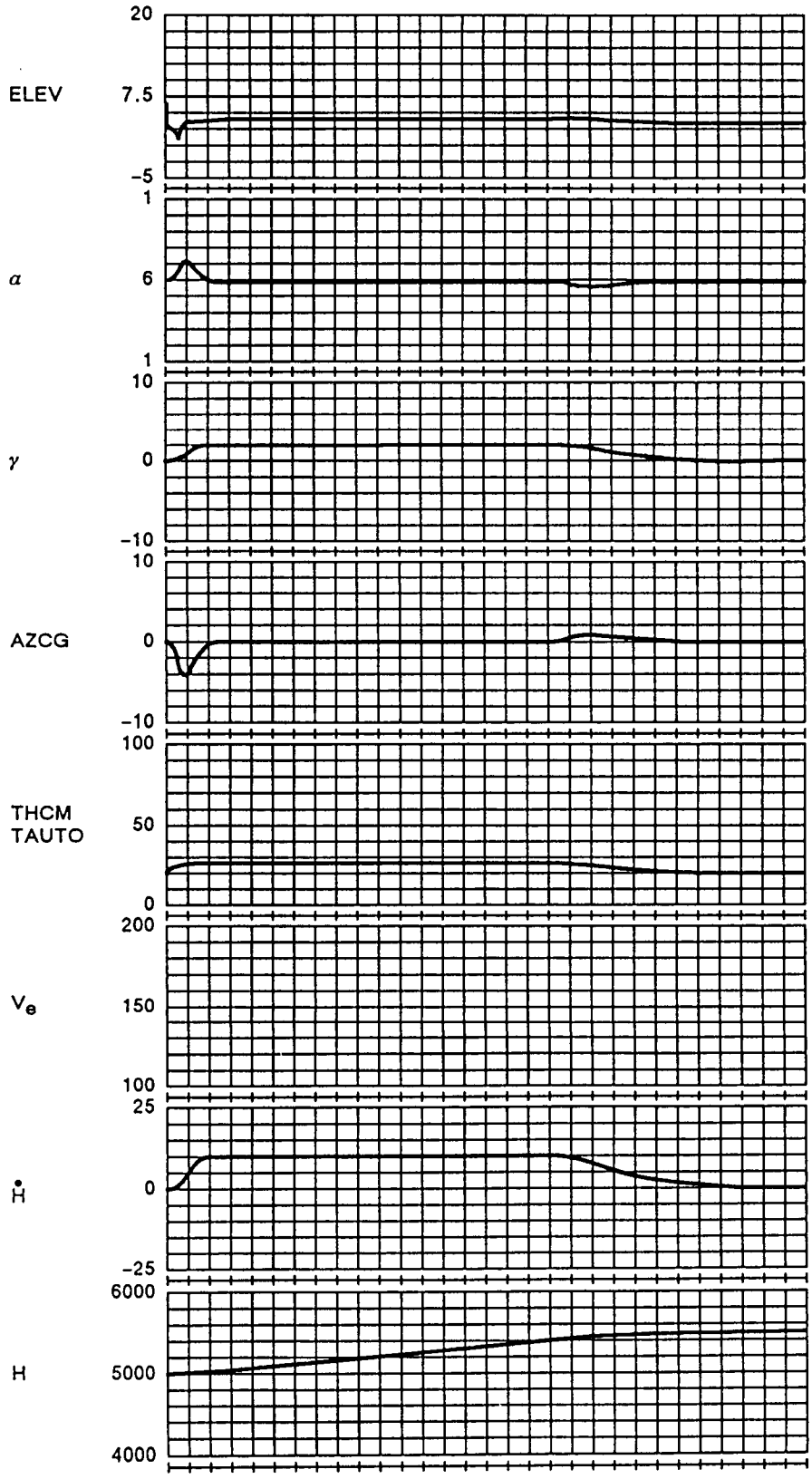

Figure 66. Altitude Preselect Mode

7-U80109R2pk14-22

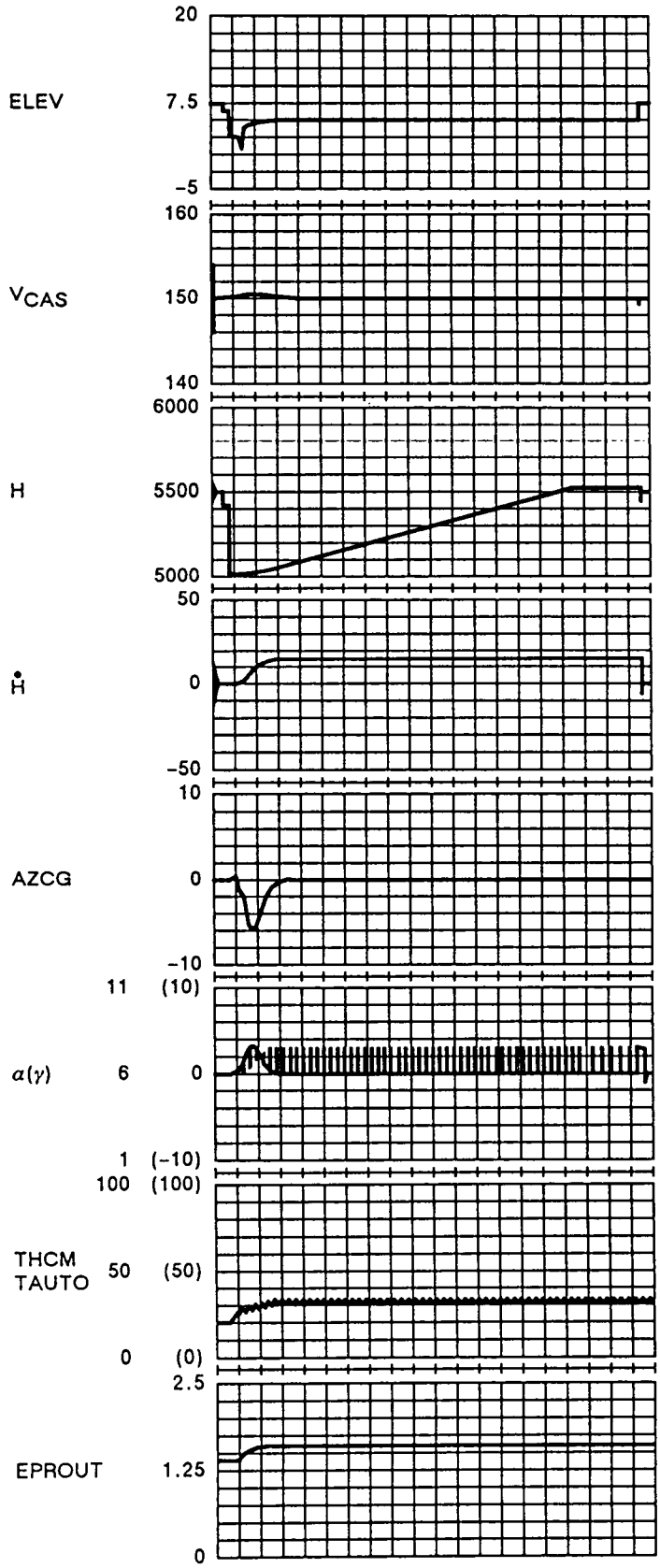

Figure 67. 3° Change in Flight Path Angle (150 kn 5000 ft)

7-U80109R2pk14-23

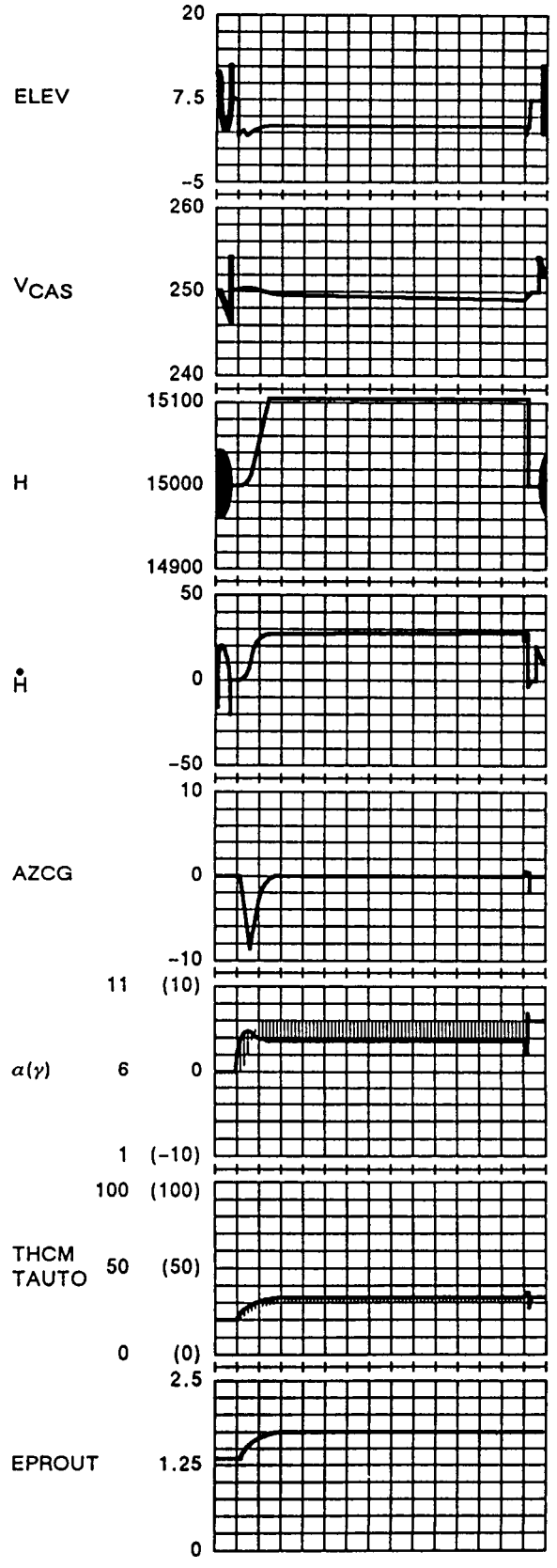

Figure 68. 3° Change in Flight Path Angle (310 kn, 20000 ft)

7-U80109R2pk14-24

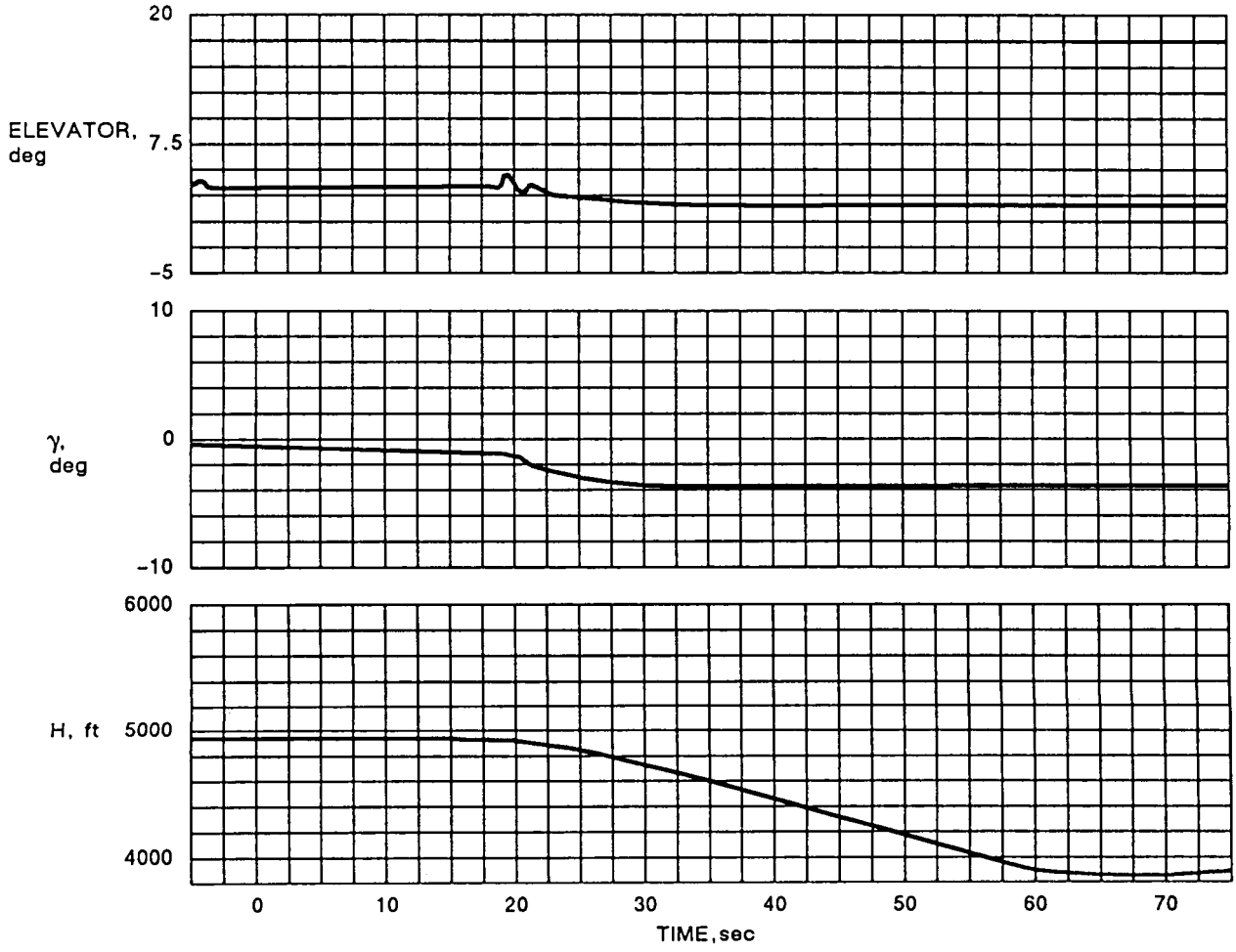

Figure 69. Glide Slope Mode

7-U80109pk13-9

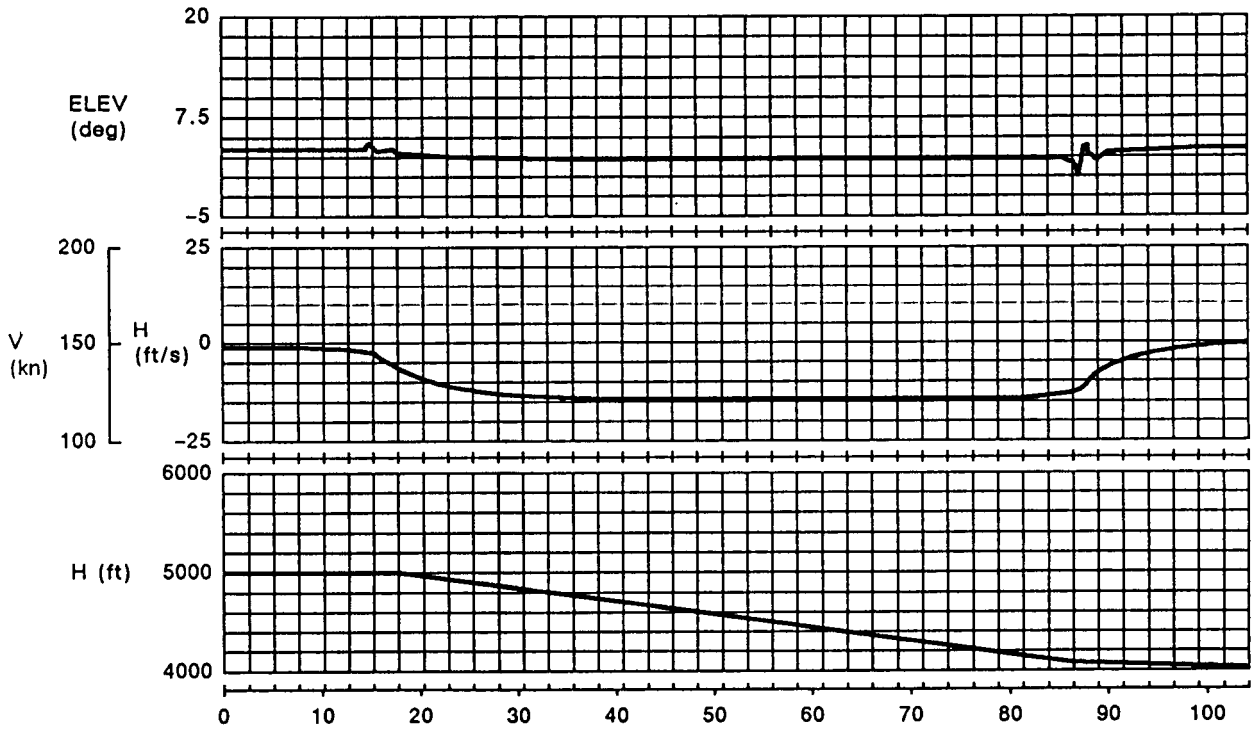

Figure 70. Vertical Path Mode

7-U80109R2pk13-25

large flight path angle (γ_{cmd} - 10°) when the maximum throttle angle has been limited to 40°. In this case, the actual FPA settles at 5° and the elevator retrims to maintain velocity. Maximum velocity error was 1.6 kn in this limiting condition.

The action of the limit is demonstrated in Figure 72a and b. In Figure 72a a 20-kt change in V_e is commanded causing the angle of attack (α) to reach in excess of 11°. The FPA deviates by a maximum of approximately 1.2°.

The result of setting α_{ref} (i.e., maximum allowable α) to 9° is shown in Figure 72b. FPA hold is maintained with approximately 1° error, but velocity is prevented from reaching the command input as α is limited at 9°.

The integrated autopilot/autothrottle includes an EPR max mode. This option is designed as a safety mode to use as a "Go Around" feature. Engagement of EPR max mode causes the engine to deliver maximum thrust as quickly as possible. Velocity hold mode is still engaged, so the airplane climbs at maximum height rate with the limits on height rate and acceleration not applying. Figure 73 shows the EPR max mode in which the throttle ramps forward at maximum rate with EPR limits at the maximum safe value (2.25). Elevator activity is considered high and velocity error reaches 5 kn. However, this is an emergency mode and these factors were acceptable.

9.5 TURBULENCE AND WIND SHEAR

The effect of wind shear and turbulence on this control law was investigated using the Harris simulator. The Velocity Control Loop employs a complementary filter to provide the derivative feedback signal (see paragraph 5.4). Simulation runs were made with horizontal turbulence (Dryden wind spectrum 1ft/s rms) to examine the result of variation of the complementary filter bandwidth ($\omega_K = 1/\tau_k$).

The standard deviation (SD) of several system states are shown plotted against ω_k in Figures 74 and 77 for two aerodynamic conditions: (1) H = 20000 ft, V = 310 kn, and (2) H = 1500 ft, V = 120 kn.

It is apparent that the SD of elevator ($\sigma_{\delta e}$) in Figure 74 and throttle (σ_{THCM} and σ_{TAUTO}) in Figure 75 were very sensitive to variation in ω_K. An increase in ω_K caused an increase in the SD. The SD in throttle command (σ_{THCM}) was larger than σ_{TAUTO} (throttle lever angle) due to backlash. The SD of height was sensitive to variation in ω_K at high altitude and speed, but remained at 2 ft ± 10% at the low speed and altitude. Variation in velocity SD was small. In vertical turbulence (ω_g = 1 ft/s rms) the response was largely independent of variation in ω_K (Table 4) at both aerodynamic conditions.

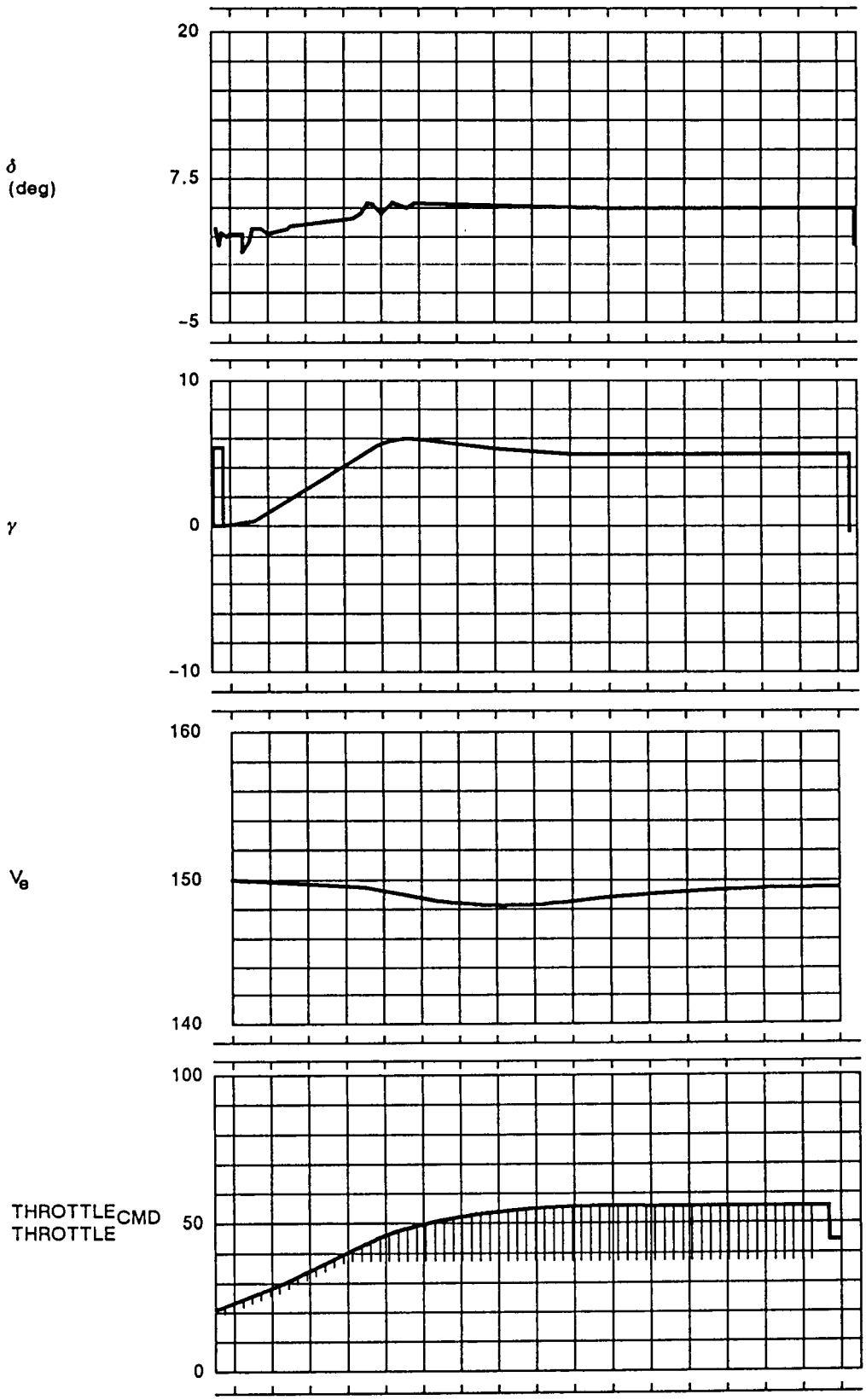

Figure 71. Throttle or EPR Limit Operation

7-U80109R2pk13-26

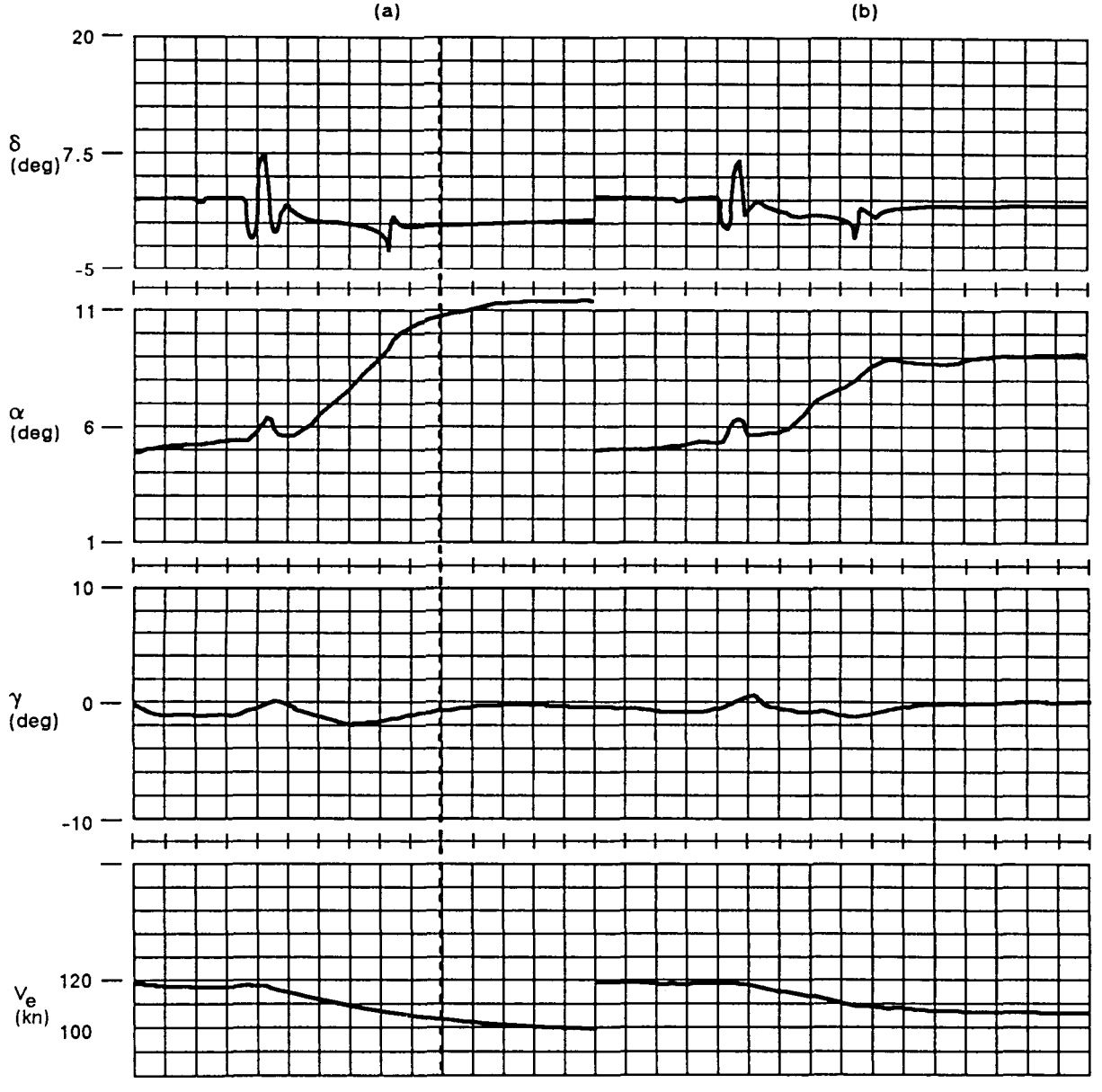

Figure 72. α Limit Operation

7-U80109R2pk14-27

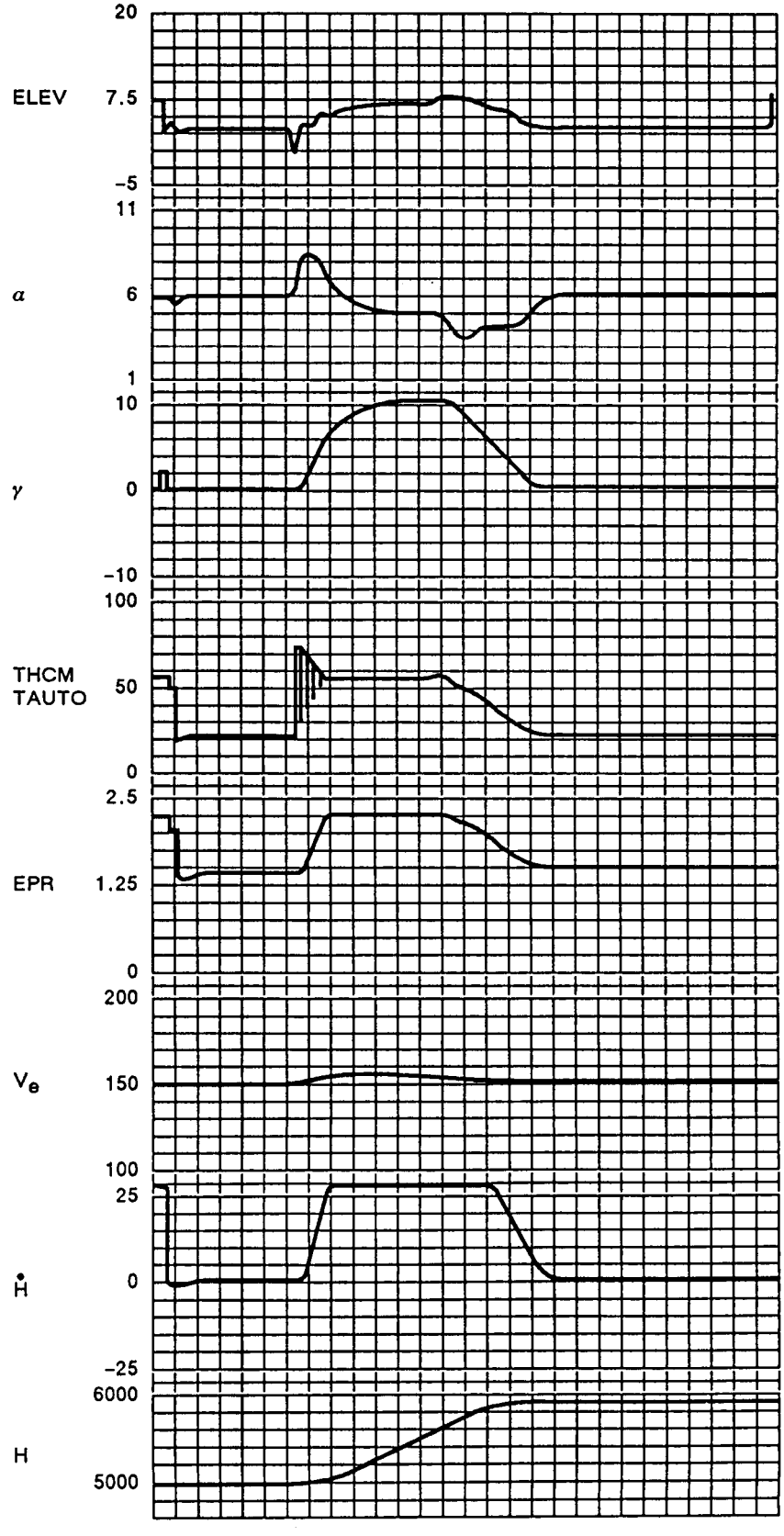

Figure 73. EPR Maximum Mode

7-U80109R2pk14-28

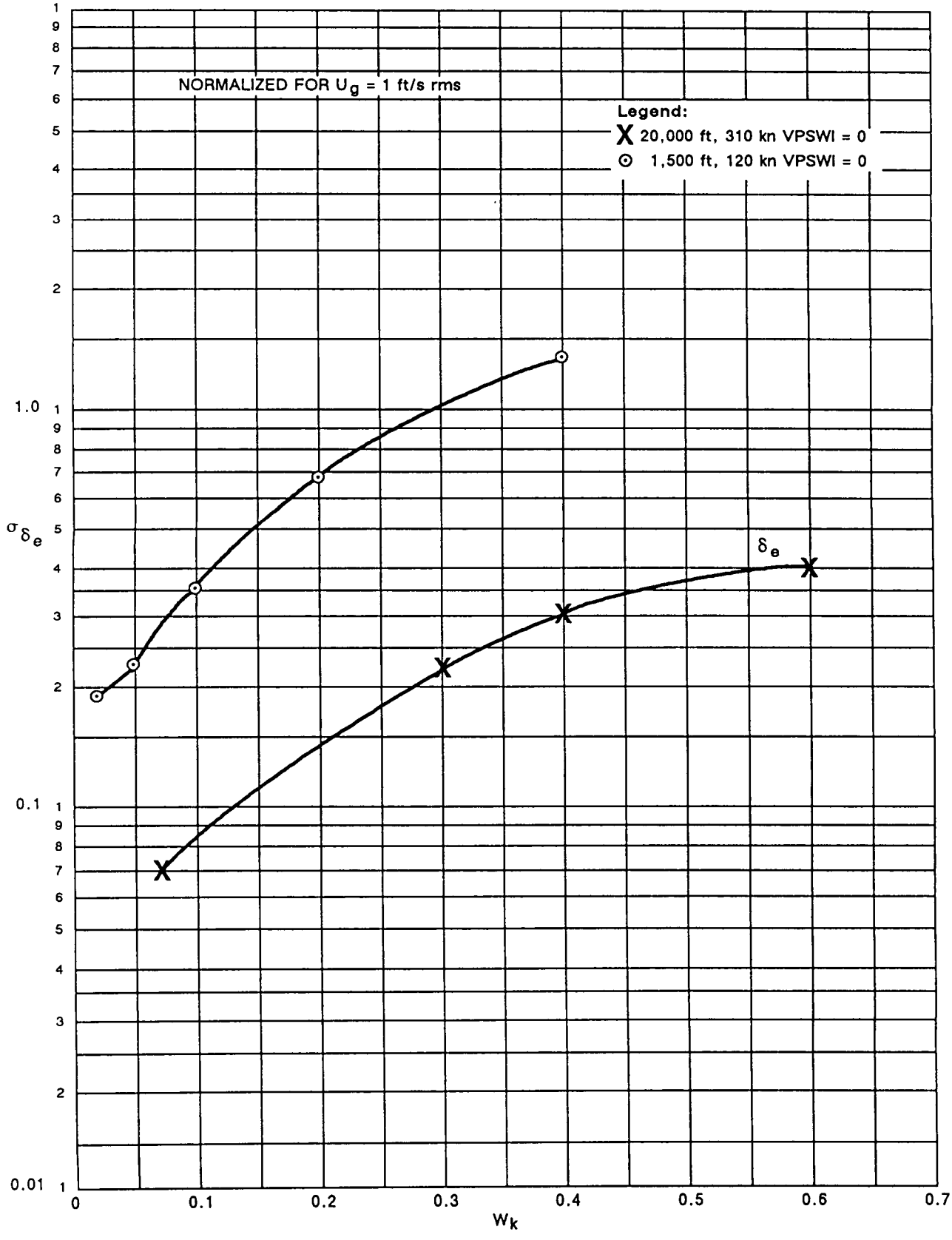

Figure 74. Horizontal Turbulence—SD of Elevator (σ_{δ_e}) Against W_k

7-U80109R2pk13-30

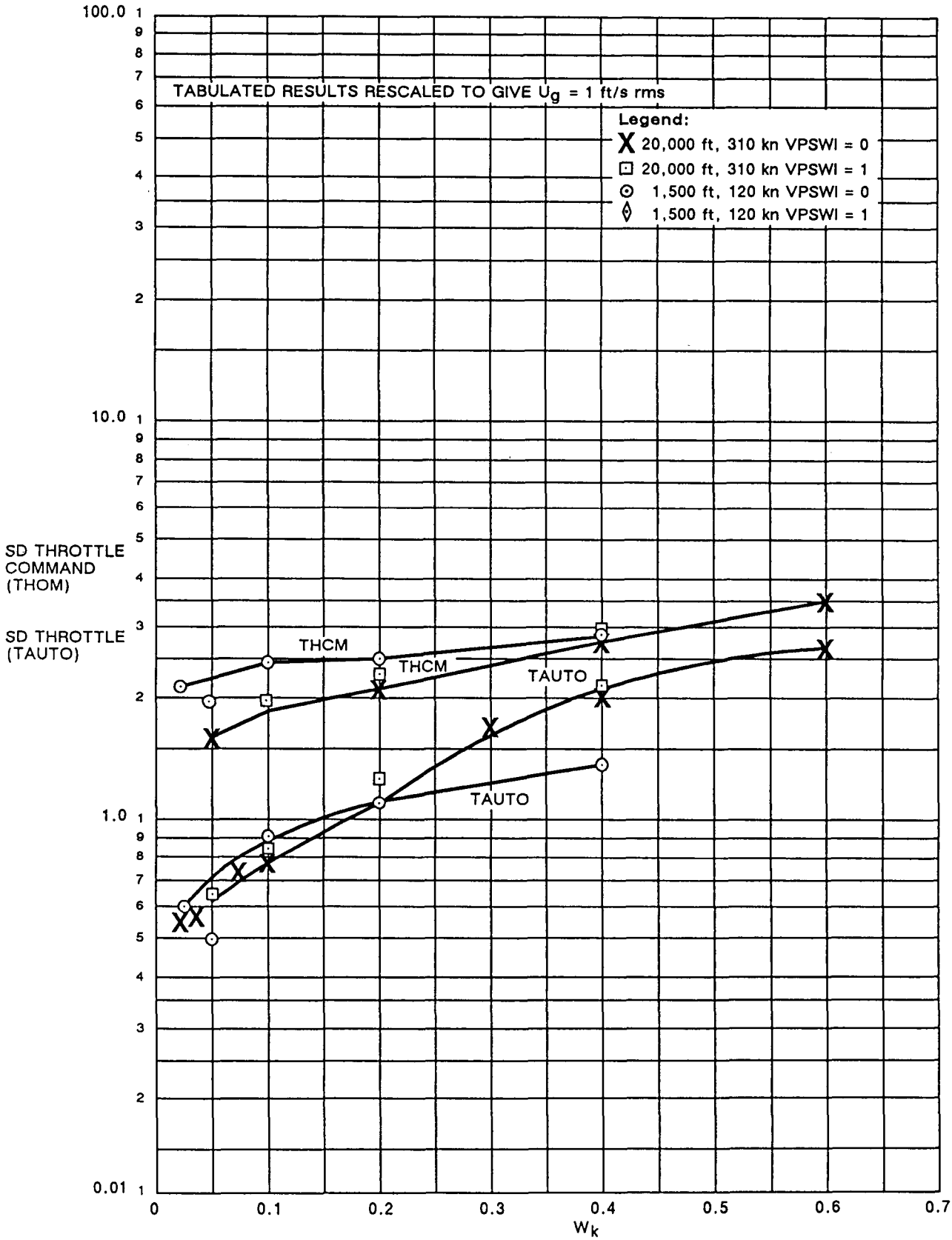

Figure 75. Horizontal Turbulence —SD of Throttle Against W_k

7-U80109R2pk13-31

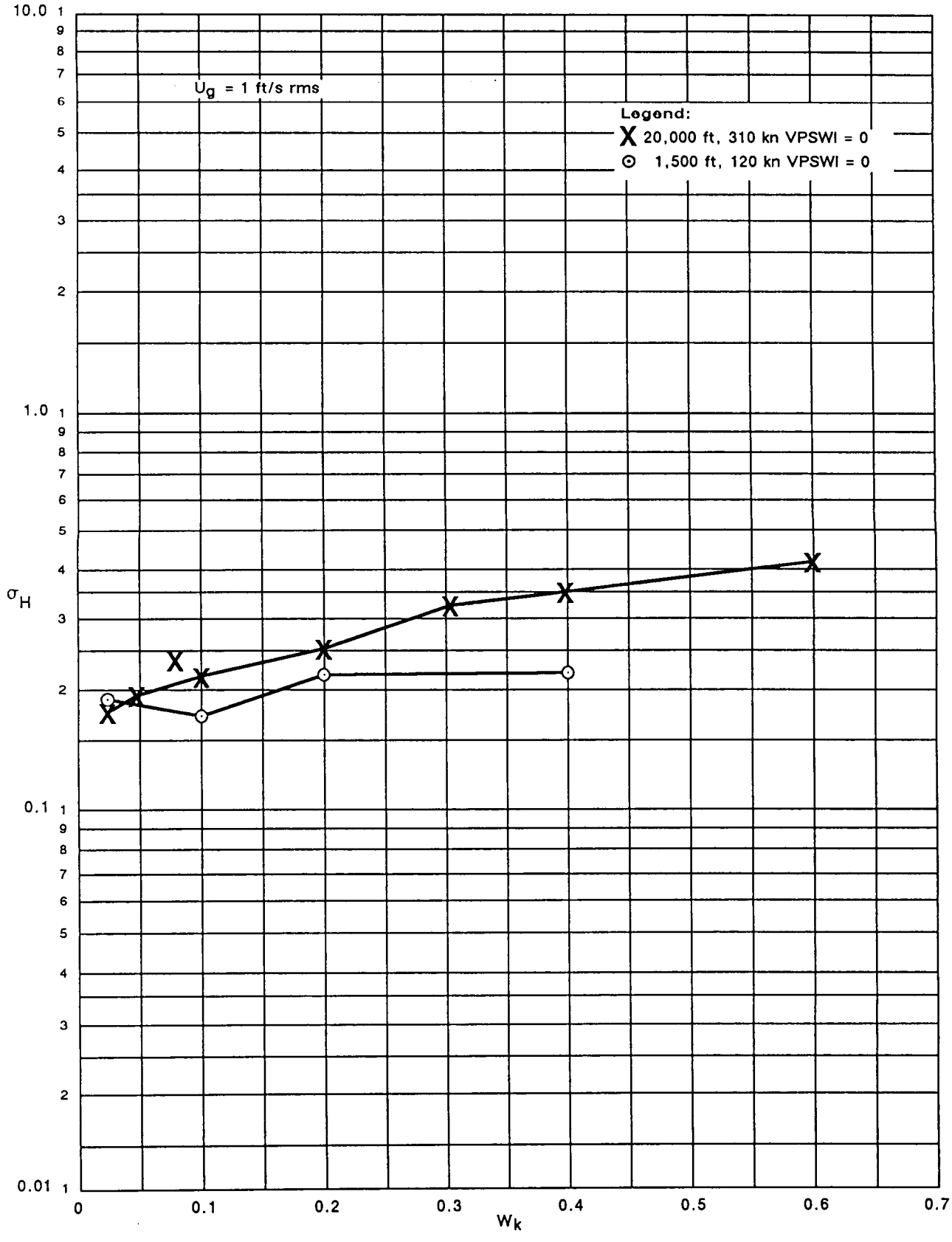

Figure 76. Horizontal Turbulence—SD of Height (σ_H) Against W_k

7-U80109R2pk13-32

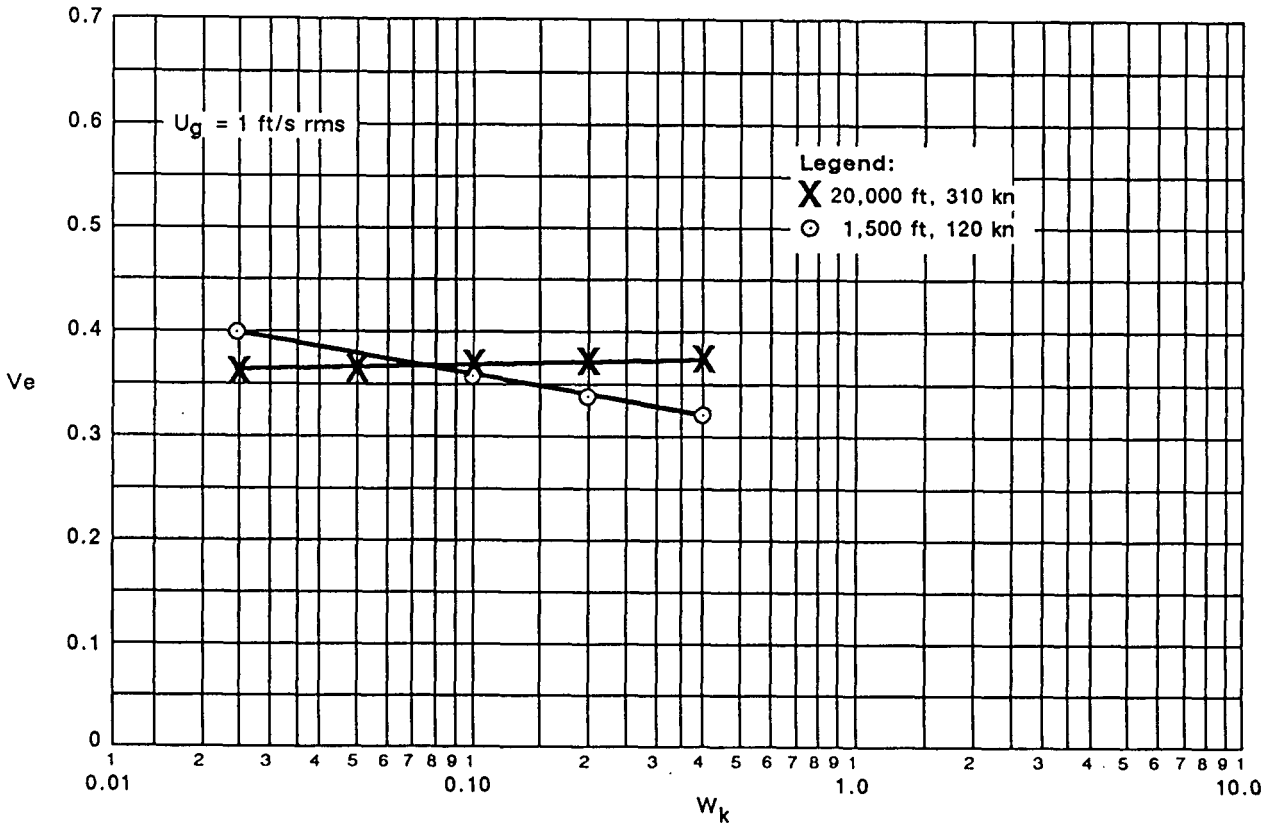

Figure 77. Horizontal Turbulence—Velocity Against W_k

7-U80109R2pk13-33

Table 4. Effect of Vertical Turbulence (1 fps rms)

	Filter Bandwidth, W_k					
	.025	.05	.1	.2	.4	.8
V	0.149	0.149	0.148	0.144	0.134	0.122
V_{CAS}	0 149	0 149	0.148	0.144	0.134	0.122
H	1.54	1.55	1.576	1.616	1.576	1.515
TAUTO	0.745	0.754	0.768	0.788	0.762	0.720
THCM	1.901	1.911	1.931	1.956	1.924	1.87
DEC	0.888	0.883	0.8736	0.856	0.811	0.7197
ELEV	0.781	0.776	0.7677	0.753	0.711	0.6276
U_g	0	0	0	0	0	0
W_g	1.038	1.038	1.038	1.0381	1.038	1.038

Height = 1500H, EAS = 120 k.

	Filter Bandwidth, W_k			
	0.05	0.1	0.2	0.4
V	0.037	0.037	0.0365	0.0354
V_{CAS}	0.041	0 041	0.040	0.03898
H	1.89	1.89	1.889	0.03898
TAUTO	0.253	0.253	0.257	0.247
THCM	1.596	1.595	1.60	1.60
DEC	0.0766	0.0766	0.0764	0.0750
ELEV	0.0437	0.0436	0.0436	0.0427
U_g	0	0	0	0
W_g	1.098	1.098	1.098	1.098

Height = 20000 ft, EAS = 310 kn

The performance of the system was examined for horizontal wind shear (modelled as a 1 kn/s ramp). Maximum velocity and height error were plotted for various valves of ω_K at the two aerodynamic conditions (high and low) previously described. Figures 78 shows that increasing the filter bandwidth ω_K (i.e., increasing the bandwidth of the velocity loop) reduces the maximum velocity error.

However this is achieved at the expense of height error which increases significantly with increase in bandwidth at high altitude (fig. 79). The effect was far less marked at low altitude and speed. An interesting comparison can be made between the wind shear and turbulence performance: Maximum error and SD of height increase with increasing filter bandwidth, whereas maximum velocity error vary significantly with filter bandwidth, with the SD of velocity insensitive at high altitude and only decreased slightly at low altitude.

The linear results plotting SD of throttle against maximum velocity error V for varying filter bandwidth (paragraph 5.4) shows that a trade-off is possible between throttle activity and velocity error wind shear. Figure 80 shows that throttle lever angle (TAUTO) activity was lower both at high and low speed than the linear predictions. However, the throttle command signal was approximately 75% higher than the linear prediction. To take advantage of the ability to trade off throttle activity in turbulence against maximum velocity error in wind shear, the system time constant (τ_K) has been programmed to vary as a function of altitude. Thus low altitude (1000 ft and below) $\tau_K = 4$, thereby reducing the velocity error due to wind shear. At higher altitude the effect of wind shear is not critical and it is desirable to minimize throttle activity. Therefore above 2500 ft τ_K is fixed at 20. Between 1000 to 2500 ft, τ_K varies in a linear manner with altitude. Details of the implementation are given in Figure 47.

The turbulence and wind shear results did not show a significant difference when either $\dot{V}_G$ or the $\dot{V}_{derived}$ signal was implemented on the Harris simulator. Further efforts in modelling the instrumentation required to determine thrust and current weight are needed before an accurate evaluation of the two methods can be made.

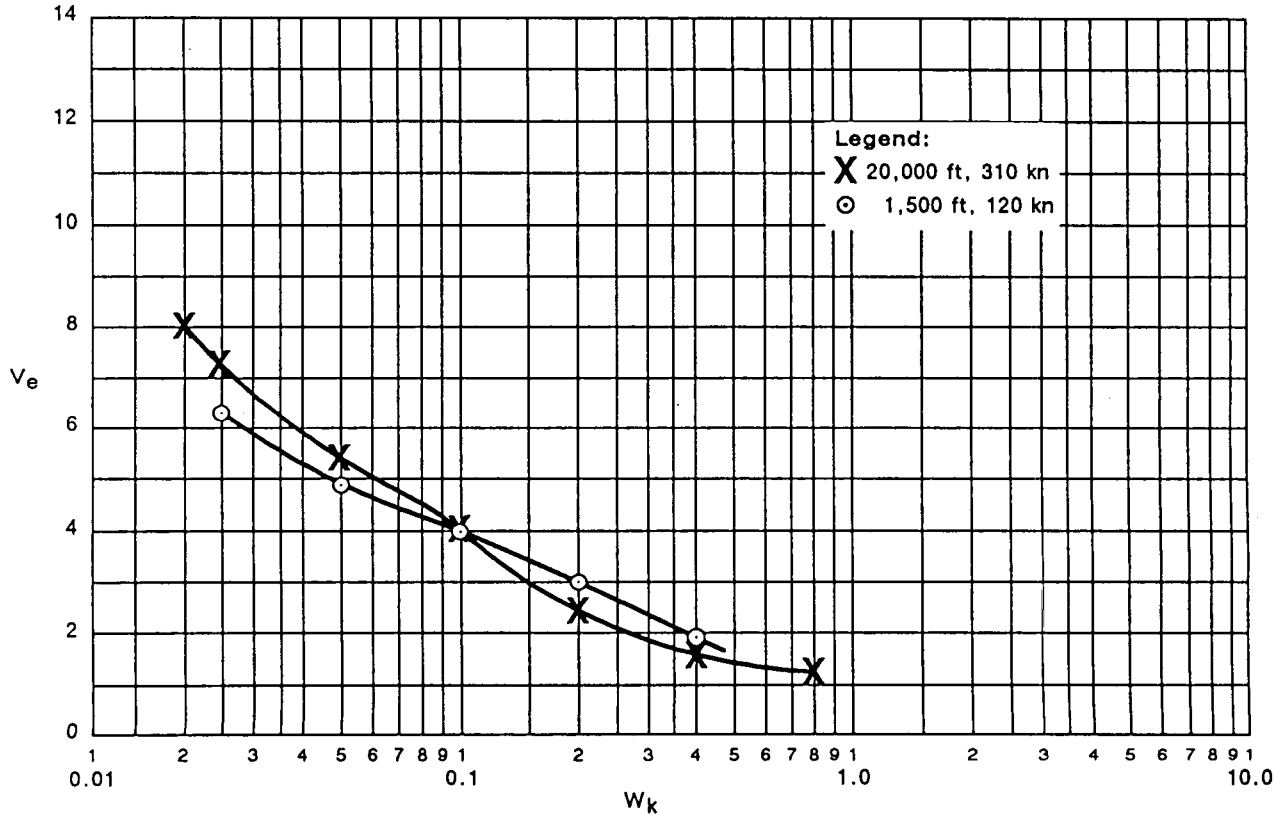

Figure 78. Horizontal Wind Shear—Velocity (V_e) Against W_k

7-U80109R2pk13-29

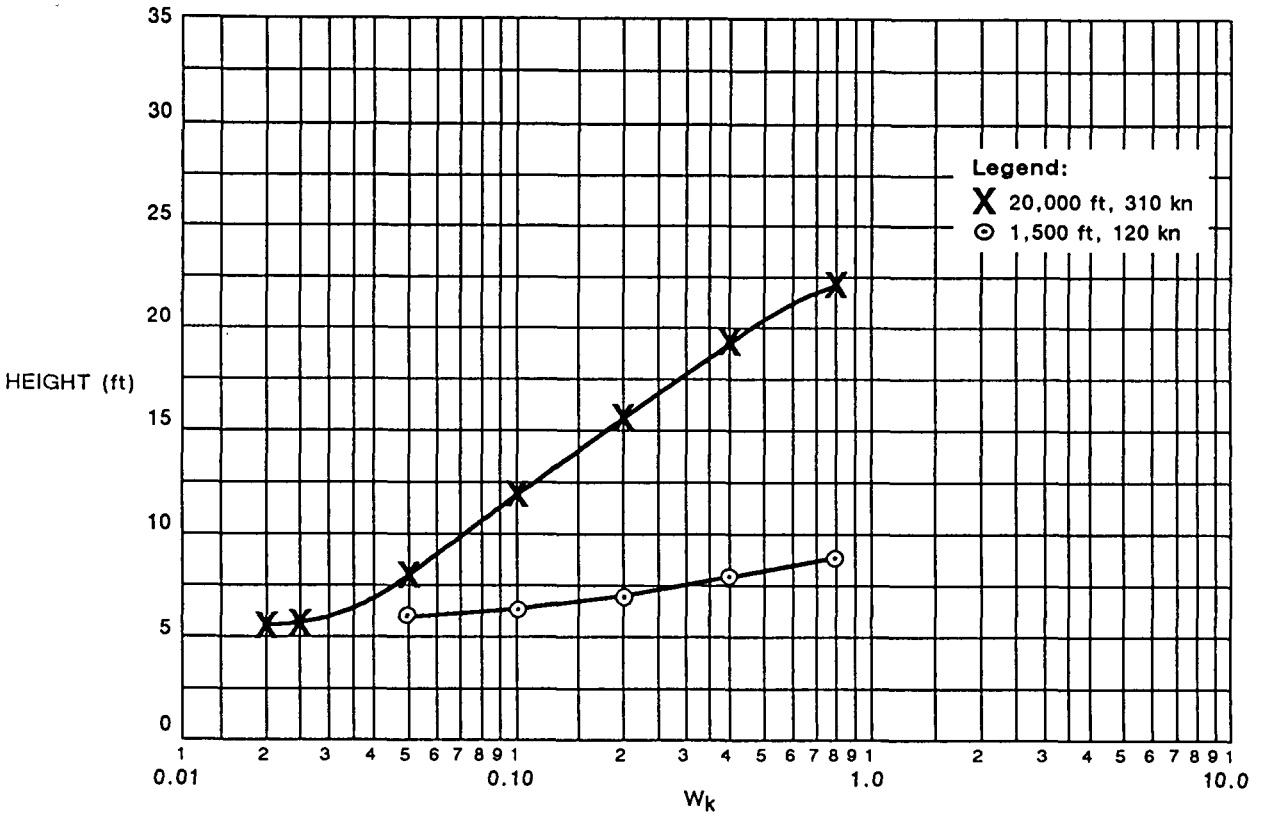

Figure 79. Horizontal Wind Shear—Height Against W_k

7-U80109R2-34

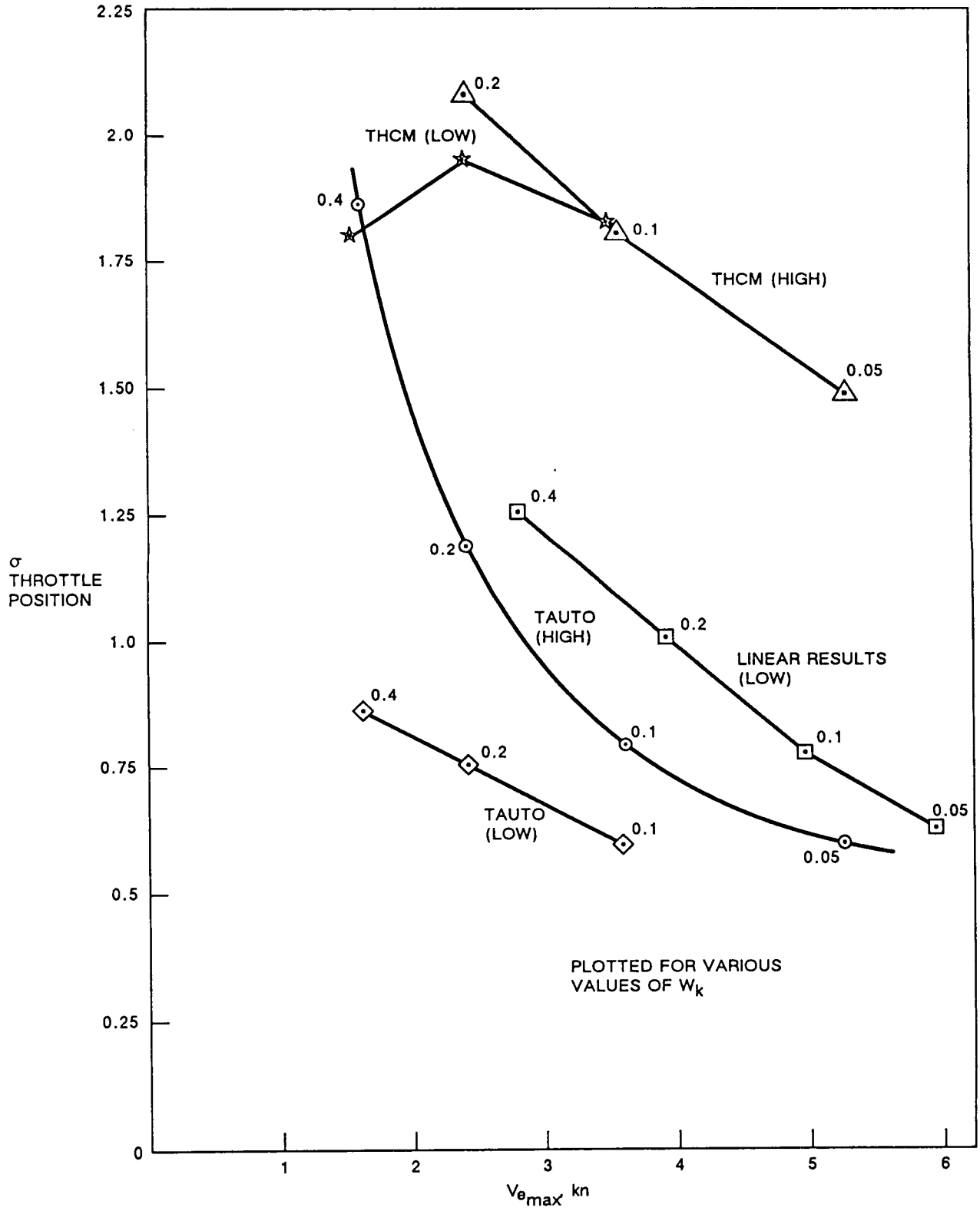

Figure 80. SD Throttle Activity Against Velocity Error ($V_{e_{max}}$) Due to Wind Shear

7-U80109R2pk13-10

10.0 CONCLUSIONS

1. The integrated autopilot/autothrottle was designed to give:

   (a) Fuel efficiency by employing the total energy control concept and minimizing throttle activity.
   (b) Low development, implementation and certification costs by designing the system around a fixed inner loop configuration.
   (c) Maximum safety by preventing stall and preventing engine overboost.

2. The original design constraints have been satisfied during normal operation (e.g., maximum velocity error during altitude maneuvers was less than 1 kn and maximum height error during velocity changes was less than 20 ft over the full aerodynamic range).

3. Wind shear performance was improved to satisfy the design requirement of 5 kn maximum error with the addition of a complementary inertial/air mass referenced acceleration. However, this improvement was achieved at the expense of throttle activity.

4. Variation of the complementary filter time constant, enabling the system to be optimized for wind shear criterion, was satisfied during approach and landing, but throttle activity was minimized during cruise.

5. The use of a 2D wind shear detector did not improve wind shear performance when compared with the preferred system.

6. Several inner loop designs were evaluated. Of these designs, linear analysis showed the optimum was an $\dot{h}/\theta/\dot{\theta}$ complementary inner loop in terms of decoupling in altitude and speed, low elevator activity, and best path velocity tracking in turbulence .

7. A feedback inner loop was selected in an attempt to provide a simple method of limiting. However, this method was not satisfactory for limiting, and stall prevention was incorporated by an additional outer loop control.

8. Future work should consider reimplementing the $\dot{h}/\theta/\dot{\theta}$ inner loop.

9. An engine controller was designed to satisfy the thrust response requirements of the autothrottle functions. Overboost of the engine was prevented by limiting the EPR command signal. In addition, the engine controller has an EPR_{MAX} mode designed as an emergency 'Go Around' feature.

10. Additional modes have been added to control ground speed (i.e., Mach or CAS) and capture the glide slope or follow a preprogrammed vertical path.

11. A mode control panel was designed to enable mode selection by the pilot. Consideration was given to the software design necessary to control arming, engagement and switching between the various modes.

12. The overall system concept and performance were evaluated using a more complex nonlinear simulation implemented on the Harris airplane simulator.

13. The Harris simulator confirmed the results achieved by linear design.

14. Future work should compare the design concept and results of this conventional design with results obtained by solving optimal control problem using a suitable cost function. This approach may yield further insight into minimizing the effect of wind shear and turbulence.

APPENDIX A. TWO-DIMENSIONAL WIND SHEAR DETECTOR

The basis of the wind shear detector is to calculate a new thrust level to compensate for accelerations due to the wind shear.

It can be shown that the vertical wind is:

$$Vw_V = -\dot{h} + V_T \tan\theta - V_T \tan\alpha \cos\Phi \qquad (A.1)$$

where $\dot{h}$ = inertial altitude rate
V_T = true air speed
θ = pitch altitude
X = true angle of attack
Φ = roll altitude

In addition it can be shown that the change in flight path angle due to vertical wind, assuming constant speed and power setting is:

$$\Delta\gamma w_V = -Vw_V/V_T \qquad (A.2)$$

Hence
$$\Delta\gamma w_V = \gamma_I + \tan\theta - \tan\alpha \cos\Phi \qquad (A.3)$$

or for small angles:

$$\Delta\gamma w_V = \gamma_I + \theta - \alpha \qquad (A.4)$$

The thrust required to compensate for such a change in flight path angle is:

$$\Delta T w_V = W \Delta\gamma w_V \qquad (A.5)$$

Where W = Weight (lbs)

Equation 4 is implemented by measuring longitudinal acceleration (a) using a body mounted accelerometer, where:

$$a_x = \dot{V}_I + g\theta \qquad (A.6)$$

where V_I = velocity rate (inertial)

Figure A.1 shows that a lagged θ (θ) can be derived by integrating the accelerometer measurement, feeding back V_{TAS} , and high pass filtering the resultant signal. This concept is used in Figure A.2 to obtain the $\Delta\gamma W_V$ signal. This signal ($\Delta\gamma W_V$) is rate limited to filter the high frequency turbulence. Finally the signal input to the throttle was divided by the throttle-to-thrust gain to get the command in terms of degrees of throttle.

It should be noted that the computation of ΔT_W is dependent on the accuracy of the angle of attack signal and that accurate determination of α has not been fully investigated.

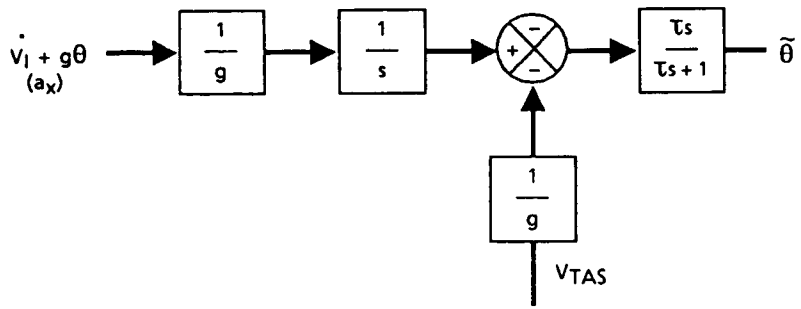

Figure A.1. Derivation of $\tilde{\theta}$

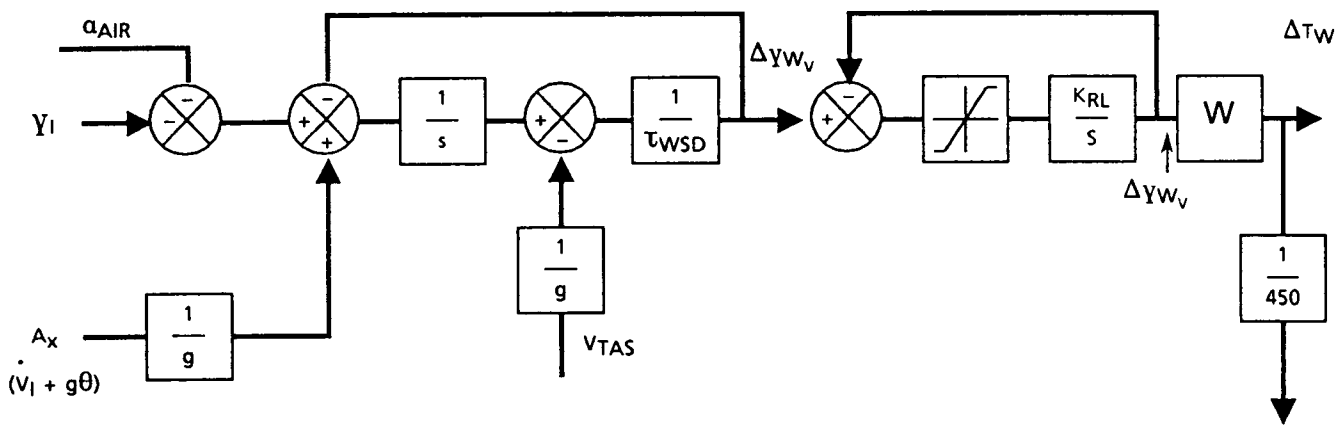

Figure A.2. Wind Shear Detector

APPENDIX B. DERIVATION OF $\ddot{h}/\dot{\theta}$ SYSTEM

Pitch rate may be expressed as:

$$\dot{\theta} = \frac{1}{V_G}\ddot{h} + \dot{\alpha} \qquad \dot{\theta},\ \dot{\alpha} \text{ in rad/sec} \tag{B.1}$$

Substitute for the state equation from the aircraft equation of motion:

$$\dot{\alpha} = (-.3133)U - (.6543)\alpha + (1.)q - (.000723)\delta_e - (.108\text{x}10^{-6})\delta_T \tag{B.2}$$

Considering small perturbations only from an initial steady state condition, constant thrust, no horizontal or vertical turbulence, and the elimination of α with $= \theta \frac{1}{V_G}\dot{h}$, the equation reduces to:

$$\dot{\theta} = \frac{1}{V_G}\ddot{h} - 33.13U - .6543\left(\theta - \frac{1}{V_G}\dot{h}\right) + 1.0q - .000723\delta_e \tag{B.3}$$

With $\dot{\theta} = q$, the equation can be solved for θ as follows:

$$\dot{\theta} = .4319\ddot{h} + .2827\ddot{h} - .063\delta_e - .1354V \tag{B.4}$$

Where $V = V_{GO}U$, θ is in degrees, $\ddot{h}$ is in ft/sec^2, δ_e is in degrees and both h and V are in ft/sec.

From Figure 18, the equation for the elevator command is:

$$\delta_{ec} = 4q + 8\left\{\theta + g/V_G\dot{h} - 1.\dot{V}_{eng} + \frac{.75}{S}\left[-.1\,V_{TAS} - \dot{V}_{eng} - g/V_G(-.1h-\dot{h})\right]\right\} \tag{B.5}$$

Substitution of equation 4 in equation 5 results in:

$$\delta_{ec} = 4q + 8\left\{.4319\ddot{h} - .135V + .283\dot{h} - .063\delta_e + g/V_G\dot{h} \right. \tag{B.6}$$
$$\left. -\dot{V}_{ng} + \frac{.75}{S}\left[-.1\, V_{TAS} - \dot{V}_{eng} - g/V_G(-.1h-h) \right] \right\}$$

The elevator position is related to δ_{ec} by the elevator servo transfer function:

$$\delta_{ec} = \frac{\delta_{ec}}{.05S+1} \tag{B.7}$$

Substition of equation 6 into equation 7 and solving for δ_e yields:

$$ec = \frac{.655}{.033S+1}\left[4q + 8\left\{.4319\ddot{h} - .135V + .283\dot{h} + g/V_G\dot{h} \right.\right. \tag{B.8}$$
$$\left.\left. -\dot{V}_{eng} + \frac{.75}{S}\left[-.1\, V_{TAS} - \dot{V}_{eng} - g/V_G(-.1h-\dot{h})\right] \right\} \right]$$

This equation represents an $\ddot{h}/\dot{\theta}$ control law that has nearly the same stability characteristics as the original system. For implementation of this system, the .03 sec lag must be replaced with the actual 0.5 sec elevator servo transfer function. This would have a very small effect on the aircraft dynamics.

REFERENCES

1. Users Manual for 737-200 (ADV) Standard Simulation Model (SSM), D6-32806, 7 November 1977, Boeing Commercial Airplanes.

2. Full Flight Regime Autothrottle - Engine Control System Characteristics and Servo Mechanism Requirements, C-1997 Rev A, 6 September 1979, Boeing Commercial Airplanes.

3. K. R. Bruce, Design and Verification by Nonlinear Simulation of a Mach/CAS Control Law for the NASA TCV B-737 Aircraft, NASA CR-178029, December 1986, NASA.

NASA
National Aeronautics and Space Administration

Report Documentation Page

1. Report No.	2. Government Accession No.	3. Recipient's Catalog No.
NASA CR-4217		

4. Title and Subtitle	5. Report Date
Integrated Autopilot/Autothrottle for the NASA TSRV B-737 Aircraft: Design and Verification by Nonlinear Simulation	February 1989
	6. Performing Organization Code
7. Author(s)	8. Performing Organization Report No.
Kevin R. Bruce	
	10. Work Unit No. 513-52-13-54
9. Performing Organization Name and Address	11. Contract or Grant No.
Boeing Commercial Airplane Company P. O. Box 3707 Seattle, WA 98124-2207	NAS1-14880
	13. Type of Report and Period Covered
12. Sponsoring Agency Name and Address	Contractor Report
NASA Langley Research Center Hampton, VA 23665-5225	14. Sponsoring Agency Code

15. Supplementary Notes

NASA Technical Monitor: Dr. J. F. Creedon
Boeing Technical Supervision: G. R. Hennig
Boeing Contract Manager: R. L. Erwin
Final Report

16. Abstract

An integrated autopilot/autothrottle was designed for flight test on the NASA TSRV B-737 airplane. The system was designed using a total energy concept and is intended to achieve:

1. Fuel efficiency by minimizing throttle activity
2. Low development and implementation costs by designing the control modes around a fixed inner loop design
3. Maximum safety by preventing stall and engine overboost

The control law was designed initially using linear analysis; the system was developed using nonlinear simulations. All primary design requirements were satisfied.

17. Key Words (Suggested by Author(s))	18. Distribution Statement
Flight Controls Autopilot Autothrottle Terminal Configured Vehicle (TCV)	Unclassified - Unlimited Subject Category 08

19. Security Classif. (of this report)	20. Security Classif. (of this page)	21. No. of pages	22. Price
Unclassified	Unclassified	124	A06

NASA-Langley, 1989